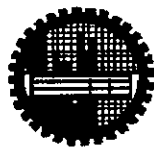
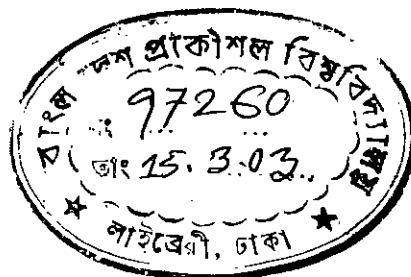


**THE EFFECT OF HEAT TREATMENT ON THE SECONDARY  
MAGNETIC EFFECTS IN IRON AND COBALT BASED AMORPHOUS  
MAGNETIC MATERIALS**

**BY**

**FARHAD ALAM**

**A DISSERTATION SUBMITTED TO THE DEPARTMENT OF PHYSICS,  
BUET, DHAKA IN PARTIAL FULFILLMENT OF THE REQUIREMENT  
FOR THE DEGREE OF MASTER OF PHILOSOPHY**



**BANGLADESH UNIVERSITY OF ENGINEERING AND TECHNOLOGY,  
DHAKA - 1000, BANGLADESH**

**FEBRUARY, 2003**


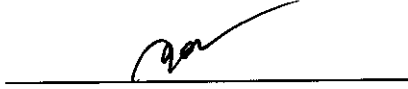


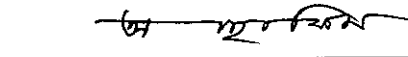


**BANGLADESH UNIVERSITY OF ENGINEERING AND TECHNOLOGY**  
**DHAKA**  
**DEPARTMENT OF PHYSICS**

**Certification of Thesis work**

The thesis titled "**The effect of heat treatment on the secondary magnetic effects in iron and cobalt based amorphous magnetic materials**" submitted by Farhad Alam Roll No. 040014021F, Session April-2000 has been accepted as satisfactory in partial fulfillment of the requirement for the degree of Master of Philosophy on 5<sup>th</sup> February, 2003.

**BOARD OF EXAMINERS**

1.   
Dr. M. Ali Asgar (Supervisor)  
Professor  
Department of Physics, BUET, Dhaka  
Chairman
2.   
Dr. Md. Abu Hashan Bhuiyan  
Professor,  
Department of Physics, BUET, Dhaka  
Member
3.   
Dr. Md. Feroz Alam Khan  
Associate Professor  
Department of Physics, BUET, Dhaka  
Member
4.   
Dr. Nazma Zaman  
Member  
Professor & Head  
Department of Physics, BUET, Dhaka  
Member
5.   
Dr. A. K. M. Abdul Hakim  
Principal Engineer  
Bangladesh Atomic Energy Commission  
Dhaka  
Member (External)

## ***Candidate's Certificate***

*This is to certify that the author is solely responsible for the work reported in this thesis and this work has not been submitted to any other University or elsewhere for the award of a degree or diploma.*



***Dr. M. Ali Asgar (Supervisor)***

***Professor***

***Department of Physics***

***Bangladesh University of Engineering and Technology***

***Dhaka-1000, Bangladesh***

## **CANDIDATE'S DECLARATION**

It is hereby declared that this thesis or any part of it has not been submitted elsewhere for the award of any degree or diploma.



---

**Farhad Alam**

**Candidate**

**Roll No.: 040014021F**

**Session: April, 2000**

*DEDICATED*

*TO*

*My Parents & Brother*

## ACKNOWLEDGEMENTS

*I am extremely delighted to express my deep sense of gratitude to my reverend supervisor Dr. M. Ali Asgar, Professor, Department of Physics, Bangladesh University of Engineering and Technology, Dhaka, for his sincere cooperation, continuous guidance, invaluable suggestions and inspiration which allowed me to complete this thesis.*

*I would like to express my sincere thanks to Dr. Nazma Zaman, Professor and Head of the Department of Physics, BUET, Dhaka and Professor Gias uddin Ahmad of the same department for their sincere cooperation.*

*I am grateful to Professor Mominul Huq, Department of Physics, BUET, Dhaka, for his valuable suggestion and inspiration.*

*I would like to thank Professor Md. Abu Hashan Bhuiyan and Professor Jiban Podder Department of Physics, BUET, for their encouragement during this work.*

*I express my gratitude to Dr. Md. Feroz Alam Khan, Associate Professor, Department of Physics, BUET, Dhaka, for his generous help in course of doing measurements with different kinds of equipment in the laboratory.*

*I would like to offer my thanks to Dr. Md. Nazrul Islam, and Dr. A. K. M. Akther Hossain of the Department of Physics for their cooperation.*

*I express my cordial thanks to Dr. S. S. Sikder, Department of Physics, B.I.T., Khulna for his endless help in preparation of the samples and Mr. Sultan Mahmud, Lecturer, The University of Asia Pacific, Dhaka, to make my work successful one.*

*I express my gratitude to my family members and to my friends and well-wishers especially, Rafia, Niyamat, Nasreen, Rafi, Jahangir, Jeffrey for their encouragement in keeping my spirit high.*

*I would like to thank Mr. Liaquat Ali for his cordial help in preparing the final script and also all the staff of the Department of Physics, BUET, Dhaka.*

*I also want to express my gratefulness to the authority of BUET for giving me the opportunity to do this research and financial support.*

*Thank you all*

## *Abstract*

Co-based amorphous magnetic materials with composition  $Co_{80-x}Fe_xB_{10}Si_{10}$  ( $x = 0, 2, 4$  and  $6$ ) have been prepared by melt spinning technique as a possible soft magnetic material. These specimens have been checked for their amorphousity by X-ray diffraction. Magnetostriction as a secondary effect, which plays one of the most important roles in determining the magnetic characteristics like coercivity, initial permeability, remanance etc. have been studied by strain gauge technique using a Wheatstone Bridge in out of balance condition. The effect of composition and temperature on magnetostriction have been measured with a sensitivity of  $10^{-6}$  as fractional strain. Since magnetostriction arises from spin orbit coupling such that a ferromagnetic material spontaneously develop lattice distortion in order to reduce magnetic anisotropy energy, the value of magnetostriction provide information regarding the magnetoelastic interaction of a magnetic material. Its importance is not only technological because low magnetostriction is related to low constrain in domain wall movement and hence higher permeability, but also of theoretical interest. Amorphous material in its perfect isotropic form should not have magnetic anisotropy and also magnetostriction but due to the mechanism used in the production of amorphous ribbons there is a strain induced anisotropy and an associated magnetostriction. The strain arises due to the tension along the length of the ribbon which the specimen is subjected to during the preparation of the ribbons. In this alloy system, the magnetic elements Iron and cobalt have positive and negative magnetostriction respectively their pure crystalline forms. It is observed that with the substitution of iron for cobalt magnetostriction has decreased gradually, which shows that iron atom has cancelled out part of the negative magnetostriction due to cobalt atoms. This result although quiet interesting in showing that one can tailor amorphous materials in respect of their

magnetostrictions and hence magnetic softness by adjusting the proportions of elements having opposite magnetostrictions, can not be deduced theoretically. Because magnetoelastic effect is a property of the structure of the material and not of its chemical composition only. Our experimental finding is therefore very important in establishing a relation and a guideline for preparing magnetically soft amorphous material. Only one sample was without iron which gave maximum negative magnetostriction value. For other samples there is monotonous decrease of magnetostriction with increasing iron substitution, maximum value is  $-21.519 \times 10^{-6}$  for composition  $Co_{80-x}Fe_xB_{10}Si_{10}$  ( $x = 2$ ) and minimum value is  $-14.308 \times 10^{-6}$  for composition  $Co_{80-x}Fe_xB_{10}Si_{10}$  ( $x = 6$ ). Maximum value for magnetostriction at liquid nitrogen temperature is  $-26.302 \times 10^{-6}$  for composition  $Co_{80-x}Fe_xB_{10}Si_{10}$  ( $x = 2$ ) for minimum value is  $-16.174 \times 10^{-6}$  for composition  $Co_{80-x}Fe_xB_{10}Si_{10}$  ( $x = 6$ ). Thermal expansion measurements have also been carried out by strain gauge technique which shows that amorphous state give rise to lower thermal expansion coefficient because of lower anharmonicity of the atomic vibrations in this system.



# Contents

|   | Page |
|---|------|
| <b>List of Figures</b>  | i    |
| <b>List of Tables</b>   | iii  |
| <b>CHAPTER – 1</b>  |      |
| 1.1 Introduction  | 1    |
| 1.2 Applications of amorphous ribbon                                | 6    |
| 1.3 Organization of the work  | 8    |
| <b>CHAPTER – 2</b>  |      |
| <b>The Structure and preparation Technique of Amorphous Ribbons</b> |      |
| 2.1 An over view of amorphous materials                             | 9    |
| 2.2 The structure of an amorphous alloy                             | 10   |
| 2.3 Condition for forming amorphous materials                       | 15   |
| 2.4 Condition necessary for preparing amorphous materials           | 18   |
| 2.5 Preparation technique of amorphous ribbons                      | 18   |
| 2.5.1 The atomic deposition method                                  | 18   |
| 2.5.2 The fast cooling of the melt                                  | 19   |
| 2.5.3 Rapid quenching method  | 20   |
| 2.6 Experimental details of the preparation of amorphous ribbon     | 22   |
| 2.6.1 Important factors to control the thickness of ribbons         | 23   |
| 2.7 Factors contributing to glass formation                         | 23   |
| 2.8 Examining the amorphousity                                      | 25   |
| <b>CHAPTER – 3</b>  |      |
| <b>Theories of Magnetostrictions</b>                                |      |
| 3.1 Physical origin of magnetostriction                             | 27   |
| 3.2 Magnetostriction with different compositions                    | 30   |
| 3.3 Low temperature magnetic moment                                 | 34   |
| 3.3.1 Models of moment variation                                    | 34   |
| 3.3.2 Band gap theory   | 35   |
| 3.3.3 Split bands   | 38   |
| 3.3.4 Coordination bond model                                       | 38   |
| 3.3.5 Environment model   | 39   |
| 3.4 Magnetic excitation   | 40   |
| 3.5 Expression for linear magnetostriction                          | 42   |
| 3.6 Magnetostriction in polycrystalline axial magnetic system       | 45   |
| 3.7 Magnetostriction in amorphous ribbons                           | 47   |
| 3.8 Engineering magnetostriction                                    | 48   |
| 3.9 Direction of linear magnetostriction                            | 49   |
| 3.10 Magnetostriction arising from domain rotation                  | 51   |
| 3.11 Magnetoresistance  | 53   |
| 3.12 Field dependence of magnetostriction                           | 54   |
| 3.13 Low temperature dependence of magnetostriction                 | 54   |
| 3.14 Application of magnetostriction                                | 55   |
| 3.14.1 Under water sound  | 56   |
| 3.14.2 Ultrasonic sound generators                                  | 57   |

## **CHAPTER – 4**

### **Theories of thermal expansion**

|     |   |    |
|-----|---|----|
| 4.1 | Theory of thermal expansion                               | 58 |
| 4.2 | Electronic and magnetic contribution to thermal expansion | 60 |
| 4.3 | Negative thermal expansion in solids                      | 63 |
| 4.4 | Thermal expansion and Invar anomalies                     | 65 |

## **CHAPTER – 5**

### **Experimental details**

|       |   |    |
|-------|---|----|
| 5.1   | Magnetostriction measurement technique                        | 70 |
| 5.2   | Strain measurements using stain gauge                         | 73 |
| 5.3   | Gauge factor  | 74 |
| 5.4   | Experimental set up for measurements of magnetostriction      | 74 |
| 5.4.1 | The D.C. Bridge   | 75 |
| 5.4.2 | The D.C. amplifier  | 75 |
| 5.4.3 | Low temperature measurement technique                         | 77 |
| 5.5   | Bridge current sensitivity and calibration of the D.C. Bridge | 77 |
| 5.6   | The choice of dummy material                                  | 79 |
| 5.7   | The specimen holder   | 79 |
| 5.8   | Specimen mounting   | 81 |
| 5.9   | The gauge cementing   | 81 |
| 5.10  | Calibration curves for magnet                                 | 82 |
| 5.11  | Bridge circuit sensitivity and calibration                    | 82 |
| 5.12  | Calibration curve for angle correction                        | 85 |

## **CHAPTER 6**

### **Results and Discussion of Co-based amorphous Ribbons**

|     |   |    |
|-----|---|----|
| 6.1 | Field dependence magnetostriction of Co-based amorphous ribbons           | 87 |
| 6.2 | Low temperature dependence magnetostriction of Co-based amorphous ribbon  | 93 |
| 6.3 | Low temperature dependence thermal expansion of Co-based amorphous ribbon | 98 |

## **CHAPTER 7**

### **Results and Discussion of Fe-based amorphous Ribbons**

|     |   |     |
|-----|---|-----|
| 7.1 | Field dependence magnetostriction of Fe-based amorphous ribbons           | 102 |
| 7.2 | Low temperature dependence magnetostriction of Fe-based amorphous ribbon  | 105 |
| 7.3 | Low temperature dependence thermal expansion of Fe-based amorphous ribbon | 108 |

|                    |     |
|--------------------|-----|
| <b>CONCLUSIONS</b> | 111 |
|--------------------|-----|

|                   |     |
|-------------------|-----|
| <b>REFERENCES</b> | 114 |
|-------------------|-----|

|                 |     |
|-----------------|-----|
| <b>APPENDIX</b> | 120 |
|-----------------|-----|

## **List of Figures**

- 2.1 *Short range order as a function of radial distance*
- 2.2 *Free energy versus temperature curve*
- 2.3 *Glass formation as function of reduced glass transition temperature*
- 2.4 *Viscosity versus temperature curve*
- 2.5 *Compositional dependence of melting point*
- 2.6 *Experimental values of critical velocity versus reduced glass transition temperature*
- 2.7 *Thin layer of molten alloy intimate contact with the outer surface of metallic rotor is quenched in to amorphous.*
- 2.8 *Temperature dependence of enthalpy  $H.G.$  and  $G'$  corresponds to glass and  $s$  corresponds to crystalline state*
- 2.9 *X-ray diffraction from the top surface of some amorphous ribbon*
- 3.1 *Physical origins of Magnetostriction*
- 3.2 *Reduced saturation magnetostriction versus reduced specific saturation magnetization for various amorphous transition metal metalloid alloys*
- 3.3 *Field dependence of the room temperature magnetostriction of non-S-State rare earth amorphous alloys*
- 3.4 *Slater-Pauling plot for amorphous  $M_{1-x}T_x$  alloys*
- 4.1 *Lattice constant of solid argon as a function of temperature*
- 4.2 *Linear thermal expansion versus reduced temperature for  $Re_2Fe_{14}B$  be serie*
- 5.1 *D. C. Bridge*
- 5.2 *Specimen holder*
- 5.3 *Current versus magnetic field*
- 5.4 *Bridge sensitivity*
- 5.5 *Variation of bridge sensitivity with current*
- 5.6 *Magnetostriction versus angular position of the field*
- 6.1 *Magnetic field versus magnetostriction of amorphous ribbon with compositions  $Co_{80-x}Fe_xB_{10}Si_{10}$  at room temperature*
- 6.2 *Magnetic field versus magnetostriction of amorphous ribbon with compositions  $Co_{80}B_{10}Si_{10}$  at room temperature*
- 6.3 *Magnetic field versus magnetostriction of amorphous ribbon with compositions  $Co_{80-x}Fe_xB_{10}Si_{10}$  at liquid nitrogen temperature*
- 6.4 *Magnetic field versus magnetostriction of amorphous ribbon with compositions  $Co_{80}B_{10}Si_{10}$  at liquid nitrogen temperature*

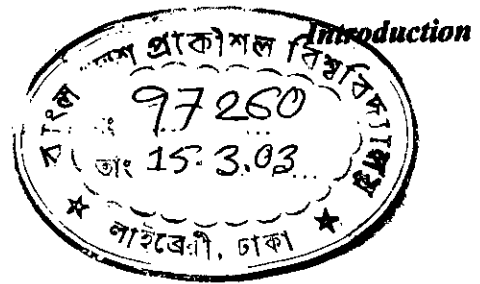
- 6.5 *Magnetostriction versus temperature of amorphous ribbon with compositions  $Co_{80-x}Fe_xB_{10}Si_{10}$*
- 6.6 *Magnetostriction versus temperature of amorphous ribbon with compositions  $Co_{80}B_{10}Si_{10}$*
- 6.7 *Temperature versus thermal expansion of amorphous ribbon with compositions  $Co_{80-x}Fe_xB_{10}Si_{10}$*
- 6.8 *Temperature versus thermal expansion of amorphous ribbon with compositions  $Co_{80}B_{10}Si_{10}$*
- 7.1 *Magnetic field versus magnetostriction of amorphous ribbon with compositions  $Fe_{90-x}Si_xB_{10}$  at room temperature*
- 7.2 *Magnetic field versus magnetostriction of amorphous ribbon with compositions  $Fe_{90-x}Si_xB_{10}$  at liquid nitrogen temperature*
- 7.3 *Magnetostriction versus temperature of amorphous ribbon with compositions  $Fe_{90-x}Si_xB_{10}$*
- 7.4 *Temperature versus thermal expansion of amorphous ribbon with compositions  $Fe_{90-x}Si_xB_{10}$*

## *List of Tables*

1. Data for Magnetic Field Strength
2. Data for Calibration of the D.C. Bridge
3. Variation of Bridge Sensitivity with Bridge Current
4. Variation of Magnetostriction with the Angle of Field
5. Table for Magnetostriction Measurement at Room Temperature ( $\text{Co}_{78}\text{Fe}_2\text{B}_{10}\text{Si}_{10}$ )
6. Table for Magnetostriction Measurement at Room Temperature ( $\text{Co}_{76}\text{Fe}_4\text{B}_{10}\text{Si}_{10}$ )
7. Table for Magnetostriction Measurement at Room Temperature ( $\text{Co}_{74}\text{Fe}_6\text{B}_{10}\text{Si}_{10}$ )
8. Table for Magnetostriction Measurement at Liquid Nitrogen Temperature ( $\text{Co}_{78}\text{Fe}_2\text{B}_{10}\text{Si}_{10}$ )
9. Table for Magnetostriction Measurement at Liquid Nitrogen Temperature ( $\text{Co}_{76}\text{Fe}_4\text{B}_{10}\text{Si}_{10}$ )
10. Table for Magnetostriction Measurement at Liquid Nitrogen Temperature ( $\text{Co}_{74}\text{Fe}_6\text{B}_{10}\text{Si}_{10}$ )
11. Table for Temperature Dependence ( $\text{Co}_{78}\text{Fe}_2\text{B}_{10}\text{Si}_{10}$ )
12. Table for Temperature Dependence ( $\text{Co}_{76}\text{Fe}_4\text{B}_{10}\text{Si}_{10}$ )
13. Table for Temperature Dependence ( $\text{Co}_{74}\text{Fe}_6\text{B}_{10}\text{Si}_{10}$ )
14. Table for Thermal Expansion Measurement ( $\text{Co}_{78}\text{Fe}_2\text{B}_{10}\text{Si}_{10}$ )
15. Table for Thermal Expansion Measurement ( $\text{Co}_{76}\text{Fe}_4\text{B}_{10}\text{Si}_{10}$ )
16. Table for Thermal Expansion Measurement ( $\text{Co}_{74}\text{Fe}_6\text{B}_{10}\text{Si}_{10}$ )
17. Table for Magnetostriction Measurement at Room Temperature ( $\text{Co}_{80}\text{B}_{10}\text{Si}_{10}$ )
18. Table for Magnetostriction at Liquid Nitrogen Temperature ( $\text{Co}_{80}\text{B}_{10}\text{Si}_{10}$ )
19. Table for Temperature Dependence ( $\text{Co}_{80}\text{B}_{10}\text{Si}_{10}$ )
20. Table for Thermal Expansion Measurement ( $\text{Co}_{80}\text{B}_{10}\text{Si}_{10}$ )
21. Table for Magnetostriction Measurement at Room Temperature ( $\text{Fe}_{82}\text{B}_8\text{Si}_{10}$ )
22. Table for Magnetostriction at Liquid Nitrogen Temperature ( $\text{Fe}_{82}\text{B}_8\text{Si}_{10}$ )
23. Table for Temperature Dependence ( $\text{Fe}_{82}\text{B}_8\text{Si}_{10}$ )
24. Table for Thermal Expansion Measurement ( $\text{Fe}_{82}\text{B}_8\text{Si}_{10}$ )
25. Table for Magnetostriction Measurement at Room Temperature ( $\text{Fe}_{80}\text{B}_{10}\text{Si}_{10}$ )
26. Table for Magnetostriction at Liquid Nitrogen Temperature ( $\text{Fe}_{80}\text{B}_{10}\text{Si}_{10}$ )
27. Table for Temperature Dependence ( $\text{Fe}_{80}\text{B}_{10}\text{Si}_{10}$ )
28. Table for Thermal Expansion Measurement ( $\text{Fe}_{80}\text{B}_{10}\text{Si}_{10}$ )



**CHAPTER - 1**



## 1.1 Introduction

Amorphous alloys, some times called metallic glasses or glassy metals, have received much attention in the last two decade due to their interesting properties and their applicability in new devices. The notion was thoroughly vindicated by 1960, the year when Duewaz<sup>[1.1]</sup> demonstrated that, by using the new technique of splat cooling, it was possible to prepare certain alloys in an amorphous state. In precisely this way the current interest in metallic glass was born. The subject is of interest to physicists, materials scientists, and electrical or electronic engineers. To physicists the attraction lies in seeing how the absence of crystal structure modifies collective magnetic phenomena, which are mainly governed by short range interactions. Materials scientists are interested in the spectrum of new materials produced by this method capable of yielding microscopically homogeneous alloys of compositions unattainable in crystals, and the new possibilities of tailoring the magnetic properties as desired. Electronic and electrical engineers will be drawn by the possible uses they can make of metallic glasses in electronic or power applications.

It was believed for many years that because of the lack of atomic ordering ferromagnetism could not exist in amorphous solids. However, in 1960 Gobanov<sup>[1.2]</sup> predicted the possible existence of ferromagnetic ordering in non crystalline solids on the basis of theoretical analysis. The first report of an amorphous metallic alloy appears to have been made by Brenner<sup>[1.3]</sup>. The present interest in amorphous metals research stems from reports by Duewaz<sup>[1.4]</sup> on the preparation technique of amorphous metallic alloys. Miroshnichenko and Salli<sup>[1.5]</sup> almost simultaneously reported a device for preparing amorphous materials spreading alloy samples in liquid stage between two mutually approaching

pistons. The theoretically expected ferromagnetic behavior in amorphous solids was first demonstrated by Mader and Nowick<sup>[1.6]</sup> in their works on vacuum deposited Co-Au alloys.

Amorphous states for pure metals like Fe, Co, Ni etc are obtained only at extremely low temperature, whereas this disorder in the amorphous state is more complex than that in the crystalline alloy. The disorder can be classified into two types – one is structural disorder which is lack of periodicity in the atomic arrangements and the other is chemical disorder in which the chemical composition losses its periodicity. The macroscopic quantities which are the average of properties in the atomic scale are more perturbed by structural disorders that interfere with each other. The effects of each kind on physical properties are difficult to isolate. There is no theory developed to explain the thermal irreversible behavior of magnetization in amorphous magnetic alloys. In the present work attempts are made to describe the unusual character of the thermodynamic parameters in amorphous ribbons using a theoretical model developed by B.T. Cong<sup>[1.7]</sup> for disordered localized Ising spin lattice. Recently soft magnetic amorphous alloys have been developed and they are used for the magnetic cores of switched-mode power supplies, magnetic recording heads and other devices by T. Miyakazki et. al.<sup>[1.8]</sup> and O-Komoto et. at.<sup>[1.9]</sup>. Most of the amorphous material useful for these applications are manufactured from Co-based amorphous ribbons as reported by H. Fujimori et. al.<sup>[1.10]</sup> with nearly zero magnetostriction. On the other hand Fe-based amorphous ribbons is reported by H. Warliment et. al.<sup>[1.11]</sup> M. A. Asgar and S.S. Sikder et. al.<sup>[1.12]</sup> are excellent in the higher saturation flux density, but they are inferior in the soft magnetic properties in comparison with Co-based amorphous ribbons.



In the past few years there have been a large contribution to both theoretical and experimental results on amorphous magnetic alloys. Many series of alloys have now been reported which are composed of transition metal alloys with a wide variety of metalloids. Zero magnetostrictive alloys have been reported in Fe-Co system. The study of the effect of the electron donar characteristics of the metalloids on magnetization and Curie temperature have led to the development of high moment and high Curie temperature alloys. The studies of the mechanisms responsible for the low temperature embrittlement and magnetic anneal instability have led to the prediction and preparation of alloys of appropriate compositions possessing greatly improved stability.

The Literature on magnetostriction of amorphous alloys is not very extensive. Simpson et. al.<sup>[1.13]</sup> prepared  $\text{Co}_{91}\text{P}_9$  by electrodes deposition and reported a value of linear magnetostriction of  $4.3 \times 10^{-6}$  for the as deposited alloy. This value of magnetostriction increased on annealing without destroying the amorphous nature of the material. The single phase crystalline alloy developed by further annealing had a value of  $\lambda$  of  $11 \times 10^{-6}$  Sherwood<sup>[1.14]</sup> reported on the magnetostriction within the ternary region of the transition metals for roller quenched amorphous ribbon with composition  $(\text{Fe-Ni-Co})_{75} \text{P}_{16}\text{B}_6\text{Al}_3$ . A zero magnetostrictive composition occurred at  $(\text{Fe}_{0.04}\text{Co}_{0.96})_{75} \text{P}_{16}\text{B}_6\text{Al}_3$ . This has approximately  $\lambda = 0$  in crystalline alloys i.e.  $\text{Fe}_8\text{Co}_{92}$ . Magnetostriction was also studied by Arai<sup>[1.15]</sup> in three series of amorphous alloys  $\text{Fe}_{80-x}\text{Ni}_x\text{P}_{13}\text{C}_7$  ( $0 \leq x \leq 40$ ),  $(\text{Fe}_{1-x}\text{Co}_x)_{80} \text{P}_{13}\text{C}_7$  ( $0 \leq x \leq 0.7$ ) and  $(\text{Fe}_{1-x}\text{Co}_x)_{75} \text{Si}_{15}\text{B}_{70}$  ( $0.75 \leq x < 1$ ). In these ribbons the values of  $\lambda_s$  were found to be not quite isotropic. The values of  $\lambda_s$  decreased nearly monotonically with increase in Ni from  $31 \times 10^{-6}$  for  $\text{Fe}_{80}\text{B}_{19}\text{C}_7$  to  $15 \times 10^{-6}$  for  $\text{Fe}_{40}\text{Ni}_{40}\text{P}_{13}\text{C}_7$ . In Fe-Co system the magnetostriction

went through zero near 96 at % Co. The magnetostrictions of the complete series of  $(\text{Fe-Ni})_{80}\text{B}_{20}$  and  $(\text{Fe-Co})_{80}\text{B}_{20}$  amorphous alloys were also reported by O. Handley<sup>[1.16]</sup>. However the effect annealing on magnetostriction of amorphous Fe-B system were also reported by M. A. Asgar and S. S. Sikder<sup>[1.17]</sup>.

The use of amorphous magnetic ribbons in devices is attractive for many reasons were also repeated by A. Hernando et. al.<sup>[1.18]</sup> and H. K. Lachowicz et. al.<sup>[1.19]</sup>. Among the applications are several that make use of the particularly strong magnetostrictive and magnetoelastic properties of suitable ribbons, together with their very good soft magnetic properties. In order to understand how the material will behave in such devices it is useful to have simplified models of the material that allow the calculation of the magnetostrictive response and elastic modulus as functions of the applied field. The magnetoelastic behaviors can be deduced from the magnetostriction and the domain structure as reported by S. Chika Zumi<sup>[1.20]</sup>. When annealing temperature was increased, the observed magnetostriction values for a particular field and also the saturation magnetostriction corresponding to the highest field needed, decreased. The results are explained in terms of strain induced anisotropy as pointed out by Predeeki et. al.<sup>[1.21]</sup> Cohen<sup>[1.22]</sup>, Hara<sup>[1.23]</sup>, Luborsky et. al.<sup>[1.24]</sup> and Egami et. al.<sup>[1.25]</sup>.

A study of the high field magnetostriction on single crystal of  $\text{Nd}_2\text{Fe}_{14}\text{B}$  has been previously reported by P. A. Algarabel et. al.<sup>[1.26]</sup> and their some linear combinations of magnetostrictive irreducible symmetry strains could be singled out, representing strictions of crystal field (CEF). Also a preliminary study of the magnetostriction in some polycrystalline compounds can be found in M. R. Ibarra et. al.<sup>[1.27]</sup>. In relation to the observation of a spontaneous volume magnetostriction i.e. the magnetic contribution to the thermal expansion below

the Curie temperature, there exists a study made by Buschon and Grössinger<sup>[1.28]</sup> on polycrystalline samples and also one on a single crystal of  $Y_2Fe_{14}B$  are reported by D. Givord et. al.<sup>[1.29]</sup>, where clear difference in the anomalous thermal expansions was observed along the a and c symmetry axes. The strain dependences

$$\sum_i \left( \frac{1}{c_i} \right) \left( \frac{\delta n_{FeFe}}{\delta \ln a_i} \right) \equiv \frac{\omega(0)}{M_{Fe}^2(0)} \text{ (with } M_{Fe}(0) = 29.9 \mu_B / f.u.)$$

where  $a_i$  are the tetragonal lattice constants,  $C_i$  the effective elastic constants and  $n_{FeFe}$  the mean field exchange constant within the Fe sublattice. Also included are the curie temperature,  $T_c$  as obtained from the invar peak anomaly in the thermal expansion co-efficient. The Grüneisen constant  $k_0$  (in  $k^{-4}$ ) used in filling of linear thermal expansion  $\left(\frac{\Delta l}{l}\right)$ .

Increased attention is being given to the production of wide ribbons and the preparation of amorphous ribbons for particular applications and for understanding the origin of the extrinsic properties. Although the primary effect like exchange interaction is important in understanding the co-operative magnetism like Ferri, Ferro and antiferromagnetic materials, the real characteristics of technical magnetic materials can be controlled by secondary effects like the magnetic anisotropy, magnetostriction, domain structure etc. The secondary effects are dependent on spin orbit interaction and as such on the atomic arrangement, crystal structure, elastic deformation, size effect etc. The magnetic softness and hardness can be controlled affectedly by changing the magnetic anisotropy and magnetostriction which arises from the crystal anisotropy and magnetoelastic interaction. In order to obtain magnetically soft materials one has to reduce magnetic anisotropy and magnetostriction as happens

in Fe-Si alloys used as transformer material. Amorphous ribbons which become a potential soft magnetic materials for high frequency uses, therefore needs to be studied in respect of the secondary effects of which magnetostriction is one of the most important parameters.

The present research involves magnetostriction and thermal expansion of amorphous ribbons of the series  $\text{Fe}_{90-x}\text{Si}_x\text{B}_{10}$  [ $x = 10$ , and 8] and  $\text{Co}_{80-x}\text{Fe}_x\text{B}_{10}\text{Si}_{10}$  [ $x = 0, 2, 4$  and 6] to see the effect of composition on these important parameters.

## 1.2 Application of Amorphous Ribbon

The class of amorphous TM-M alloys with TM = Fe, Co or Ni and M = B, P, C, Al or Si have received much attention for their magnetic properties favorable for various technical devices such as power generators, transformer, magnetic head, and magnetic shield etc. The suitability of amorphous ribbons as magnetic materials are determined both by its static and dynamic properties. For suitable application of amorphous ribbons besides the magnetic properties the temperature coefficient of thermal expansion, the stability of the ribbons as metallic glass and cost of materials need to be considered. The properties available in the amorphous ribbons cover a wide range by changing alloy composition and heat treatment, as has been discussed. The properties are easily varied by changing the induced anisotropy. The wide range of dc and ac properties provide characteristics suitable for different types of applications. Generally amorphous ribbons are characterized by a high electrical resistivity, high mechanical strength, good corrosion resistance, the absence of crystalline

anisotropy, structural defects and grain boundaries due to the noncrystalline state. The magnetic properties such as saturation flux density, Curie temperature, magnetostriction and induced anisotropy can be controlled by the alloy composition and a subsequent thermal treatment. The Fe-based amorphous ribbon exhibit the highest saturation flux density and the Co-based amorphous ribbons are characterized by low magnetostriction, very high permeabilities and low magnetic losses.

Amorphous ribbons with high  $B_r/B_s$  are practically suited to devices such as switch cores, high gain magnetic amplifiers and frequency inverters and transformers where hystereses and eddy current losses need to be minimized. The high electrical resistivity and the small thickness of the melt-quenched ribbons lead to low eddy current losses. The low hysteresis losses, results and very low core losses are needed for power electronics at high frequencies. For application in small electronic devices, the amorphous ribbons have somewhat poorer respect of losses and permeabilities than the conventional Fe-Ni-B ribbon, but are a better than the Fe-Co-B-Si and Fe-B-Si ribbons in these respect. The design optimization requires the lower cost of the amorphous ribbons, their higher induction compared to the Fe-Ni-B ribbons or their lower losses compared to the Fe-Co-B-Si, Fe-Si-B and the Fe-Ni-B at higher frequencies. Co-based amorphous ribbons are also suitable soft magnetic materials for magnetic shielding due to their high permeability. Amorphous ribbons have many refined applications like development of magnetic bubbles for computer memory, amorphous supper conductors etc.

Research for the understanding and development of amorphous ribbon can thus be very useful.

### 1.3 Organization of the Work

The present work is aimed at the experimental determination of magnetostriction and heat treatment on amorphous iron cobalt ribbon is presented. The samples collected were as prepared.

The problems associated with strain gauge technique as applied to thin magnetic ribbons are discussed, magnetostriction measurements as a function of applied field are evaluated for its dependence on temperature to see the effect of heat treatment on the domain structure affecting magnetostriction.

The differential thermal analysis of the thin ribbon was taken to find the anomalies in the temperature versus time curve at the Curie temperature, glass transition temperature and crystalization phase transformation.

There are two phases in our work. These are as follows:

- (a) Development and calibration of equipment which include.
  - (i) Setting and calibration of an electromagnet.
  - (ii) Construction of DC Bridge.
  - (iii) Construction of specimen holder.
  - (iv) Construction of a Rotator for the measurements of angular position of specimen.
  - (v) Calibration of vibrating sample magnetometer.
  
- (b) The use of strain gauge technique for the measurement of magnetostriction of amorphous iron-cobalt ribbons.
  - (i) Measurements as function of field at room temperature.
  - (ii) Measurements as a function of temperature.
  - (iii) Thermal expansion of different samples.



**CHAPTER - 2**

## **2.1    An overview of Amorphous Metallic Ribbons**

Amorphous metallic ribbons, some times called metallic glasses or glassy metal. These metallic glasses are characterized by a structural disorder where each atom constitutes a structural unit. The magnetic properties of amorphous ribbon are strongly affected by the bond and chemical disorder causing a distribution in the magnetic moments and exchange interaction. Thus amorphous ribbon in which nearest neighbor central forces dominate from structures similar to the random packing of hard spheres. The principal order present is imposed by the roughly constant separation of nearest neighbors. Other types of order may be directional ordering due to magnetic or stress annealing. The first report of an amorphous metallic alloy appears to have been made by Brenner et al<sup>[2.1]</sup>. In this work they electro-deposited nickel-phosphorus alloys, observing only one broad diffuses peak in the X-ray scattering pattern in the non-magnetic high phosphorus alloys. The present- great interest in amorphous metallic glass in 1960 by Dewez et. al. <sup>[2.2]</sup> in the same year Gobonov<sup>[2.3]</sup> predicted the possible resistance of ferromagnetic ordering in non crystalline solids on the basis of theoretical analysis. The interest in amorphous materials is increasing steadily for technological application and scientific understanding. A real technological interest developed after Pond and Maddin in 1969<sup>[2.4]</sup> reported on the preparation of continuous ribbons of amorphous alloys. The theoretically expected retention of ferromagnetic behavior in amorphous solids was first demonstrated by Moder and Nowick in 1965<sup>[2.5]</sup> in their works on vacuum deposited Co-Au alloys and soon there after by Tsuei and Duwez in 1966<sup>[2.6]</sup> in their works on split-cooled Pd-20 at % Si containing some ferromagnetic element partially substituted for the Pd.



Amorphous states of pure metals like Fe, Co, Ni etc can be obtained only at a very low temperature. Alloys of these metals with glass forming materials can be obtained in the amorphous state by cooling the melt at a relatively lower rate of million degrees per second which can remain in the metastable state over an extended range of temperature. Two important classes of amorphous magnetic materials are being studied intensively in recent time. They are the transition metal metalloid (TM-M) glass and the rare-earth transition metal glass (RE-TM) reported by T. Mizozuchi<sup>[2.7]</sup>, R. Alben et. al.<sup>[2.8]</sup>, E. M. Gyorgy<sup>[2.9]</sup> and G. S. Cargill<sup>[2.10]</sup>. TM-M glasses are stable for composition around 75-80% of TM (Fe, Co, Ni etc or in their combinations) and 25-20% of the metalloid (P, C, Si, B or in their combinations).

Typical composition for RE-TM glass is RE<sub>33</sub> – TM<sub>67</sub> where RE is one of the heavier rare-earth metals like Gd, Tb, Dy, Y etc and TM is one of the 3d transition metals like Fe, Co or Ni. Recently the metalloids in TM-M glass are replaced by non-magnetic metals like Zr, Hf etc by T. Masumoto et al<sup>[2.11]</sup>. The new amorphous and metastable alloys prepared by such techniques were used in the early works to explore the many possibilities opened up by these new rapid quenching technique.

## **2.2 The Structure of an Amorphous Alloy**

The structure of amorphous alloys have been given by Cargill<sup>[2.12]</sup> and also a detail discussion is given by Asgar<sup>[2.13]</sup> and S. S. Sikder<sup>[2.14]</sup>. An amorphous material has no long range order and the correlation that exist must be of short

range order in the sense that certain values of the interatomic distance  $\gamma$  are more common than others. There is a continuous transition from amorphous via nearly crystalline, involving nanocrystals to the microcrystalline structure depending on composition preparation process and the conditions for local atomic ordering. The stability increases with the number of components in an amorphous ribbon. The disorder can be classified into two types following Alben et. al. (1977)<sup>[2.15]</sup>.

- (1) Structural disorder – lack of periodicity in atomic arrangement and
- (2) Chemical disorder – lack of periodicity in chemical environment.

The chemical species and relative positions of the nearest neighbors of an atom are thus randomly altered in a chemically disordered solid. The amorphous structure can be studied by means of X-ray, electron and neutron diffraction as well as by extended X-ray absorption fine structure (EXAFS) measurements by Cargill III in 1975b<sup>[2.16]</sup>. The amorphous structures do not show any sharp diffraction peaks due to the absence of long range periodicity.

The structural arrangement of the atoms in amorphous solids can be given in terms of a radial distribution function. For identical atoms this describes the average number of atoms at distance between  $r + dr$  from some chosen atom as origin. This is averaged by taking each atom in turn as the origin. The average number of atoms between spheres of radii  $r$  and  $r + dr$  is then given by  $4\pi r^2\rho(r) dr$ , where  $\rho(r)$  is the atomic density.

The average distribution of atoms can be described by the radial – distribution function (RDF) is sometimes presented in slightly different from

$$F(r) = 4\pi r^2 \rho(r) \quad (2.1)$$

The number of atoms

$$N = 4\pi \int_{r_1}^{r_2} \rho(r) r^2 dr \quad (2.2)$$

between  $r_1$  and  $r_2$ . It is convenient to use the reduced radial distribution function,

$$\text{as } G(r) = 4\pi r [\rho(r) - \rho_0] \quad (2.3)$$

$\rho_0$  denotes the average atomic density. If we consider the density  $\rho_0$  is constant then

$$F(r) = 4\pi \rho_0 r^2 \quad (2.4)$$

Since the density is constant so  $F(r)$  follows the parabolic distribution

$$W(r) = \frac{F(r)}{4\pi r^2 \rho_0} = \frac{4\pi r^2 \rho(r)}{4\pi r^2 \rho_0} = \frac{\rho(r)}{\rho_0} \quad (2.5)$$

when  $\rho(r) = \text{constant}$ , then  $W(r) = 1$ . Theoretical curve of the radial distribution function as a function  $r$  is shown in figure 2.1.

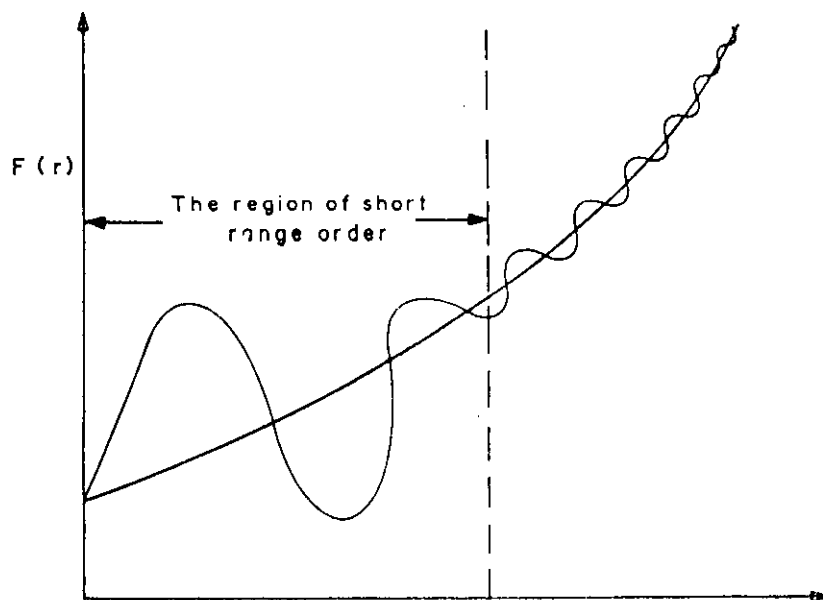
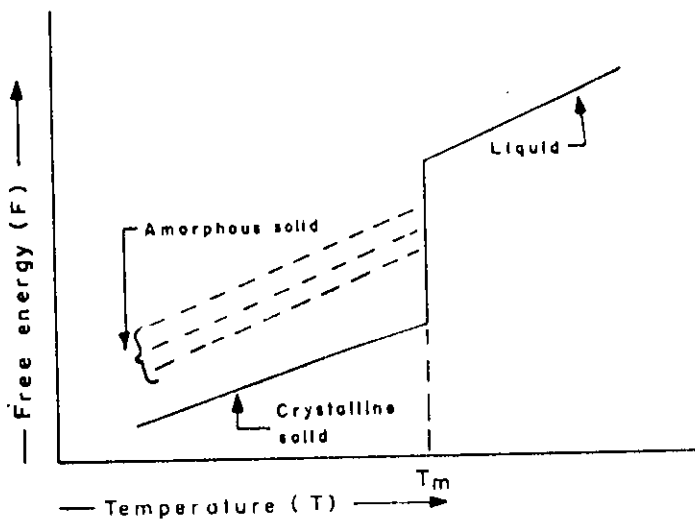


Fig. 2.1: Short range order as a function of radial distance

The structure of an amorphous solid can be discussed on many levels. For example, in terms of the external size and shape of the solid, in terms of cracks, voids, inclusions, composition gradients and other heterogenetics resolvable by optical microscopy or other technique.

Amorphous solid can be considered as a super cooled liquid. A metallic glass is distinct from a liquid or a solid, because of its deviation from thermodynamic equilibrium while both a melt and its corresponding crystalline phase have minimum free energy, an amorphous materials because of its non equilibrium state is at a higher values of free energy. Free energy as a function of temperature for a crystalline solid an amorphous solid and a liquid is shown in figure 2.2.



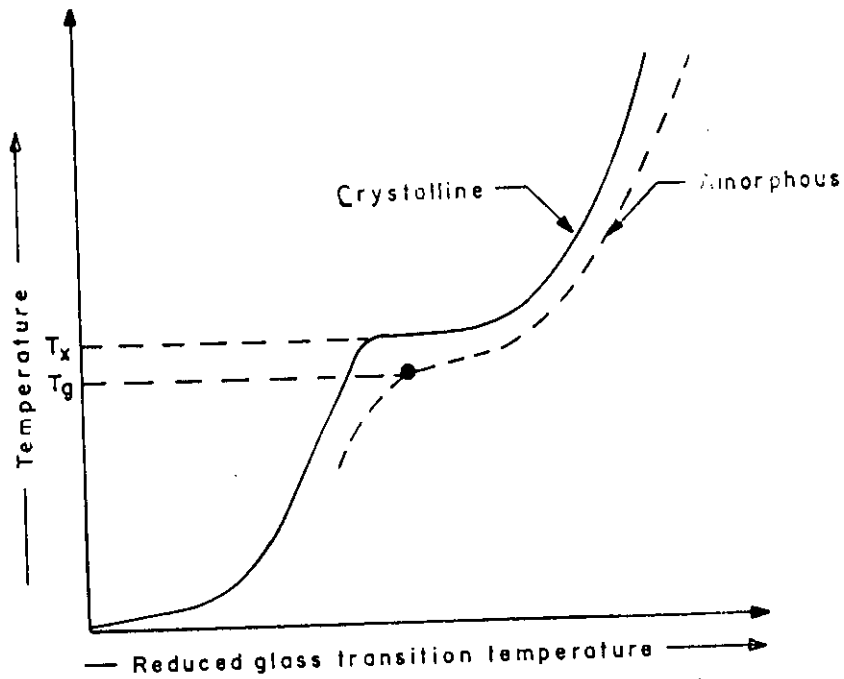
**Fig. 2.2: Free energy versus temperature curve.**

Figure 2.3 shows the reduced glass transition temperature  $\tau = T_g/T_m$  for amorphous solids compared to crystalline solids. It is to be noted that for higher values of  $\tau$  only glass formation is possible.

When a melt is cooled too rapidly, its viscosity and relaxation time increase to the point where the internal equilibrium can no longer be maintained and the equilibrium configuration become inaccessible.

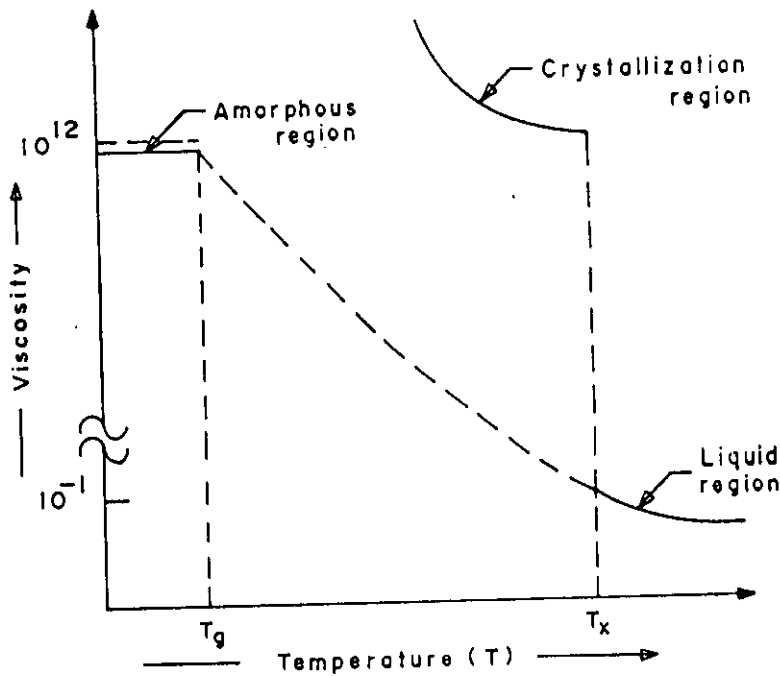
**Two ways of solidification**

- (1) Crystallization process and
- (2) By increasing Viscosity



**Fig. 2.3: Glass formation as a function of reduced glass transition temperature.**

Mechanical hardness of the condensed matter is dependent on the viscosity such that although amorphous materials structurally resemble a liquid state, their viscosity become comparable to that of a solid and this determines the stability of amorphous materials. Figure 2.4 represents the variation of viscosity of amorphous materials with temperature.

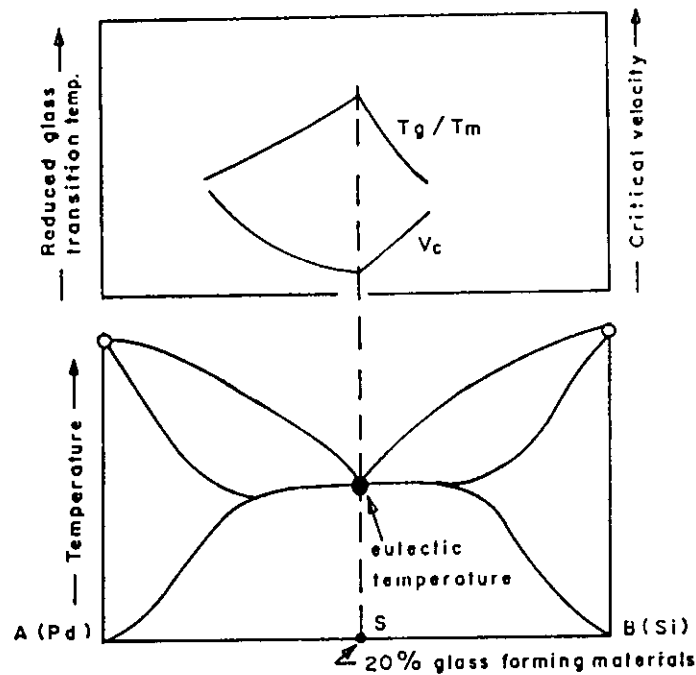


**Fig. 2.4: Viscosity versus temperature curve.**

### **2.3 Conditions for forming amorphous Material**

It is very difficult to get pure metals in the amorphous state. It is necessary to add glass forming materials to pure metals or alloys to get the amorphous state and to bring the cooling rate within a reasonable rate. Usually around 20% of glass forming materials like B, Si, P, C etc which have atomic radii relatively small compare to these of metallic atoms and the glass forming atoms occupy the voids left between the bigger atoms of metals when they are closely packed. It can be showed that when there is random close packing of hard spheres there is about 20% voids created between these atoms. The glass forming materials which have smaller atoms occupy these voids which explain the importance of the glass forming material in the preparation of an amorphous ribbons. The glass forming material also reduces the melting point of the alloys and there by the separation

between the glass forming temperature and the crystallization temperature is reduced. In fact  $T_g/T_m$  which is called the reduced glass transition temperature is an important parameter determining the glass forming tendency of an alloy.

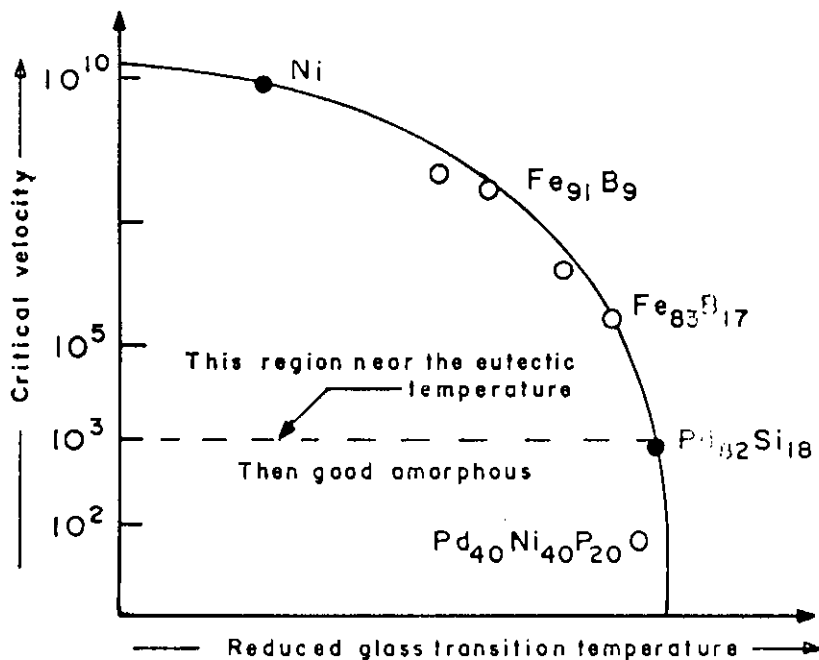


**Fig. 2.5: Compositional dependence of melting point.**

The more complex an alloy is greater is the possibility of forming the amorphous state. This is because the arrangement of the atoms in the crystalline form of complex system takes more time which means a greater relaxation time. The presence of glass forming materials contributes to this complexity and there by increases the relaxation time. The stability of a metallic glass is also increased due to the presence of the glass forming material. Since a metallic glass is in a metastable state the stability with respect to temperature is determine by the local potential barrier produced by the disordered state of the amorphous material. When  $T_g/T_m$  is large the cooling rate needed for glass formation may be reduced, this mean that critical velocity of the Copper disk can be reduced. The

dependence of reduced glass transition temperature and the phase diagram indicating the dependence of melting point on composition of the melt is shown in figure 2.5.

To increase the stability it is necessary to introduce some atoms of B, Si, or P (i.e. atoms with smaller radius) in the matrix. From statistics we know that the amorphous material has a porosity of 20% on the average therefore  $TM_{80}M_{20}$  ( $M = B, P, Si, C$  etc = 20% at atomic) is generally introduced to form a good amorphous material. From figure 2.6 it is observed that the minimum linear velocity of the drum is around 10m/min for preparation of an amorphous ribbon by melt spinning technique.



**Fig. 2.6: Experimental values of critical velocity versus reduced glass transition temperature.**



## **2.4 Conditions necessary for Preparing Amorphous Materials**

In terms of viscosity and diffusion co-efficient we can find the condition for formation of glass.

- (i) For metals atomic bonding is metallic and the viscosity is lower than diffusion co-efficient and mobility is high.
- (ii) In the case of amorphous materials viscosity is very high and the mobility and the diffusion co-efficient is low. Atomic bonds tend to be covalent as in the case of Silicate ( $\text{SiO}_2$ ).

## **2.5 Preparation Technique of Amorphous Ribbons**

There are various techniques in use to produce a metallic alloy in arrangements have no long range periodicity. The different experimental techniques developed to produce amorphous metallic glass can be classified into two groups

- (i) The atomic deposition methods, and
- (ii) The fast cooling of the melt.

### **2.5.1 The atomic deposition methods**

Deposition can be described in terms of whether the added atom is prevented from diffusing more than an atomic distance before it is fixed in position due to cooling and increased viscosity. The atomic deposition methods include condensation of a vapor on a cooled substrate by

- (a) Vacuum deposition
- (b) Sputter deposition
- (c) Electro deposition and
- (d) Chemical deposition

### **2.5.2 The fast cooling of the melt.**

For producing an amorphous state by any of the liquid quenching devices the alloy must be cooled through the temperature range from the melting temperature ( $T_m$ ) to the glass transition temperature ( $T_g$ ) very fast allowing no time for crystallization. The factors controlling  $T_g$  and crystallization are both structural and kinetic. The structural factors are concerned with atomic arrangement, bonding and atomic size effects. The kinetic factors as discussed by Turnbull<sup>[2.17]</sup> are the nucleation, crystal growth rate and diffusion rate compared to the cooling rate. The interest in this method stems from the wide variety of alloys that can be made as well as from the potential low cost of preparation. In the pioneering work of Duwe et. al.<sup>[2.18]</sup> a number of devices have been reported for obtaining the necessary high quenching rates and for producing continuous filaments. The methods using the principle of fast cooling of melt techniques are

- (i) The gun technique
- (ii) Single roller rapid quenching techniques
- (iii) Double roller rapid quenching techniques
- (iv) Centrifuge and rotary splat quencher techniques
- (v) Torsion catapult techniques
- (vi) Plasmat jet spray techniques
- (vii) Filamentary casting techniques
- (viii) Melt extraction techniques
- (ix) Free jet spinning techniques
- (x) The melt spinning techniques

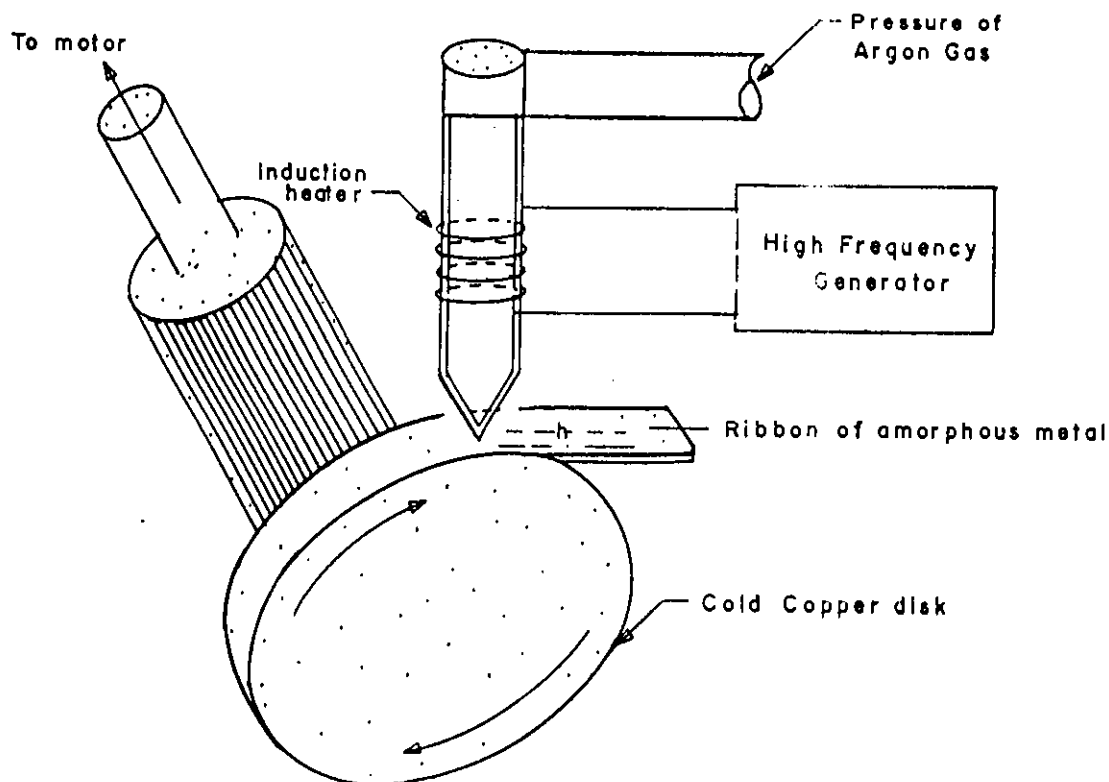
Although the different methods used in preparing amorphous metallic ribbons are mentioned here, only the single roller rapid quenching technique which was used to prepare the specimens for the present work will be discussed.

### **2.5.3 Rapid quenching method**

As shown in a schematic diagram in figure 2.7 the rapid quenching technique apparatus consists mainly of a Copper roller, an induction heater and a nozzle. The roller was driven by a variable speed motor via a tooth belt. The angular velocity was 2000 rev./min. Use of log wheel rotation enable us to vary surface velocity in the range 20 to 30 m/s. The diameter of the Copper roller was 10 cm. The use of Copper for the roller material was chosen for its good conductivity and mechanical softness, which allowed cleaning and polishing to be carried out easily. For room temperature work, it showed no contamination of the ribbon from the roller material and the careful preparation of the surface was more important than the material of the roller.

In this process one has to consider that vibration of the roller should be well below the high frequency vibration of the melt puddle to avoid any influence of it on the geometry and uniformity of the ribbon. One has to be careful and see that the ribbon does not remain in contact with the surface of the roller for a whole revolution and be hit, from the back. A bigger diameter is thus preferred for the roller. The induction heater coil is made of hollow copper tubing which is cooled simultaneously by circulating water through its inner hole. The shape and diameter of the induction heater as also its winding is to be adjusted to produce proper temperature gradient. This is to avoid, sudden cooling of the melt in its way out of the crucible and blocking the nozzle. The quartz tubing having outer

diameter 20mm which is narrowed down conically to 1mm with a hole for the nozzle 0.1 to 0.2 mm.



**Fig. 2.7:** Thin layer of molten alloy intimate contact with the outer surface of metallic rotor is quenched in to amorphous.

The nozzle geometry is selected to minimize the contraction in the cross-sectional area of the molten jet as it leaves the nozzle orifice. Quartz tube is suitable for repeated use in several successful runs and should be transparent to

make the melting process visible. It should withstand the sudden fast changes in temperature.

## **2.6    *Experimental Details of the Preparation of Amorphous Ribbon***

The amorphous ribbons are prepared in a furnace in an argon atmosphere (0.2 to 0.3 atoms). The buttons prepared are about 50 grams each. Care is taken to ensure through mixing and homogeneity of the alloy composition by turning over and remelting each button few times. The mother alloys which are formed in the form of buttons in a furnace by sudden cooling and is then cut into small pieces and is introduced in the quartz tube. The quartz tube is connected from the top by the rubber 'O' rings and metal rings to the argon cylinder through a valve and a pressure gauge.

After proper cleaning of the roller surface and adjusting its speed to the desired value, as measured by stroboscope, the induction furnace is powered using high frequency generator. When the melting temperature is reached as observed through a protective spectacle, the injection pressure is applied by opening the pressure valve. To avoid the turbulence of the wind, arising from the high speed of the roller in disturbing the melt puddle, cotton pad and metallic shield are usually used just beneath the roller. To avoid oxidation of the ribbon during its formation an inert atmosphere can be created around the roller by a slow stream of helium gas.

The speed of the roller, the volumetric flow rate, the orifice diameter, the substrate orifice distance, the injection angle etc are adjusted by trial and error to get the best result in respect of the quality and the geometry of the ribbons.

**2.6.1 Important factors to control the thickness of ribbons.**

- (1) Rotating speed
  - (a) Angular velocity  $\omega = 2000$  rev./min and
  - (b) surface velocity  $v = 20$  m/s
- (2) Gap between nozzle and rotating copper drum  $h = 100$  to  $150 \mu\text{m}$
- (3) Oscillation of the rotating copper drum both static and dynamic have maximum displacement  $1.5$  to  $5 \mu\text{m}$ .
- (4) Pressure =  $0.2$  to  $0.3$  argon atmosphere
- (5) Temperature of metals  $T_m \sim 1500^\circ\text{C}$ . The temperature did not exceed  $1800^\circ\text{C}$  other wise quartz these would be melt.
- (6) Stability was ensured for the drop in the surface of drum,

**2.7 Factors contributing to Glass Formation**

There are three interrelated factors that determine glass forming tendency. These are thermodynamic conditions that favor the liquid phase relative to the crystalline phase, the kinetic conditions that inhibit crystallization and the process factors that arise due to experimental conditions.

The thermodynamic factors for glass formation are liquidus temperature  $T_m$  at which the alloy melts, the heat of vaporization and the free energy of all the phase that arise or could potentially arise during solidification process. Viscosity of the melt, the glass transition temperature  $T_g$  and the homogeneous nucleation rate belongs to kinetic parameters. The glass transition temperature is defined as

the temperature at which the super cooled liquid takes on the rigidity of a solid or more specifically at which the viscosity approaches 15 poise.

Processing parameters are the cooling rate, the heterogeneous nucleation rate and the super cooling temperature interval. The temperature of the glass transition is slightly dependent on the cooling rate. At each cooling rate the glass will freeze in a different state of internal energy. This is shown in figure 2.8.

At the melting point  $T_m$ , the enthalpy  $H$  of a crystal includes latent heat of fusion due to long range order. In the case of rapid cooling of the melt the free energy decreases since long range order do not take place, thus leaving the system at a higher energy state. Heat treatment, relaxation and stability are thus important considerations in metallic glass. The glass forming tendency also arises from as size difference between the constituent elements. It appears that appreciable size difference between the components in the glass alloy is a necessary condition for ready glass formation.

A single parameter that expresses glass forming tendency is the ratio of the glass transition temperature to the melting temperature defined as

$$\tau = \frac{T_g}{T_m}$$

Higher values of  $\tau$  obviously favor glass formation. For metallic glass to be formed by rapid cooling,  $\tau$  should be greater than 0.45 by H. S. Chen<sup>[2,19]</sup>. Based on alloy composition there are two major groups that rapidly form glasses. In one of these groups the metal is from Fe, Co, Ni, Pd or Pt and the metalloid is B, C, Si, Ge or P these metallic glasses constitute soft amorphous magnetic materials. Our working sample prepared shown by table 1.

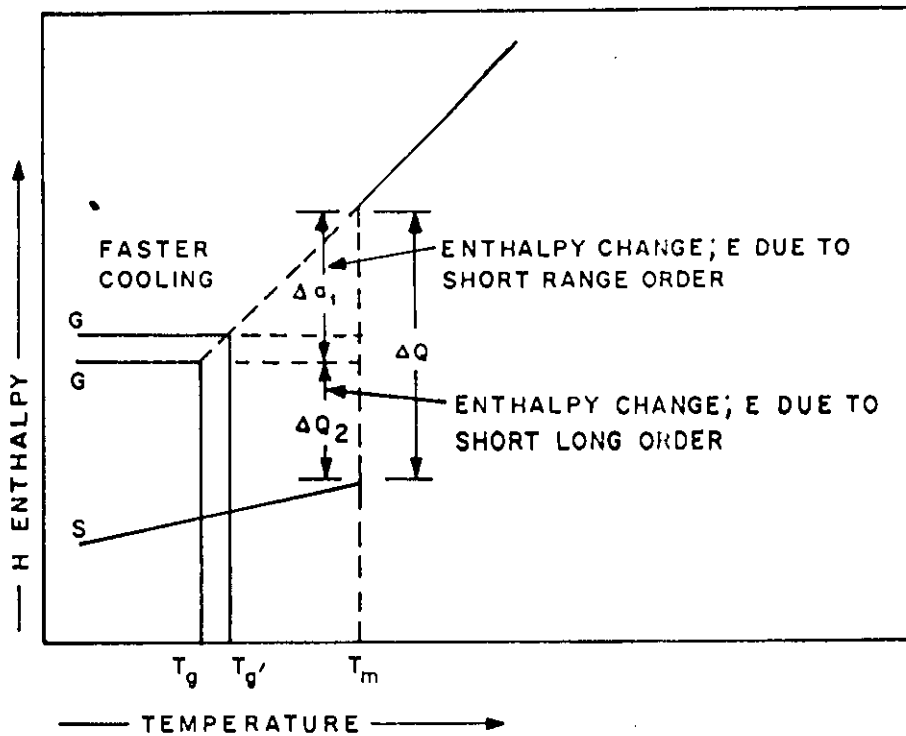


Fig. 2.8: Temperature dependence of enthalpy H. G and G' corresponds to glass and S corresponds to crystalline state.

Tabel – 1

| Fe-based ribbons                                  | Thickness | Co-based ribbons  | Thickness |
|---|-----------|---|-----------|
| Fe <sub>80</sub> Si <sub>10</sub> B <sub>10</sub> | 26μm      | Co <sub>80</sub> B <sub>10</sub> Si <sub>10</sub>                 | 21 μm     |
| Fe <sub>82</sub> Si <sub>8</sub> B <sub>10</sub>  | 34μm      | Co <sub>78</sub> Fe <sub>2</sub> B <sub>10</sub> Si <sub>10</sub> | 28μm      |
|   |           | Co <sub>76</sub> Fe <sub>4</sub> B <sub>10</sub> Si <sub>10</sub> | 26μm      |
|   |           | Co <sub>74</sub> Fe <sub>6</sub> B <sub>10</sub> Si <sub>10</sub> | 26μm      |

### 2.8 Examining the Amorphousity

The amorphousity of all the ribbons have been confirmed by X-ray diffraction using Cu-K<sub>α</sub> radiation. All the ribbons were found to be amorphous as shown in figure 2.9.



The ribbons showed broad diffraction maximum and no low angle scattering. These ribbons were also ductile and those cases for which low angle scattering appear and the broad diffraction peak are subdued there is some presence of micro crystalline phase. These could be removed if the speed of the roller was increased. The thickness of an amorphous is controlled by the linear speed of the roller, the gap between the nozzle and the rotating drum which was about 1.5 to 5 $\mu$ m, oscillation of the drum, both static any dynamic pressure and temperature of the melt and the stability of the drop on the surface of the drum. The nature of the broad diffraction peak as observed is shown in figure for some of the samples.

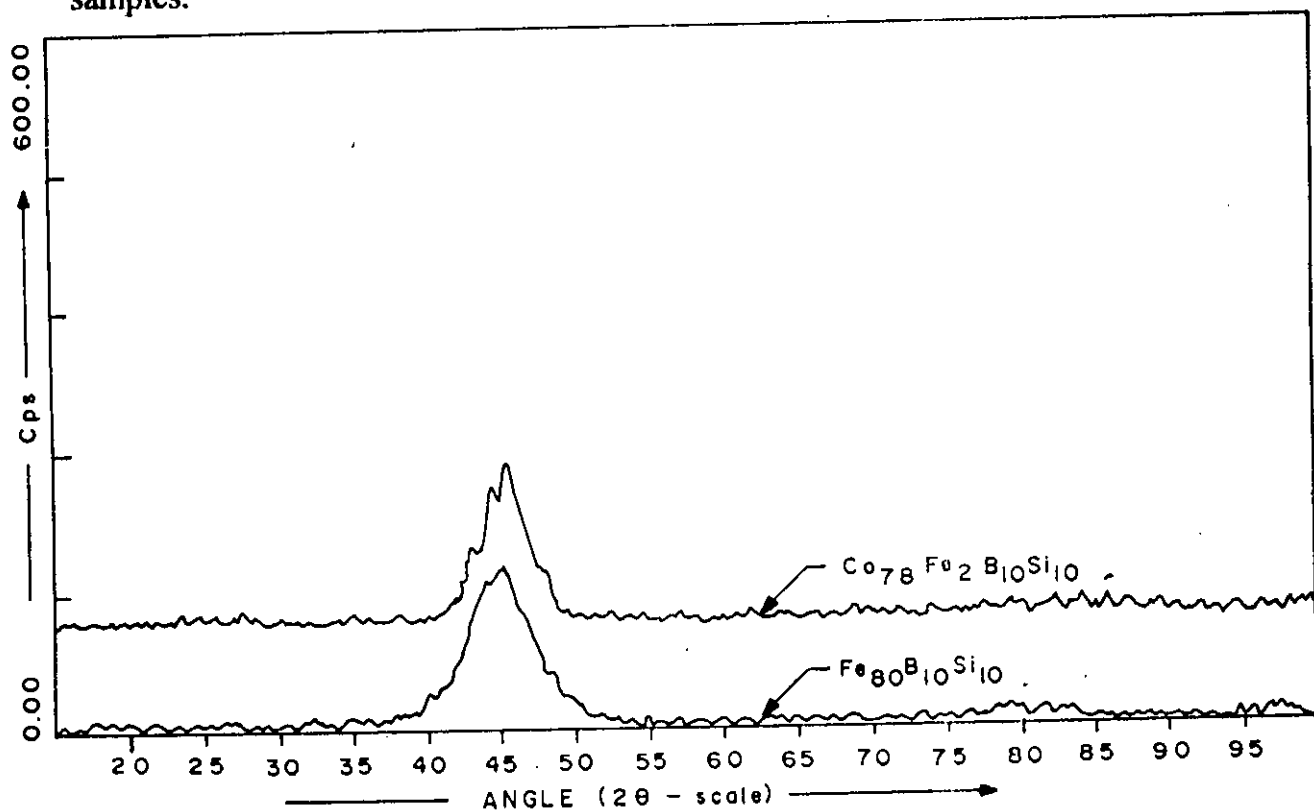


Fig. 2.9: X-ray diffraction from the top surface of some amorphous ribbon.



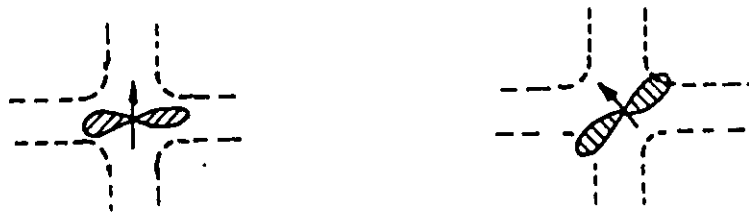
**CHAPTER - 3**

### 3.1. Physical Origin of Magnetostriction

Magnetostriction is usually analysed in terms of a general formalism, where the free energy, as in the classical use, or the Hamiltonian as in the quantum mechanical case, is expressed in polynomial forms, there is little agreement between theoretical prediction and observed results except in a qualitative way. This shows the dominant role of experiments in determining the coefficients representing the magneto-elastic interaction-Although magnetostriction originates in the interaction between the atomic magnetic moments and one would prefer to treat it within the framework of quantum mechanics, it has not been developed at present to the point of quantitative usefulness. Magnetostriction which is commonly defined as any change in dimension of body caused by a change in its magnetic states is a property which can be considered as being among the most important intrinsic materials parameter. The physical origin of magnetostriction is explained by M. A. Asgar<sup>[3.1]</sup> along the following lines.

For non S-state ions the orbital angular momentum has non-zero value of  $L$  with  $(2L+1)$  degeneracy in the lowest energy ground state. The orbital charge distribution for these ions is highly symmetrical. When these paramagnetic ions are surrounded by crystal, the orbital degeneracy is removed and the resultant wave function form new linear combinations, which reflect the local symmetry of the crystal. The rotation of the charge distribution lobes alters the orbital angular momentum, because of spin orbit coupling. The magnetization associated with spin will thus be related.

Spin-orbit coupling also contributes to the anisotropy by way of another mechanism called anisotropic exchange introduced by Van Vleck<sup>[3,2]</sup>. From S-state ions the orbital angular momentum is zero and the charge distribution is some what distorted by the crystal field. The spin-orbit coupling thus contributes to the anisotropy energy and the magnetostriction in this case as well although of much smaller magnitude. Exchange energy can make contributions to magneto-elastic energy due to the strain dependence of the exchange integral  $J_{ij}$ . When the magnetic moments of neighboring ions are rotated.



(a) CRYSTAL FIELD ANISOTROPY



(b) EXCHANGE ANISOTROPY



(c) EXCHANGE STRICTION

Fig. 3.1: Physical Origins of Magnetostriction.

There are three mechanism of anisotropy:

- (i) Crystal field anisotropy
- (ii) Exchange anisotropy and
- (iii) Exchange striation

Which is shown schematically in figure (3.1a, 3.1b and 3.1c) respectively. The picture applies to a localized model and an extension of the one ion model to metallic elements in conjunction with band theory necessitates the consideration of different correlation functions. The temperature and magnetic field dependence of the macroscopic magnetostriction coefficients are then related to these correlation functions. Callen and Callen<sup>[3.3]</sup> have shown that three distinct types of correlation functions enter the theory. These are self-correlation function  $\langle S_i^2 \rangle$ , the isotropic correlation  $\langle S_i \cdot \bar{S}_j \rangle$ , and the longitudinal correlation function  $\langle S_i^z S_j^z \rangle$ .

Using a band model, Berger<sup>[3.4]</sup> has interpreted magnetostriction as resulting from 3d-band degeneracy which is partially lifted by spill-orbit interaction. In polycrystalline FeNi and CoNi alloys. Singularities are observed in extraordinary Hall effect at the electron concentration of 27.7 per atom, in magnetostriction as well as in magnetoresistance, and magnetostriction and extraordinary Hall coefficients showing zero value, and magnetoresistance showing maximum. All the three properties are attributed to spin-orbit interactions.

It is interpreted that magnetostriction and extra-ordinary Hall coefficient are proportional to the spin-orbit energy shift of the d-bands at the fermi-energy and hence change sign as the fermi-level moves through the lifted degeneracy.

Campbell<sup>[3.5]</sup> again using band model, relates magnetostriction to charge in Fermi- wave vectors parallel and perpendicular to the direction of magnetization. Electrons and holes have effects of opposite sign such that magnetostriction becomes zero when the Fermi-surface has compensation from electron and hole characters.

### 3.2 Magnetostriction with Different Compositions

The use of amorphous magnetic ribbons in devices is attractive for many reasons<sup>[3.6-3.7]</sup>. Among the applications are several that make use of the particularly strong magnetostrictive and magneto elastic properties of suitable ribbons, together with their very good soft magnetic properties. The magnetoelastic behavior can be deduced from the magnetostriction and the domain structure<sup>[3.8]</sup> early model of the  $\Delta E$  effect<sup>[3.9, 3.10]</sup> assumed the simplest possible domain structure consisting of transverse stripe domains.

The magnetostrictive effects in amorphous alloys originate from the magnetoelastic interactions associated with the local anisotropies and the local strains controlling the local direction of the magnetic moments. The origin of the local strains have been discussed in terms of the single ion model with random local axis<sup>[3.11-3.23]</sup>. The macroscopic magnetostriction representing the relative

changes in length and volume is related to the macroscopic magneto-elastic constants, which have to be considered as an average over the local elastic contribution. The linear magnetostriction can be expressed by

$$\lambda_s = \frac{3}{2} \lambda_s \left( \cos^2 \theta - \frac{1}{3} \right) \quad 3.1$$

where  $\theta$  is the angle between the magnetization and the strain,  $\lambda_s$  represents the saturation magnetostriction constant.

$$\lambda_s = \frac{3}{2} (\lambda_{||} - \lambda_{\perp}) \quad 3.1a$$

Where  $\lambda_{||}$  and  $\lambda_{\perp}$  refer to the relative changes in length parallel and perpendicular to the direction of magnetization. The spontaneous volume magnetostriction  $\omega_s$  can be written as

$$\omega_s = \lambda_{||} - 2\lambda_{\perp} \quad 3.1b$$

some typical values for amorphous transition metal metalloid alloys are compiled in figure 3.2. Fe-rich alloys exhibit a large positive saturation magnetostriction in contrast to polycrystalline iron. Many Co-rich alloys exhibit a small negative  $\lambda_s$ , in agreement with that of crystalline cobalt, but with increasing Co-content  $\lambda_s$  becomes positive. The different sign of  $\lambda_s$  in these alloys has led to the development of zero-magnetostriction alloys which are of interest for different applications<sup>[3.24-3.25]</sup>. Low magnetostriction can easily be reached using Co-based alloys with some additives<sup>[3.26-3.34]</sup>. The temperature dependence of  $\lambda_s$  can be well described in terms of the single-ion model for uniaxial symmetry predicting the relation<sup>[3.35]</sup>.

$$\lambda_s(T) = \lambda_s(0) \hat{I}_{\frac{3}{2}}(x) \quad 3.2$$

where  $\hat{I}_{\frac{3}{2}}(x)$  is the reduced Bessel function

$$\hat{I}_{\frac{1}{2}}(x) = 1 + \frac{3}{x^2} - \frac{3}{x} \coth x$$

and  $X$  is related to the relative magnetization,  $m_s(T) = M_s(T)/M_s(O)$ , by

$$m_s(T) = \frac{1}{x} + \coth x \quad 3.3$$

The temperature variation of the reduced linear saturation magnetostriction versus reduced saturation magnetization is displayed in figure 3.3 for different amorphous alloys<sup>[3.29-3.36]</sup>. The data follow well the line calculated from equation (3.2), confirming the dominance of single-ion contributions in these alloys. Co and Co Fe based alloys again deviate from the pure single-ion behavior and their temperature dependence suggests the presence of two ion contributions<sup>[3.29,3.37, 3.38]</sup> which are proportional to  $m_s^2(T)$ . Then  $\lambda_s$  can be expressed by

$$\lambda_s(T) = \lambda_1 \hat{I}_{\frac{1}{2}}(x) + \lambda_2 m_s^2(T) \quad 3.4$$

with  $\lambda_1 < 0$ ,  $\lambda_2 > 0$  and  $x$  defined by equation (3.3).

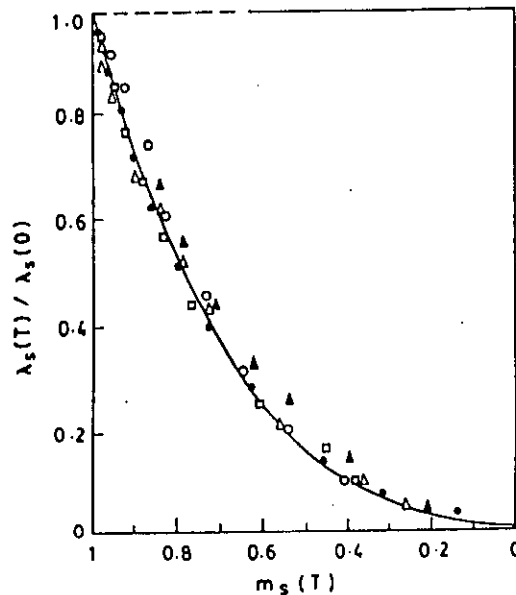


Fig. 3.2: Reduced saturation magnetostriction versus reduced specific saturation magnetization for various amorphous transition metal metalloid alloys<sup>[3.29]</sup>.



The occurrence of a compositional and temperature compensation of  $\lambda_s$  in Co Fe based alloys confirms the presence of these two mechanisms contributing to  $\lambda_s$ .

However, also the competition between two single-ion contributions was discussed to cause  $\lambda_s = 0$  in B-CoMn alloys<sup>[3.39]</sup>. The magnetostriction arising from a disorder caused by randomly oriented easy axes follows a power law  $\lambda_s(T) = \lambda_s(0) m_s(T)^n$  with  $n < 3$ <sup>[3.40]</sup>.

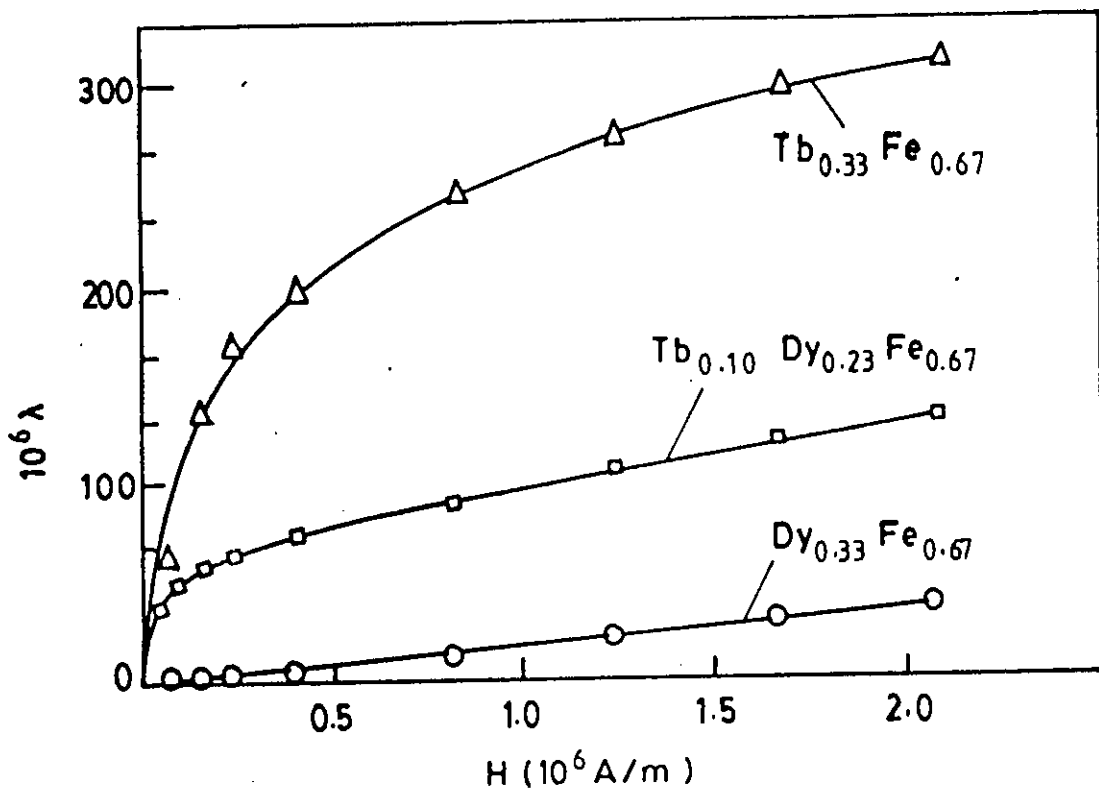


Fig. 3.3: Field dependence of the room temperature magnetostriction of non-S-State rare earth amorphous alloys<sup>[3.41]</sup>.

Magnetic saturation can only be reached at much larger magnetic fields. The field dependence is displayed in figure (3.3) revealing an increase of  $\lambda$  in fields up to  $2 \times 10^6$  A/m<sup>[3.41]</sup>.

### 3.3 Low Temperature Magnetic Moment

#### 3.3.1 Models of moment variation

The average magnetization is based on the exchange coupled magnetic moments which are correlated to the sum of spin up and spin down d-electrons outside the last filled shell. The magnitude of the magnetic moment per atom and its temperature dependence have been discussed in terms of two extreme picture of fully localized electrons (Heisenberg model) and fully it inerrant electrons (Stoner model). The localized model cannot account for the fractional values of the observed moments and leads to a much too low curie temperatures while the it inerrant model gives rise to a curie temperature which is an order of magnitude too high and also the moments in the paramagnetic state are completely destroyed. Thus, various approaches have been made to improve or combine these theories. An essential element of the disordered local moment theories<sup>[3.42-3.62]</sup>, and the local band theories<sup>[3.54-3.62]</sup>, is the introduction of a fluctuating mean field which means that a local mean field is introduced, whose direction may vary in space and time. In the disordered local moment theories, the mean fields are assumed on lattice sites with no correlation among them, while for the local band theories it is assumed that the excitations maintain sufficient short range magnetic order even above  $T_c$ . The real difference between these two view points is not the absolute scale of short range magnetic order, but

in whether or not local ordering plays significant role in the energetic of creating local magnetic strength<sup>[3.62]</sup>.

Although these theories account for various basic features of ferromagnetism of 3d metal, there remain still some unsolved problems. Therefore, a basic theory for amorphous alloys with 3d metals which involves the additional problem of structural disorder is not yet available different models were developed to interpret the trends in magnetic property variation with alloy constant. The first two model discussed focus on the valence per atom or the splitting of bands for alloys but take no account of the particular atomic structures and nearest neighbor environments. The bond model is based on the local symmetry or coordination and the chemical bonding and was applied to explain primarily the magnetic moment variation of transition metal metalloid crystalline and glassy alloy.

### 3.3.2 Band-gap theory

The moment variation with the average number of electrons (slater-pauling curve) was first discussed in the concept of virtual bond sates<sup>[3.63,3.64]</sup>. This model has been extended and reinterpreted<sup>[3.65, 3.66]</sup> and expressed in a more generalized form referred as band-gap theory<sup>[3.67, 3.68]</sup>. The atom-averaged magnetic moment in alloys of composition  $M_{1-x}T_x$  with  $T = \text{Fe, Co or Ni}$  and  $M$  the solute can be expressed in terms of the atom averaged number of spin up and spin down electrons.

$$\bar{\mu}_T = \mu_B (N^\uparrow - N_\downarrow) \quad 3.5$$

The average atomic valence  $Z$  is related to  $N^\uparrow$  and  $N_\downarrow$  by

$$Z = N^\uparrow + N_\downarrow \quad 3.6$$

Combining equation (3.5) and (3.6), one obtains

$$\bar{\mu}_T = \mu_B (2N^\uparrow - Z) \quad 3.7$$

There by, the total number of spin-up electrons consists of d and sp electrons and thus

$$N^\uparrow = N_d^\uparrow + N_{sp}^\uparrow \quad 3.8$$

In the alloy, Z has to be considered as an averaged number of the T and M atoms,

$$\bar{Z} = (1-x)Z_M + xZ_T \quad 3.9$$

and thus  $\bar{\mu}_T$  can be expressed in the form<sup>[3.66]</sup>.

$$\bar{\mu}_T(x) = \mu_B \left[ (1-x)(2N_{dM}^\uparrow - Z_M) + x(2N_{dT}^\uparrow - Z_T) + 2N_{sp}^\uparrow \right] \quad 3.10$$

where  $2N_{dT}^\uparrow = 10$  for Fe and elements to its right and  $2N_{dT}^\uparrow = 0$  for elements to its left.

For  $\mu_T^o = \mu_B (2N_{dT}^\uparrow - Z_T) + 2\mu_B N_{sp}^\uparrow$  and  $2N_{dM}^\uparrow = 0$ , equation (3.10) reduces to the form<sup>[3.69]</sup>.

$$\bar{\mu}_T(x) = \mu_T^o - (1-x)(10 + Z_M - Z_T)\mu_B \quad 3.11$$

This relation predicts a linear reduction of the average transition metal moment with increasing  $\mu$  concentration,  $(1-x)$ , where  $\mu_T^o$  is the T moment in the pure metal. Some typical averaged moment  $\bar{\mu}_T$  per transition metal atom at  $T = 4.2$  K are complicated.

The Fe moment variation for amorphous B-Fe-Ni and B-P-Fe-Ni alloys of  $\bar{\mu}_T$  expressed in the form

$$\bar{\mu}_T = Z_m + \mu_B 2N_{sp}^\uparrow$$

3.12

and expressed versus the average magnetic valence

$$Z_m = (1-x)(2N_{dT}^\uparrow - Z_T) + x(2N_{dM}^\uparrow - Z_M)$$

and  $N_{sp}^\uparrow = 0.3$  (full line) for amorphous B-Co alloys<sup>[3.66]</sup>.

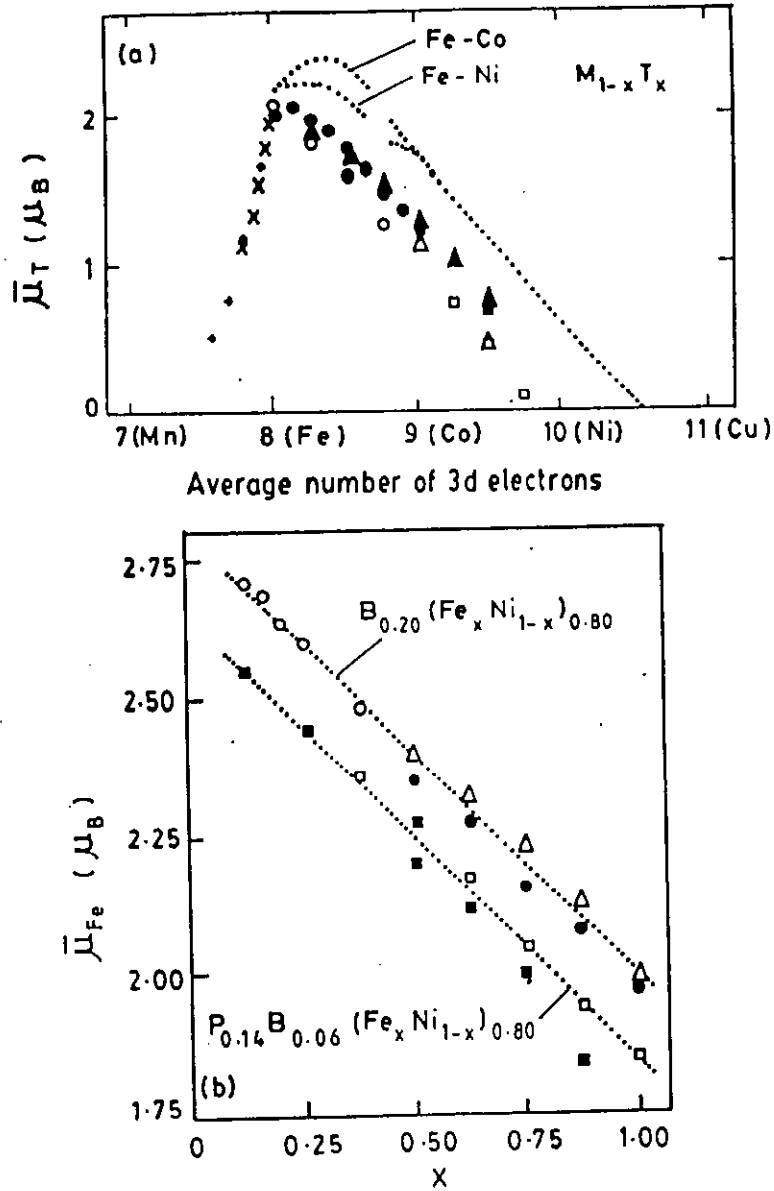


Fig. 3.4: Slater-Pauling plot for amorphous  $M_{1-x}T_x$  alloys.

Random ferromagnetism can be attributed to a broad distribution of Fe-Fe exchange interactions including a significant of antiferromagnetic bonds. Ferromagnetic alloys are magnetic order takes place at much higher concentrations as compared to the corresponding Fe or Co alloys.

### 3.3.3 Split bands.

Valence band of  $M_{1-x}T_x$  alloys split into two resolvable parts at different energies when the difference in atomic number is greater or equal to two<sup>[3.70, 3.71]</sup>. The split band character is a consequence of polar d-d bonding and was experimentally confirmed for various amorphous alloys<sup>[3.72]</sup>. The concept of split bands, originally applied to crystal line alloys, was extended to amorphous alloys. The interpretation of magnetostriction<sup>[3.73, 3.74]</sup> measurements for amorphous  $B_{0.20}(FeCoNi)_{0.80}$  alloys indicate that Fe and Ni indeed contribute to the valence-band density of states at different energies and thus a minimum in the density of states is present. This model was shown to account well for the compositional variation of the magnetostriction and spoon tenuous Hall effect in these alloys.

### 3.3.4 Co-ordination bond model

This model was derived from valence-bond theory to account for the magnetic moment variation of crystalline and glassy transition metal metalloid (M-T) alloys<sup>[3.75, 3.76]</sup>. It assumes that the average T moment is suppressed according to the number of M neighbors and the strength of the M-T bonds. The model is based on a strong p-d bonding, causing a T moment reduction of one fifth of its moment for each 3d electron participating in the nonmagnetic covalent T-M

bond. This leads to an average T moment suppressing for  $M_{1-x}T_x$  alloys of the form

$$\bar{\mu}_T(x) = \mu_T^o \left[ 1 - \left( 1 + \frac{Z_M^T}{5} \right) (1-x) \right] \quad 3.13$$

representing a linear decrease  $\bar{\mu}_T$  with the metalloid concentration  $(1-x)$ ,  $Z_M^T$  is the number of T atoms surrounding an M atoms. This model accounts for the moment variation for various M-T alloys<sup>[3.77-3.79]</sup> the band-gap model appears to be able to explain more general trends in a wider class of alloys. Although these models are contradictory in their basic origin, both lead to a linear decrease of  $\bar{\mu}$  according to the relation

$$\bar{\mu}_T(x) = \mu_T^o [1 - P(1-x)] \quad 3.14$$

where the slope P differs according to the assumptions made in these models

### 3.3.5 Environment model

The third picture to interpret the moment variation is based on the structural disorder and accounts for the different environment of a transition metal<sup>[3.80]</sup>. The probability of a T atom to have  $j$  nearest T neighbors out of a maximum number  $n$  is given by

$$P(x, k, n) = \frac{n!}{K!(n-k)!} \quad 3.15$$

Assuming a minimum number  $j$  of nearest T neighbors to be necessary for a T atom to carry a moment  $\mu_1$  and for less than  $j$ , T neighbors a moment  $\mu_2$ , then

$\bar{\mu}(x)$  can be expressed in the form

$$\bar{\mu}(x) = \mu_1 p_j(x) + \mu_2 [1 - p_j(x)] \quad 3.16$$

$$\text{where } p_j(x) = \sum_{k=j}^n p(x, k, n) \quad 3.17$$

In the case  $\mu_1, \mu_2 \neq 0$ , no critical concentration is expected. For  $\mu_2 = 0$ , a critical concentration can be calculated from the transient of the turning point of  $\bar{\mu}(x)$  at

$$x = x_t \text{ by } x_c = \frac{x_o}{p_j(x_t)}, \text{ where } x_t \text{ is determined by } p_j^{(1)}(x_t) = 0$$

The models so far discussed can account for the moment variation for various alloys, but there are also various counter examples where  $\bar{\mu}(x)$  cannot be explained in terms of one of these models. This is associated with the extreme assumptions that are made in the case of the band-gap model disregarding certain influences of structure and local environment and in the case of the coordination bond or environment model where particular band features are ignored.

### 3.4 Magnetic Excitations

Single particle and collective particle excitations contribute to the excitations contribute to excitation spectrum of magnetic materials. The spin waves or magnons are the excitations of lowest energy and involve a deviation of the moment from the parallel or anti-parallel alignment of the ground state. This requires an exchange energy  $Dk^2$  <sup>[3.81]</sup> where D is the spin wave stiffness constant which is related to the exchange constants and K is the wave, D is a function of temperature and can be expressed by

$$D(2) = D(o) \left[ 1 - a \left( \frac{T}{T_c} \right)^n \right] \quad 3.17$$

where  $n = 5/2$  for an ideal Heisenberg ferro-magnet <sup>[3.82, 3.83]</sup>.



Typical values for  $D(0)$  is expected to scale with  $T_c$ . This indeed was found for many Co-based alloys<sup>[3.84, 3.85]</sup>. For Fe-based alloys the  $D(0)$  also increase with  $T_c$  but the data do not follow straight lines<sup>[3.85]</sup> which is probably associated with the non-linear magnetic structure for Fe-rich alloys and those with compositions near  $x_c$ .  $D(T)$  is correlated to the coefficient  $B$  of the  $T^{3/2}$  term<sup>[3.81]</sup> governing the low temperature variation of the saturation magnetization.  $D(T)$  can be determined from the spin wave excitations using standing spin waves in thin films, from Brillouin Scattering, magnetization data or neutron-scattering experiments. The spin wave resonance condition for the resonance field applied normal to the film plane reads.

$$w = \gamma \left[ H_n - 4\pi M_s + \frac{D}{g\mu_B} \left( \frac{n\pi}{h} \right) \right] \quad 3.18$$

$h$  is the film thickness and  $H_n$  is the resonant field of the  $n$ th spin wave mode. The temperature dependence of  $D(T)$  obeys the  $T^{3/2}$  law for some amorphous alloys such as B-Fe<sup>[3.86]</sup> or Gd-CoMo<sup>[3.87]</sup>, while for other measured by in elastic neutron scattering for an amorphous B-Si-Fe alloy<sup>[3.88]</sup>.  $D(T)$  is related to the micro magnetic exchange stiffness constant  $A(T)$  by

$$A(T) = \frac{M_s(T)}{2g\mu_B} D(T) \quad 3.19a$$

where  $g\mu_B$  and  $g$  denotes the gyro magnetic ratio,  $A(T)$  is related to the domain wall energy  $\sigma_w$  of a  $180^\circ$  Bloch Wall by  $\sigma_w = 4\sqrt{Ak_w}$ . Thus  $D(T)$  also can be estimated from wall energy measurements.  $A(T)$  can be expressed in terms of the exchange constant<sup>[3.89]</sup>.

$$A(T) = \frac{1}{6} \sum_i N_i S_i(T) \sum_j J_{ij} Z_{ij} r_{ij}^2 S_j(T) \quad 3.19b$$

where,  $N_i Z_{ij}$  and  $r_{ij}$  are the number of  $i$  atoms per unit volume, the number  $j$  nearest neighbors and the atomic distance between the atoms  $i$  and  $j$  respectively combinations in ferri magnets. The temperature dependence of  $A(T)$  obtained from standing spin wave spectra in an amorphous Gd-Fe film<sup>[3.90]</sup>.

The presence of non-S-state rare earth gives rise to a strong coupling between the spin system and the lattice via spin-orbit coupling yielding high line width in the resonance spectra<sup>[3.91]</sup> which presents the determination of  $D(T)$ .

It should be noted that strong differences were observed for  $D(0)$  values evaluated from magnetization and neutron diffraction experiments. This discrepancy was attributed to additional low lying magnetic excitations<sup>[3.92]</sup>.

### 3.5 Expression for Linear Magnetostriction

The standard expression for strain along an arbitrary direction in terms of magnetostriction constants and the direction of the applied field, we shall consider here a simple microscopic model used by Néel<sup>(3.93)</sup>. The model postulates certain properties of the energy of interaction of the neighboring atoms without investigating the origin of this energy. The justification being only experimental, the model should not be taken too seriously. Néel developed in his paper on magnetic annealing and surface anisotropy is as follows, when the distance between the atomic magnetic moments is variable, the interaction energy is expressed by

$$W(r, \cos\phi) = g(r) + l(r) \left( \cos^2\phi - \frac{1}{3} \right) + q(r)$$

$$\left( cs^4 \phi - \frac{6}{7} cs^2 \phi + \frac{3}{35} \right) + \dots \tag{3.20}$$

If the interaction energy is a function of  $r$ , the crystal lattice must be deformed upon the generation of a ferromagnetic moment, because such interaction tends to change the bond length in a different way depending on the bond direction. The first term  $g(r)$  is the exchange interaction term and is of relevance only when volume magnetostriction is considered as manifested in thermal expansion anomaly at the magnetic ordering temperature.

If  $\bar{\alpha}$  denotes the direction of domain magnetization and that of the bond direction, we can write

$$W = g(r) + l(r) \left\{ (\alpha_1 \gamma_1 + \alpha_2 \gamma_2 + \alpha_3 \gamma_3)^2 - \frac{1}{3} \right\} + q(r) (\alpha_1 \gamma_1 + \alpha_2 \gamma_2 + \alpha_3 \gamma_3)^4 - \frac{6}{7} (\alpha_1 \gamma_1 + \alpha_2 \gamma_2 + \alpha_3 \gamma_3)^2 + \frac{3}{35} + \dots \tag{3.21}$$

Considering a deformed cubic lattice and relating the direction cosines  $\gamma_1$  to the strain tensor  $L_{ij}$ , we can get the expansion for magneto-elastic energy. Since the magnetoelastic energy has a linear dependence on strain the crystal will deform without limit unless it is counter balanced by the elastic energy which increases rapidly because of its quadratic dependence on strain.

By differentiating the

$$\text{Total energy} = E_{\text{mag,elastic}} + E_{\text{elastic}}$$

With respect to the strain components, and setting the partial derivatives equal to zero, for minimum energy condition, one can obtain the relation for the fractional change in length of the crystal in any arbitrary direction  $\bar{\beta}$  as

$$\lambda_p = \sum_{i,j=1} h_{ij} \beta_i \beta_j \quad 3.22$$

Substituting the values of the strain components as obtained by minimizing total energy coming from magnetoelastic and elastic terms, we can get an expression for

$$\begin{aligned} \lambda_p = h_0 + h_1 \left( \sum \alpha_i \beta_i^2 - \frac{1}{3} \right) + 2h_2 c_{ij} (\alpha_i \alpha_j \beta_i \beta_j) + h_3 S + h_4 \\ \left( \sum \alpha_i^4 \beta_j^2 + \frac{2}{3} S - \frac{1}{3} \right) + 2h_5 c_{ij} [\alpha_i \alpha_j (1 - \alpha_i^2 \alpha_j^2) \beta_i \beta_j] + \dots \end{aligned} \quad 3.23$$

where  $c_{ij}$  indicates a summation over terms with cyclic permutation of the indices and  $h_0 \rightarrow h_5$  are the magnetostriction constant defined by

$$\begin{aligned} h_0 = \frac{-b_0}{c_{11} + 2c_{12}}, h_1 = \frac{-b_1}{c_{11} - c_{12}}, h_3 = \frac{-b_3}{c_{11} + 2c_{12}} \\ h_4 = \frac{-b_4}{c_{11} - 2c_{12}} \text{ and } h_5 = \frac{-b_5}{2c_{44}} \end{aligned} \quad 3.24$$

where the coefficients  $b_n$  are magnetoelastic coupling coefficients. The above relations are specific to cubic symmetry. For hexagonal crystals, the relation become modified due to different symmetry conditions and have been treated in detail by Mason and Lewis<sup>[3,94]</sup>. Taking the first three terms only in equation (3.21) and assuming magnetostriction to be zero for a demagnetized specimen for cubic crystal

$$\begin{aligned} \lambda_p = \frac{3}{2} \lambda_{100} \left( \alpha_1^2 \beta_1^2 + \alpha_2^2 \beta_2^2 + \alpha_3^2 \beta_3^2 - \frac{1}{3} \right) + \\ 3\lambda_{111} (\alpha_1 \alpha_2 \beta_1 \beta_2 + \alpha_2 \alpha_3 \beta_2 \beta_3 + \alpha_3 \alpha_1 \beta_3 \beta_1) \end{aligned} \quad 3.25$$

where  $\lambda_{100}$  and  $\lambda_{111}$  indicates strains along (100) and (111) direction respectively.

### 3.6 Magnetostriction in Polycrystalline Axial Magnetic Systems.

For a single crystal of axial symmetry (which is the case for the tetragonal symmetry materials), if we neglect the magnetic anisotropy within the basal plane, the magnetostriction is given by<sup>[3.95]</sup>.

$$\begin{aligned} \lambda(\alpha, \beta) = & \frac{1}{3} \lambda_{11}^{\alpha} + \frac{1}{2\sqrt{3}} \lambda_{12}^{\alpha} \left( \alpha_2^2 - \frac{1}{3} \right) + 2\lambda_{21}^{\alpha} \left( \beta_2^2 - \frac{1}{3} \right) + \sqrt{3} \lambda_{22}^{\alpha} \left( \alpha_2^2 - \frac{1}{3} \right) \\ & \times \left( \beta_2^2 - \frac{1}{3} \right) + 2\lambda^{\gamma} \left\{ \frac{1}{4} (\alpha_x^2 \alpha_y^2) \times (\beta_x^2 \beta_y^2) + \alpha_x \alpha_y \beta_x \beta_y \right\} + \\ & \lambda^{\gamma} \{ \alpha_y \alpha_z \beta_y \beta_z + \alpha_x \alpha_z \beta_x \beta_z \} + \text{higher order terms} \end{aligned} \quad 2.26$$

where the  $\lambda_{ij}^{\alpha}$  phenomenological magnetostrictive constant have their usual meaning<sup>[3.96]</sup>, being functions of the temperature and the applied field, i.e.  $\lambda_{ij}^{\alpha} = \lambda_{ij}^{\alpha}(T, H)$ . In equation (3.26)  $\alpha \equiv (\alpha_x \alpha_y \alpha_z)$  represents the magnetization direction and  $\beta \equiv (\beta_x \beta_y \beta_z)$ , the direction in which the strain  $\lambda$  is measured.

Making  $\alpha = \beta$ , we will have the magnetostriction measured parallel to the applied field  $H_j$  if the angle formed by the magnetization vector  $M_s$ , with  $H$  is  $\theta$ , we obtain, neglecting higher order terms.

$$\begin{aligned} \lambda_{11} = & \frac{\lambda_{11}^{\alpha}}{3} + \left( \frac{1}{2\sqrt{3}} \lambda_{12}^{\alpha} + 2\lambda_{21}^{\alpha} \right) \left( \cos^2 \theta - \frac{1}{3} \right) + \sqrt{3} \lambda_{22}^{\alpha} \left( \cos^2 \theta - \frac{1}{3} \right)^2 + \\ & \frac{\lambda^{\gamma}}{2} \sin^4 \theta + 2\lambda^{\gamma} \cos^2 \theta \sin^2 \theta \end{aligned} \quad 3.27$$

The parallel magnetostriction in a polycrystalline sample can be calculate by averaging equation (3.27) over all the directions within a sphere, assuming all of them being equally probable, i.e.

$$\langle \lambda_{11} \rangle_{pol} = \frac{1}{4\pi} \int_0^{2\pi} \int_0^\pi \lambda_{11}(\theta, \varphi) \sin\theta \, d\theta \, d\varphi$$

The result is

$$\lambda_{11} = \frac{1}{3} \lambda_{11}^\alpha + \frac{4}{45} \sqrt{3} \lambda_{12}^\alpha + \frac{4}{15} \lambda^r + \frac{2}{15} \lambda' \quad 3.29$$

The transverse magnetostriction,  $\lambda_\perp$ , can be conveniently obtained from the expression  $\lambda_\perp = \frac{\lambda_1}{2}$ , where  $\omega$  is the volume striction. One takes a frame of axes ( $x'$ ,  $y'$ ,  $z'$ ), randomly oriented with respect to the one where  $M$ , has the  $\alpha$  direction.

The volume magnetostriction,  $\omega$ , will be

$$\omega = \lambda_{x'} + \lambda_{y'} + \lambda_{z'} \quad 3.30$$

i.e. the sum of strains measured along the three random axes. Expressing the direction cosines of  $x'$ ,  $y'$  and  $z'$  in terms of the polar angles denoting the position of the  $o'$  origin, substituting them into equation (3.26) and going to equation (3.30) yields

$$\omega = \lambda_{11}^\alpha + \frac{1}{2\sqrt{3}} \lambda_{12}^\alpha \left( \cos^2\theta - \frac{1}{3} \right) \quad 3.31$$

which averaged in the form of equation (3.28) for the polycrystalline sample gives

$$\langle \omega \rangle_{pol} = \lambda_{11}^\alpha \quad 3.32$$

Therefore the volume strain is only contributed to by the uniform exchange striction mode  $\lambda_{11}^\alpha$ , which in this case can be completely separated out, even with measurements on a poly-crystal, obtaining now  $\lambda_\perp$ , we end up with the following expression for the anisotropic

$$\lambda_1 = \lambda_{11} - \lambda_\perp$$

magnetostriction for a poly-crystal

$$\lambda_1 = \frac{2}{15} (\sqrt{3} \lambda_{22}^a + 3\lambda' + 2\lambda^e) + \text{higher order terms} \quad 3.33$$

This means that the single-ion crystal field modes representing the  $C/a$  ratio distortion ( $\lambda_{22}^a$ ), the shear breaking of the basal plane cylindrical symmetry ( $\lambda'$ ) and the shear tilting the  $c$ -axis, are cast together within  $\lambda_1$ . Notice that no exchange striction terms ( $\lambda_{11}^a$  and  $\lambda_{12}^a$ ) are present at all in  $\lambda_1$ .

### 3.7 Magnetostriction in Amorphous Ribbon

For amorphous we can apply the same approximation as in the case of polycrystalline magnetic material such that

$$\lambda_{100} = \lambda_{111} = \lambda_s$$

We get equation (3.25)

$$\begin{aligned} \lambda_\rho &= \frac{3}{2} \lambda_s \left( \alpha_1^2 \beta_1^2 + \alpha_2^2 \beta_2^2 + \alpha_3^2 \beta_3^2 - \frac{1}{3} \right) + 3\lambda_s (\alpha_1 \alpha_2 \beta_1 \beta_2 + \alpha_2 \alpha_3 \beta_2 \beta_3 + \alpha_3 \alpha_1 \beta_3 \beta_1) \\ &= \frac{3}{2} \left[ \alpha_1^2 \beta_1^2 + \alpha_2^2 \beta_2^2 + \alpha_3^2 \beta_3^2 + 2\alpha_1 \alpha_2 \beta_1 \beta_2 + 2\alpha_2 \alpha_3 \beta_2 \beta_3 + 2\alpha_3 \alpha_1 \beta_3 \beta_1 - \frac{1}{3} \right] \quad 3.34 \\ &= \frac{3}{2} \left[ (\alpha_1 \beta_1 + \alpha_2 \beta_2 + \alpha_3 \beta_3)^2 - \frac{1}{3} \right] \end{aligned}$$

$$\text{Hence } \alpha_1 \beta_1 + \alpha_2 \beta_2 + \alpha_3 \beta_3 = \text{Cos } \theta$$

where  $\theta$  is the angle between the direction of magnetization and that of observation. When the domain magnetization rotates toward the direction of the applied field, the fractional change is given by

$$\lambda_{\beta} = \frac{\Delta l}{l}$$

becomes equation (3.34)

$$\frac{\Delta l}{l} = \frac{3\lambda_s}{2} \left( \cos^2 \theta - \frac{1}{3} \right) \quad 3.35$$

where  $\frac{\Delta l}{l}$  is the strain,  $\lambda_s$  is the magnetostriction constant and  $\theta$  is the angle between the spontaneous magnetization and the direction in which the strain is measured. If a tensile stress  $\sigma$  is applied to the material, then the change in energy density is

$$E_{\sigma} = -\frac{3}{2} \lambda_s \sigma \cos^2 \theta \quad 3.36$$

$\lambda_s$  is dimensionless. A positive value of  $\lambda_s$  indicates that the axis of tension becomes the easy direction of magnetization.

### 3.8 Engineering Magnetostriction

The components of strain along the ribbon axis for the two types of domain are given by

$$\epsilon_1 = \frac{3}{2} \lambda_s \left[ \cos^2(\theta - \phi_1) - \frac{1}{3} \right] \quad 3.37$$

$$\text{and } \epsilon_2 = \frac{3}{2} \lambda_s \left[ \cos^2(\theta + \phi_2) - \frac{1}{3} \right] \quad 3.38$$

The engineering magnetostriction  $\lambda_e$  defined as the average axial strain of the whole ribbon, is given

$$\lambda_e = \alpha \epsilon_1 + (1 - \alpha) \epsilon_2 \quad 3.39$$



For  $\epsilon_1, \epsilon_2$  from equation (3.37) and equation (3.38) dropping the constant  $\frac{1}{3}$  one finds for the effective length change

$$\frac{\lambda_e}{\lambda_s} = \frac{3}{2} \left\{ \frac{1}{2} [\cos^2(\theta - \phi_1) + \cos^2(\theta + \phi_2)] + \left( \frac{x}{d} \right) [\cos^2(\theta - \phi_1) - \cos^2(\theta + \phi_2)] \right\} \quad 3.40$$

equation (3.40) may now be used to give the complete expression for  $\lambda_e$  in the wall movement regime as

$$\begin{aligned} \frac{\lambda_e}{\lambda_s} = & \frac{3}{2} \left\{ \frac{1}{2} [\cos^2(\theta - \phi_1) + \cos^2(\theta + \phi_2)] + \left[ \frac{C}{4}(1-r) \right] [\cos^2(\theta - \phi_1) + \cos^2(\theta + \phi_2)] \right. \\ & h[\cos(\theta - \phi_1) + \cos(\theta + \phi_2)] - \frac{1}{2} (\sin^2 \phi_1 - \sin^2 \phi_2) - \\ & \left. \gamma [\sin^2(\theta - \phi_1) - \sin^2(\theta + \phi_2)] \right\} \quad \text{When } \left( x \leq \frac{d}{2} \right) \end{aligned} \quad 3.41$$

As before, at a critical value of the applied field wall movement is complete, and further increase in field result in the simpler expression

$$\frac{\lambda_e}{\lambda_s} = \frac{3}{2} [\cos^2(\theta - \phi_1)] \quad \text{when } (x > d/2) \quad 3.42$$

### 3.9 Direction of Linear Magnetostriction

Experiments have shown that the deformation depends upon the direction of magnetization. For a cubic crystal magnetize in the direction given by the direction cosines  $\lambda_1, \lambda_2$  and  $\lambda_3$  (defined with respect to the cubic axes). This deformation expressed in strain components  $\epsilon_{ij}$  ( $i, j = x, y, x$ ) become in first approximation.

$$\begin{aligned}
 \varepsilon_{xx} &= \frac{3}{2} \lambda_{100} \left( \alpha_1^2 - \frac{1}{3} \right) \\
 \varepsilon_{yy} &= \frac{3}{2} \lambda_{100} \left( \alpha_2^2 - \frac{1}{3} \right) \\
 \varepsilon_{zz} &= \frac{3}{2} \lambda_{100} \left( \alpha_3^2 - \frac{1}{3} \right) \\
 \varepsilon_{xy} &= \frac{3}{2} \lambda_{111} \alpha_1 \alpha_2 \\
 \varepsilon_{yz} &= \frac{3}{2} \lambda_{111} \alpha_2 \alpha_3 \\
 \varepsilon_{zx} &= \frac{3}{2} \lambda_{111} \alpha_3 \alpha_1
 \end{aligned} \tag{3.43}$$

The extra terms  $(-\frac{1}{3})$  make the total change of volume nil (trace of matrix is zero). The factors  $-\frac{1}{3}$  ensure that the strain in the direction of magnetization with respect to the non-magnetized state ( $\alpha_1^2 = \alpha_2^2 = \alpha_3^2 = \frac{1}{3}$ ) is  $\lambda_{100}$  and  $-\frac{1}{2}\lambda_{111}$ , in the [100] and [111] directions respectively.

The strain in a direction perpendicular to  $\lambda_{100}$  and  $-\frac{1}{2}\lambda_{111}$  respectively. In an arbitrary direction we then have parallel to the magnetization

$$\lambda_{(\alpha_1, \alpha_2, \alpha_3)} = \lambda_{100} + 3(\lambda_{111} - \lambda_{100})(\alpha_1^2 \alpha_2^2 + \alpha_2^2 \alpha_3^2 + \alpha_3^2 \alpha_1^2) + \dots \tag{3.44}$$

For the ferromagnetic materials the values of  $\lambda$  at room temperature are found to be

$$\text{Fe} : \lambda_{100} = 25 \times 10^{-6} \text{ and } \lambda_{111} = -19 \times 10^{-6}$$

$$\text{Ni} : \lambda_{100} = -46 \times 10^{-6} \text{ and } \lambda_{111} = -25 \times 10^{-6}$$

In discussing the effect of a unidirectional stress it is convenient to divide materials into two classes which have

- i) Positive magnetostriction
- ii) Negative magnetostriction

In materials of class i) the magnetization is increased by tension (except at  $I = 0$  or  $I_s$ ) and the magnetization is decreased by tension and the material contracts when magnetized.

### 3.10 Magnetostriction Arising from domain rotation.

Magnetostriction is associated with domain orientation. The change in dimension of a single domain can be rotated in simple quantitative way to change in direction of magnetization in the domain as follows

$$\lambda_1 = \frac{3}{2} \lambda_s \left( \cos^2 \theta - \frac{1}{3} \right) \quad 3.45$$

Here  $\theta$  is the angle between the direction in which the change in length is measured. It is assumed now that magnetostriction is independent of the crystallographic direction of magnetization and that the change in volume is zero. The zero point of  $\lambda_1$  is chosen so that the change in volume is zero. The zero point of  $\lambda_1$  is chosen so that it is equal to the longitudinal change in length  $\lambda_s$ , where  $\theta = 0$  at saturation. When the length is measured at right angle to the direction of magnetization (Transverse effect)  $\theta = 90^\circ$  and the change in length

$$\lambda = -\frac{\lambda_s}{2}$$

For polycrystalline or amorphous material the domain are initially oriented at random. The same relation is applicable if one use the average of  $\text{Cos}^2\theta$  over all the domains. When the material is unmagnetized,

$$\langle \text{Cos}^2\theta \rangle_{av} = \frac{1}{3} \quad \text{and } \lambda = 0$$

Upon application of a strong field  $\theta$  becomes zero and  $\lambda = -\lambda_s$ .

If the domain are not initially random, one can use the relation

$$\begin{aligned} \lambda &= \frac{3}{2}\lambda_s \left[ \langle \text{Cos}^2\theta \rangle_{av} - \frac{1}{3} \right] - \frac{3}{2} \left[ \langle \text{Cos}^2\theta \rangle_o - \frac{1}{3} \right] \\ &= \frac{3}{\lambda} \lambda_s \left[ \langle \text{Cos}^2\theta \rangle_{av} - \langle \text{Cos}^2\theta \rangle_o \right] \end{aligned} \quad 3.46$$

where  $\langle \text{Cos}^2\theta \rangle_o$  = initial domain distribution,  $\langle \text{Cos}^2\theta \rangle_{av}$  = domain distribution at any time.

If the domain are oriented originally so that  $\theta = 0$  fir half of them and  $\theta = 180^\circ$  for other half  $\langle \text{Cos}^2\theta \rangle_o = \langle \text{Cos}^2\theta \rangle_{av} = 0$  (the reference point); in a strong field  $\theta = 0$  and there is no change in  $\text{Cos}^2\theta$  and  $\lambda = 0$ . When used in this sense,  $\lambda$  depends decidedly on the initial domain distribution while  $\lambda_s$  is a constant of the material. The constant  $\lambda_s$  can be determined in any specimen by measuring  $\lambda$  when a saturation field is applied first parallel and then at  $90^\circ$  to the direction of measurement of  $\lambda$ . The total change in length caused by the change in field in the polycrystalline or amorphous material is then

$$\frac{\Delta l}{l} = \frac{3}{2}\lambda_s \quad 3.47$$

in dependent of the initial domain distribution.

### 3.11 Magnetoresistance

Magnetoresistance is another serious drawback of strain gauge at room temperature for measurements in the presence of a magnetic field is very dependent on temperature, chemical composition of gauge, particularly magnetic impurity, the strength of the magnetic field and perhaps the state of strain in the gauge. The differential magneto-resistance in the gauges we have used was less than  $10^{-7}$  when reduced to strain. The effect of rotation of a magnetic field of 4.16 kilo gauss showed an ever smaller differential magneto-resistance. Measurements which require only rotation of the field, thus are not seriously affected provided that the dummy gauge is placed parallel to the active gauge.

The use of Durofix facilitated the removal of the gauges from the Copper discs for subsequent use with proper glue. The possibility of bad bondage with Durofix was checked by observing the differential strain. The whole success of this method, however, lies in the proper choice of a glue which can give proper bondage throughout the temperature range and at the same time can easily be dissolved without damaging the gauges. To measure differential magneto-resistance, it is not of course essential to get as good a grip as needed for measurements of, say magnetostriction or thermal expansion, because the strain arising from the application of magnetic field is small. The purpose of the glue is mainly to keep the gauge flat on the specimen to avoid bending.

### 3.12 Field Dependence of Magnetostriction

We have performed an extensive and through study of the field dependence of the parallel and perpendicular magnetostrictions in the present series of Co and Fe based amorphous ribbons at room temperature up to maximum field 4.16 kilo gauss. The sequence followed below for the field dependence analysis presentation is only for a matter of convenience and clarity. Two types of effective anisotropy field are deal with:  $H_c^k$ , the applied along the c-axis are needed to saturate the system against the anisotropy keeping the magnetization,  $M_s$ , in the basal plane, and conversely,  $H_{Kb}$ , the field needed to be applied along the basal plane to saturate against the anisotropy keeping  $M_s$  along the C-axis. Such a field dependence for magnetostriction associated with a 3d electron band. Field dependence magnetostriction to be mainly of exchange origin and comes form the Fe or Co sub-lattice as well.

### 3.13 Low Temperature Dependence of Magnetostriction

We have performed on extensive study of low temperature dependence of the parallel and perpendicular magnetostriction in the present series of Co and Fe-based amorphous ribbon, from around 70 k upto room temperature and up to a maximum applied field of 4.2 kilo gauge. This field is so weak due to the proximity to the spin reorientation transition toward the C-axis. In contrast  $W$  increases with field at all temperatures, in agreement again, with a 3d band striation associated to the Fe sub-lattice. The present series of amorphous

ribbons, there are two main contributions to the magnetostrictive distortions respectively due to the magneto-elastic coupling within the TM-M sub-lattices. The thermal dependence is as may be observed, too complex to be ascribed to a simple single-ion axial magnetostriction of just second order kind. The complicated low temperature behavior depicted of the competition between the different single-ion distortion modes. The complex behavior low temperature dependence of the anisotropic magnetostriction associated with TM sub-lattice, needs recourse to high-order crystal field single-ion interaction.

### 3.14 Application of Magnetostriction

Materials that subjected to an alternating magnetic field, a hysteresis loop will trace under the variation of B (or M) with H. At the same time, the variation of  $\lambda$  with H traces out another loop. Actually, the latter is a double loop, as illustrated for nickel in figure 3.6 because the magnetostrictive strain is independent of the sense of the magnetization. The material therefore vibrates at twice the frequency of the field to which it is exposed. This magnetostrictive vibration is the major source of the humming sound emitted by transformers. (A transformer contains a "Core" of magnetic material subjected to the alternating magnetic field generated by the alternating current in the primary winding).

Conversely if partially magnetized body is mechanically vibrated, its magnetization will vary in magnitude about some mean value because of the inverse magnetostrictive effect and this alternating magnetization will induce an alternating emf in a coil wound around the body.

These two effects are exploited in the magnetostrictive transducer. It is one of a large group of electro-mechanical transducers, which can convert electrical energy into mechanical energy, and vice versa. The shape and size of a magnetostrictive transducer depends on the nature of the applications one simple form is a ring carrying a toroidal winding. Magnetostrictive transducers are best suited for operation at frequencies of about 20 to 100 kHz. They have two main applications.

### 3.14.1 Under water sound

The detection of an under water object, such as a submarine is accomplished by a sonar (sound navigation and ranging) system. An "active" sonar generates a sound original with a transmitting transducer and listens for the sound reflected from the submerged object with a receiving traducer, called a hydrophone. A "passive" sonar listens for sound, such as engine noise, generated by the submerged object. An echo sounder is an active sonar designed to measure the depth of the ocean bottom. While magnetostrictive transducers still have a role to play in under water sound applications, they have been largely replaced by piezoelectric transducers. A piezoelectric material, like barium titanate or quartz, is one which becomes electrically polarized when it is mechanically strained i.e. electric charges of opposite sign are formed on its ends. Conversely it becomes strained when subjected to an electric field. The analogy between these electrical effects and certain magnetostrictive effects have caused magnetostrictive transducers to be some times called piezomagnetic transducers. The analogy is not exact, however, and the word piezomagnetic should be reserved for those few antiferro-magnetic single crystal which develop a small magnetic moment when mechanically strained in the absence of a field,  $\text{CoF}_2$  and  $\text{Mn F}_2$  are examples.



**3.14.2 Ultrasonic sound generators**

There are also transducers, but here the emphasis is not on sound as a signal but on sound as a mechanical disturbance, usually in some liquid medium, capable of bringing about some desired effect. Probably the most important application of this kind is ultrasonic clearing of metal and other parts during manufacturing operations, such as before electroplating or final assembly. The parts to be cleaned are immersed in a solvent, which is agitated by an ultrasonic generator. Remove of dirt and grease is much faster by this method than by simple immersion.

Magnetostriction finds another application in the acoustic delay line. a delay line is a device designed to delay the passage of an electrical signal for a predetermined length of time. A purely electrical line, such as a coaxial cable, will produce delays of the order of microseconds, due chiefly to the capacitance of the cable. For longer delays of the order of milliseconds, acoustic delay lines are needed; these involve the conversion of an electrical pulse into an acoustic pulse. Since the velocity of an electrical signal along a conducting wire is about equal to the velocity of light,  $3 \times 10^{10}$  cm/sec and the velocity of sound in a metal is about  $5 \times 10^5$  cm/sec, an acoustic pulse travels with a velocity some  $10^{-5}$  times that of an electrical.



**CHAPTER - 4**

### 4.1 Theory of Thermal Expansion

We may understand thermal expansion by considering for a chemical oscillator the effect of anharmonic terms in the potential energy on the mean separation of a pair of atoms at a temperature  $T$ . We take the potential energy of the atoms at a displacement  $x$  from their equilibrium separation at absolute zero as

$$U(x) = cx^2 - gx^3 - fx^4 \quad 4.1$$

with  $c, g,$  and  $f$  all positive. The term in  $x^3$  represents the asymmetry of the mutual repulsion of the atoms and the term in  $x^4$  represents the softening of the vibration at large amplitudes. The minimum at  $x = 0$  is not an absolute minimum, but for small oscillations the form is an adequate representation of an inter atomic potential.

We calculate the average displacement by using the Boltzmann distribution function, which weights the possible values of  $x$  according to their thermodynamic probability

$$\langle x \rangle = \frac{\int_{-a}^a dx x e^{-\beta U(x)}}{\int_{-a}^a dx e^{-\beta U(x)}} \quad 4.2$$

with  $\beta = \frac{1}{k_B T}$ , for displacements such that the anharmonic terms in the energy are such in comparison with  $k_B T$ , we may expand the integrands as

$$\int dx x e^{-\beta U} = \int dx e^{-\beta cx^2} (x + \beta gx^4 + \beta fx^5) = \left(3\pi^{\frac{1}{2}}\right) \left(g/c^{\frac{3}{2}}\right) \beta^{-\frac{3}{2}} \quad 4.3$$

where  $\langle x \rangle = \frac{3g}{4c^2} k_B T$  in the classical region, In equation (4.3) we have left  $cx^2$  in the exponential, but we have expanded  $\exp(\beta gx^3 + \beta fx^4) \cong 1 + \beta gx^3 + \beta fx^4 + \dots$ . Measurements of the lattice constant of solid argon as shown in figure 4.1. the slope of the curve is proportional to the thermal expansion coefficient. The expansion coefficient vanishes as  $T \rightarrow 0$ . In lowest order the thermal expansion does not involve the symmetric term  $fx^4$  in  $U(x)$ , but only the antisymmetric term  $gx^3$

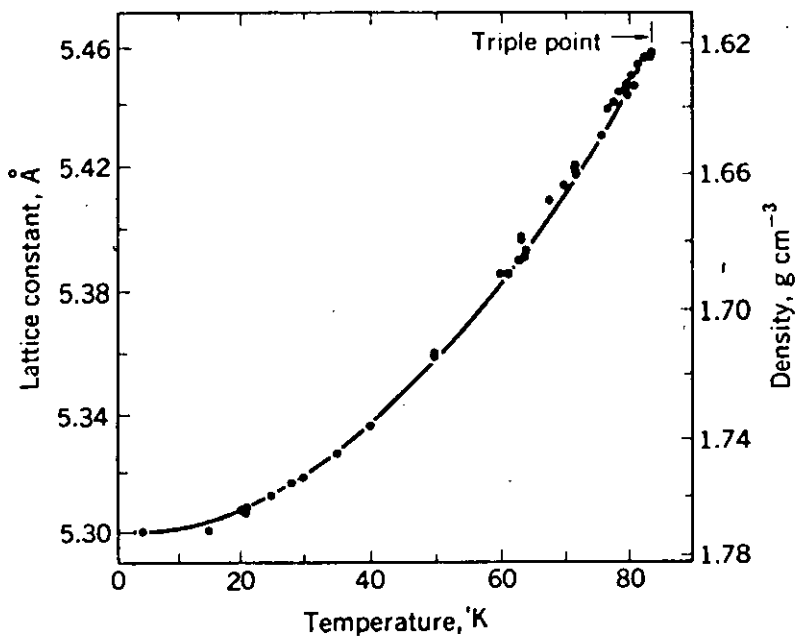


Fig. 4.1: Lattice constant of solid argon as a function of temperature, or measured by various workers<sup>[4.1]</sup>.

## 4.2 Electronic and Magnetic Contribution to Thermal Expansion.

In a metal the total contribution to the entropy arises from lattice variations, conduction electrons and magnetic interactions. If we write the entropy as

$$S = S_l + S_e + S_m \quad 4.4$$

then the specific heat is given by

$$C_v = T \left( \frac{\partial s}{\partial T} \right)_v = C_{vl} + C_{ve} + C_{vm} \quad 4.5$$

The thermal expansion is given by the relation

$$\left( \frac{\partial s}{\partial T} \right)_T = \left( \frac{\partial p}{\partial T} \right)_v = \frac{\beta}{\lambda_T} \quad 4.6$$

If the different contributions to the entropy are functions  $S_i(\theta_i/T)$  where  $\theta_i$  is a characteristic temperature, then

$$\left( \frac{\partial s_i}{\partial V} \right)_T = \frac{\gamma_i C_{vi}}{V} \quad 4.7$$

$$\text{where } \gamma_i = -\frac{V}{\theta_i} \left( \frac{\partial \theta_i}{\partial v} \right)_T \quad 4.8$$

is the corresponding Grüneisen parameter. We could, therefore, write

$$\beta = \frac{\lambda_T}{V} (\gamma_l C_{vl} + \gamma_e C_{ve} + \gamma_m C_{vm}) \quad 4.9$$

It is well known that the conduction electrons in a metal contribute a term to the specific heat proportional to the temperature  $T$ . So we should expect in a metal a contribution to thermal expansion coefficient from the conduction electron which would be linear in temperature. At low temperature where the lattice contribution to the expansion coefficient varies as  $T^3$ , we could write  $\alpha$  as

$$\alpha = BT + DT^3 \quad 4.10$$

By plotting  $\alpha/T$  against  $T^2$  the values of Band D can be found. From the value of B and the measured electronic specific heat one could obtain the value of  $\gamma_e$ .

Varley has derived the following theoretical expression for  $\gamma_e$ .

$$\gamma_e = 1 + \left( \frac{\partial \ln n(E_F)}{\partial \ln V} \right)_{E_F, T} - \frac{N}{n^2(E_F)} \cdot \left( \frac{\partial n(E_F)}{\partial E_F} \right)_V \quad 4.11$$

$$\left[ 1 + \left( \frac{\partial \ln V}{\partial \ln V} \right)_{E_F, T} \right] + \frac{C_{ve}}{\beta V n^3(E_F)} \cdot \left( \frac{\partial n^2(E_F)}{\partial E_F} \right)_V$$

Here  $n(E_F)$  is the number density of states per unit volume at the Fermi level  $E_F$ ;  $N$  is the total number of conduction electron per unit volume in the metal. For a single band free electron model  $n(E_F)$  depends only on  $E_F$  and

$$\frac{N}{n^2(E_F)} \cdot \left( \frac{\partial n(E_F)}{\partial E_F} \right) = \frac{1}{3} \quad 4.12$$

$\gamma_e$  for such a case should be  $\frac{2}{3}$ , where the single band free electron model is not applicable the value of  $\gamma_e$  can be very different from  $\frac{2}{3}$ . The magnitude and sign of  $\gamma_e$  will depend on: (i) how rapidly and in what direction  $n(E_F)$  varies with energy at the Fermi level; and (ii) how sensitive  $n(E_F)$  is to changes in volume  $V$ . In exceptional cases the electronic Grüneisen parameter could be negative yielding a negative contribution to the thermal expansion coefficient.

In ferromagnetic materials at the Curie temperature and in antiferro-magnetic materials at the Néel temperature the onset of ordering of the spins is accompanied by an anomaly in thermal expansion. This effect has been observed in many cases. In such ordered spin arrays at very low temperatures there could be excitations involving spin reversal on a few of the atoms. These excitations are called spin waves and where quantized these elementary excitations go under

the name of magnons. It is well known that in ferromagnetic and ferrimagnetic materials these spin waves obey a quadratic dispersion law:  $\left( \omega(\vec{q}) \propto q^2 \right)$  and yield a magnon contribution to the heat capacity varying as  $T^{3/2}$  at low temperatures. This magnon contribution to the heat capacity has been observed in magnetite. In ferromagnetic metals this contribution is superposed on the electron contribution to the specific heat and it becomes difficult to separate the two effects. In ferrimagnetic materials the electronic contribution is absent and the magnon contribution can be easily detected. Magnon must also contribute to the thermal expansion of these materials. The corresponding Grüneisen parameter is a measure of the volume dependence of the effective exchange interaction determining the quadratic dispersion relation in the materials. Lord has in discussed the magnitude of the magnon contribution to thermal expansion in Yttrium iron garnet and Europium oxide. He concludes that in YIG it may be just possible to detect the magnon contribution around 4°K; but in Europium oxide the effect is very considerable and should be easily observable with the existing experimental techniques. These measurements can be correlated with the measurements of the pressure dependence of the transition temperature in these material.

In an antiferromagnetic material, on the other hand, one gets a linear dispersion relation if the anisotropic magnetic energy is neglected in comparison with the exchange energy. In such a case the magnon contribution to the low temperature specific heat varies as  $T^3$ . Since the lattice contribution at these low temperatures also has the same temperature dependence it would not be possible to separate the magnon contribution unless the Néel temperature is low compared to the Debye temperature. In such a case the magnetic contribution will be several

times the lattice contribution which can be calculated from the elastic constant data. If the anisotropy energy is not negligible, then the dispersion relation is modified and there is a finite energy gap. In such a case the specific heat at low temperatures varies faster than  $T^3$ . One would expect such a behavior in  $\text{CuCl}_2 \cdot 2\text{H}_2\text{O}$  in which the Néel temperature is about  $4^0\text{K}$  and the anisotropy energy is half as much as the exchange energy. However, Peterson and Philips have only observed a  $T^3$  dependence of the magnon heat capacity in this material. One would expect a similar contribution to the thermal expansion in the antiferromagnetic materials. There are no experiments so far on the magnon contribution to thermal expansion in ferro-, ferri-, and antiferro-magnetic materials.

### 4.3 Negative Thermal Expansion in Solids

In the systems like glasses and crystals having diamond like structure the negative value for  $\alpha$  arises at low temperatures from the vibrational energy of the lattice. An explanation for the possible existence of negative  $\alpha$  in these solids was proposed by Blackman in a series of papers by adopting Barron's theoretical treatment. Using the relation

$$\gamma_i = \frac{d \ln(V^{-1/3} v_i)}{d \ln V} \quad 4.13$$

Blackman arrived at the form

$$\gamma_i = -\frac{1}{6\rho v_i^2} \left[ \frac{d(\rho v_i^2 r)}{dr} \right]_{r=r_0} \quad 4.14$$

where  $v_i$  = velocity of propagation of the  $i$ th elastic mode ( $i = 1, 2, 3$ )



$\rho$  = density

$2r$  = lattice constant

$C_{kl} = v_i^2 \rho$ , is the elastic constant

$\partial_i$  = Grüneisen parameter for the  $i$ th mode, and

$V$  = molar volume

Two models we discussed by him. In the NaCl model, based on pure ionic interaction potential having columbic and repulsive forms, Blackman found that  $\gamma_i$  assumes negative values for transverse modes. Calculations for ZnS structure indicate that as long as the next nearest neighbor interactions are columbic, the transverse modes in the ZnS structure show negative values  $\gamma_i$  for long range nearest neighbor interactions.

Diamond- structure solids, for instance, are said to have a low-lying transverse acoustic branch which at low temperatures is predominant in absorbing energy. In the case of glasses the presence of low-lying transverse optic modes, which are propagated with longitudinal waves, is said to yield negative  $\gamma$  values at low temperatures. At these temperatures only acoustic vibrations are present, and the average value of  $\gamma$  can also become negative in which case the material possess negative  $\alpha$ . The large effect of the transverse modes in all these materials is due to open structure of these solids which result in large value of the shear elastic compliances associated with these modes. however, in NaCl, almost all the modes have positive  $\gamma$ .

On the other hand, anisotropic solids like  $\text{FeF}_2$ ,  $\text{RuO}_2$ ,  $\text{CrO}_2$  exhibit negative values of  $\alpha$  at high temperatures along one of the two principal directions. Therefore the explanation given above cases to have any sense in these materials. This may be understood probable in the same way as in the case of rutile. In rutile Kirby suggests that the thermal expansion arises from the contributions from the acoustic and optic modes such that optic modes are more effective in the c-direction whereas the acoustic modes are highly predominant along directions normal to the c-axis.

Negative values of  $\alpha$  found in a few metals, for example, chromium invar and galolinium, arise from magnetic interaction or the electron gas White, Klein and Mountain. White has presented a simple picture to explain qualitatively the occurrence of negative values of  $\alpha$  in crystal.

#### 4.4 Thermal expansion and Inver Anomalies

Inver anomalies starting at the Curie temperatures,  $T_c$ , as a result of the competition between the anharmonic phonon lattice THE and the exchange (spontaneous magnetostriction). In as much as the compound  $\text{Y}_2\text{Fe}_{14}\text{B}$  shows such an effect, and the anomaly starts at almost the same temperature mainly to the lattice dependence of the Fe-Fe pair exchange interaction. Noticeable is that for the  $\text{Nd}^{[4.2]}$  and Er compounds, weak anomalies are displayed in the THE coefficient at precisely the temperatures,  $T_{SR}$ , at which the spin reorientation transition starts.

Useful information about the spatial dependence of the exchange interactions can be obtained from the above anomalies. Therefore, in order to separate the lattice contribution (LC) from the magnetic one, we assume that the LC follows the simple Grüneisen law

$$\frac{\Delta l}{l} = K_G T^4 \quad 4.15$$

and in fact, we can observe that such dependence is extremely well followed in the paramagnetic regime. The values of the obtained  $K_G$  Grüneisen coefficients are given and as can be seen, they are similar for the whole series.

The difference between the extrapolated Grüneisen curve within the magnetically ordered region and the actual THE can be ascribed to the spontaneous exchange magnetostriction within the Fe sub-lattice. A mean-field model for magnetovolume effects in ferromagnetic transition metals has been developed by Shiga<sup>[4.2]</sup> and a modified version of it will be introduced here in order to explain our results. We assume that the exchange free energy, its strain-dependent part (per unit volume) and the elastic energy can be described by the expression,

$$F = F_{ex} + F_{el} = \sum_{i=1}^3 \left( n_{RR} + \frac{\partial n_{RR}}{\partial a_i} \Delta a_i \right) M_R^2 + \sum_{i=1}^3 \left( n_{RFe} + \frac{\partial n_{RFe}}{\partial a_i} \Delta a_i \right) M_R M_{Fe} \quad 4.16$$

$$+ \sum_{i=1}^3 \left( n_{FeFe} + \frac{\partial n_{FeFe}}{\partial a_i} \Delta a_i \right) M_{Fe}^2 + \frac{1}{2} \sum_{i=1}^3 C_i \left( \frac{\Delta a_i}{a_i} \right)^2$$

where the indexes  $I = 1, 2, 3$  refer to the  $a_1, a_2$  and  $a_3 \equiv c$  axes of the tetragonal structure,  $n_{ij}$  are the mean field (MF) exchange constants.  $M_i$  the sub-lattice average magnetizations and  $C_j$  the appropriate effective elastic constants. In a first stage, minimization of  $F$  will provide us with the equilibrium strains, the volume strain becoming

$$\omega = \sum_{i=1}^3 \left( \frac{\Delta a_i}{a_i} \right)_i = \sum_{i=1}^3 \frac{a_i}{C_i} \left( \frac{\partial n_{FeFe}}{\partial a_i} M_{Fe}^2 + \frac{\partial n_{RFe}}{\partial a_i} M_R M_{Fe} + \frac{\partial n_{RR}}{\partial a_i} M_R^2 \right) \quad 4.17$$

In obtaining equation (4.16), the assumption has been made that the Fe and RE sub-lattice magnetizations are lattice cell-size independent. This assumption is, in fact, an oversimplification because it does not take into account the volume dependence of the Fe magnetic moment,  $\mu_{Fe}$ , amounting for  $Y_2Fe_{14}B$ , to  $\partial(\ln \mu_{Fe})/\partial \omega \cong 0.18^{[4.4]}$ , which must be attributed to the increase in atomic volume. The latter is inherently associated with an increase in magnetic moment in itinerant ferromagnets. This constitutes a consequence of the lattice variation derived from the inner electronic pressure appearing within the itinerant electron magnetic system as the electron kinetic energy increases with the magnetization, due to the transfer of electrons to the majority sub-band<sup>[4.5]</sup>.

A solution of the series of equations in the  $\Delta a_i/a_i$  unknowns obtained from the minimization conditions  $\partial F/\partial(\Delta a_i/a_i) = 0$  is extremely complex, and therefore, owing to the afore-mentioned similarity of the Curie points for the whole series with the  $Y_2Fe_{11}B$  system, we will neglect, in the following calculation, the MF interactions  $n_{RR}$  and  $n_{RFe}$ , weaker compared with the dominant  $n_{FeFe}$  one. Therefore, if we assume that the Fe sub-lattice magnetization varies with the strain in the form

$$M_{Fe} = M_{Fe}(0) + \left( \frac{\partial M_{Fe}}{\partial a_i} \right)_{a_i^0} \Delta a_i \quad 4.18$$

where  $a_i^o$  is the paramagnetic lattice constant, it is easy to show that equation (4.16) transforms to

$$\omega = \sum_{i=1}^3 \frac{a_i}{C_i} \left[ \frac{\partial n_{FeFe}}{\partial a_i} M_{Fe}^2 + \left( \frac{\partial n_{RFe}}{\partial a_i} M_R + 2 \frac{\partial n_{FeFe}}{\partial a_i} \right) M_{Fe} + \frac{\partial n_{RR}}{\partial a_i} M_R^2 \right] \quad 4.19$$

where  $\partial M_{Fe} / \partial a_i = \text{const} + N_{Fe} (\partial \mu_{Fe} / \partial a_i)$ ,  $N_{Fe}$  being the number of Fe atoms per unit volume.

This means that we should expect a dependence of the spontaneous magnetostriction with  $M_{Fe}$  including quadratic and linear terms.

In accord with the previous discussion we have scaled  $\omega$  against the reduced magnetization,  $m_{Fe} = M_{Fe}(T)/M_{Fe}(0)$ , of the Fe sub-lattice alone, taking for this the  $Y_2Fe_{14}B$  magnetization<sup>[4,6]</sup>. In figures 3a and b we have plotted the thermal dependence of the magnetic contribution to the THE superposing on it the dependence of  $m_{Fe}^2(T)$  alone. The agreement is reasonable, giving support to the previous assumption of ascribing the spontaneous volume striction essentially to the Fe sublattice. The values of the quantities proportional to the strain derivatives,  $\sum_i (1/C_i) (\partial n_{FeFe} / \partial \ln a_i)$ , for the Fe-Fe, exchange interactions. The values obtained are not too different, indicating a similar strain dependence for the Fe-Fe exchange interaction along the series as could be anticipated.

However, a fit of the spontaneous volume striction,  $\omega$ , versus the reduced magnetization,  $M_{Fe}$ , according to equation (4.19) also gives excellent results, as can be observed, indicating the presence in  $\omega$  of a linear term in  $M_{Fe}$  as well, the result of the lattice constant dependence of the MF  $n_{RFe}$  exchange interaction plus the Fe magnetic moment strain dependence. The values of the fitting parameters to an expression of the form.

$$\frac{\omega(T)}{3} = K_{FeFe} m_{Fe}^2 + K_{RFe} m_{Fe} + K_{RR} \tag{4.20}$$

where the correspondence with the coefficients in equation (5) is immediate. Except for the Pr compound, all of them are correspondingly similar, again indicating a similar strain dependence of the MF  $n_{ij}$  exchange constants and, probably, of  $\partial \mu_{Fe} / \partial a_i$ . Plots of  $\omega/m_{Fe}(T)$  versus  $m_{Fe}(T)$  give, in fact, good straight lines for all the compounds.

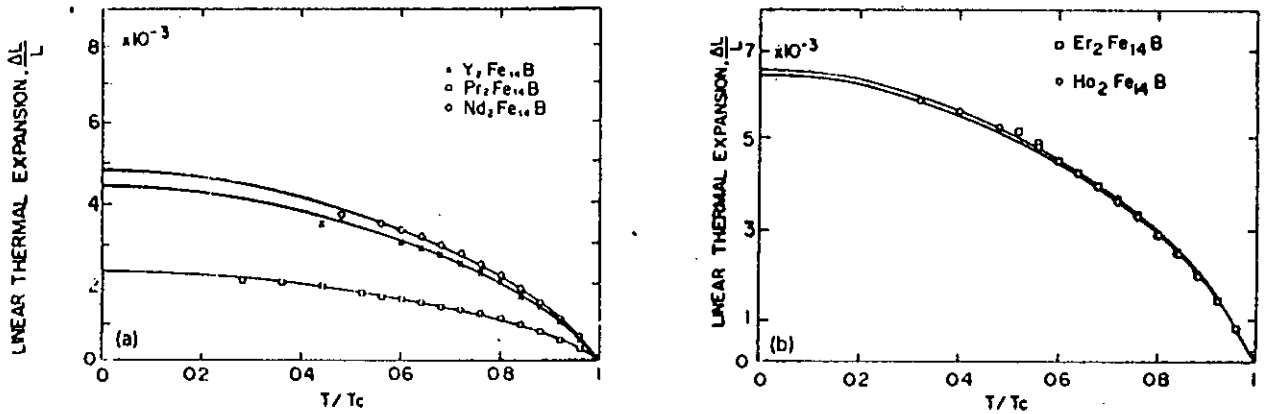


Fig.4.2 Linear thermal expansion,  $\Delta l/l$ , vs. the reduced temperature  $T/T_c$  ( $T_c$  is the Curie temperature) for the  $RE_2Fe_{14}B$  series. The lines are the theoretical fits by  $\omega = \sum_i (a_i / C_i) (\partial n_{FeFe} / \partial a_i) M_{Fe}^2$



**CHAPTER - 5**

## 5.1 Magnetostriction Measurement Technique

Depending on what aspects of the magnetostriction interaction one is going to investigate, one can choose from the various experimental techniques that has been developed. For static magnetoelastic interaction measurement, one can use X-ray<sup>[5.1]</sup> three terminal capacitance diameter<sup>[5.2]</sup> optical and mechanical levels<sup>[5.3]</sup> or electrical resistance strain gauge<sup>[5.4]</sup>.

To determine the strength of the spin-phonon coupling in dynamic magnetoelastic interaction, we can measure the absorption of microwave phonons, low temperature thermal conductivity of otherwise pure metal doped with magnetic impurities, inelastic neutron scattering broadening of ferromagnetic resonance line width or Mossbauer effect under stress to the rotation of magnetization. Vibrating reed technique can be used to measure magnetomechanic pole effect specially in amorphous ribbons<sup>[5.5]</sup> and to measure magnetomechanical coupling factor, impedance measurement of the existing coil can be done<sup>[5.6]</sup>.

Here the magneto-mechanical coupling factor  $K$  is related to the elastic energy  $U_E$  and the magnetic excitation  $U_m$  by the relation

$$K^2 U_m = (1 - K^2) U_E \quad 5.1$$

This technique, since the time of its introduction by Goldman<sup>[5.7]</sup> has gradually replaced almost entirely all other methods of magnetostriction measurement. The reason for this successes, as also the problems associated with this method and use of this technique as developed by Asgar<sup>[5.8]</sup> are as follows:



Magnetostriction measurements are set with a large number of problems, strain develops in a magnetic specimen when magnetized. This small strain is dependent both on the direction of magnetization and its magnitude. Also the state of zero average external magnetization may not correspond to the zero magnetic strain, because the demagnetized multidomain state is neither unique nor well defined.

In the displacement method Nazaoka<sup>[5.3]</sup> combined optical and mechanical method. Here the specimen, by the displacement of its free end, the other end being fixed, rotates a spindle to which a mirror is attached.

The difficulty with this method is that one has to use a big specimen to get sufficient sensitivity. Again it is difficult to magnetize a big specimen in different direction using rotating field maintained at uniform field and steady temperature. Again this method can not provide the strain difference of two well defined magnetic states and one has to assume equal distribution of the domains in all the easy direction of magnetization in the demagnetized state, which may not be true.

The X-ray diffraction technique which was first used by Rooksby and Willis<sup>[5.9]</sup> to determine spontaneous magnetostriction, measures the distortion of crystal axes by determining directly splitting of X-ray reflection spots from different crystal planes.

However, X-ray diffraction method besides being less sensitive is difficult to use with different directions of magnetization. In using strain gauge technique one can get over many of these difficulties. The gauges can be used on a very small

disk shaped specimen cut in a definite crystallographic plane and the gauge can be bonded in a precisely determined direction.

The strain gauge works on the principle that when a fine wire in the form of a grid or a thin foil, and embedded in a paper or epoxy film is bonded firmly on a specimen and shows a change in resistance proportional to the strain.

We can write then relation as

$$\frac{dR}{R} = G \frac{dL}{L} \quad 5.2$$

where  $\frac{dR}{R}$  is the fractional change in resistance, G is the gauge factor and  $\frac{dL}{L}$  is the strain along the gauge direction.

The magnetic strain in the crystal is determined from the change in resistance of the gauge fixed on the specimen in relation to the resistance of another dummy gauge bonded on a reference specimen using a resistance bridge in the out of balance.

The mechanics of resistance change of the gauge wire under strain can thus be quite complex. Moreover, the gauge may not follow the strain of the material of which it is bond. Thus there is a affected bonding factor. In addition one has to consider the thermally induced resistance change, when the dummy and active gauges are at different temperature. The most important difficulty with the use of strain gauge is dummy gauge on a suitably chosen non magnetic materials which have the same thermal and thermoelastic properties as the magnetic material. This ensures that the dummy and the active gauges are subjected to the same strain and temperature except for the magnetic strain.

## 5.2 Strain Measurements Using Strain Gauge

In 1947 Goldman was the first to measure magnetostriction by the use of strain gauge a folded metal wire, which can have a resistance of the order of 100 ohms.

The strain gauge technique is based on the fact that any strain characteristic of the specimen on which the gauge is affixed is transmitted faithfully to the electrically sensitive zone of the gauge and is observed as a resistance changes which can be measured with the help of Wheatstone bridge. When the temperature of the specimen is changed there is a further contribution to the resistance change due to thermal expansion of the gauge wires, the gauge matrix, the bonding glass specimen and the resistivity change and the change in gauge factor of the gauge materials. Similar strain gauge known as dummy gauge is in the other arm of Wheatstone bridge to compensate as far as possible for temperature influence.

The measurement can be carried out with direct current or low frequency alternating current ( $f < 100$  c/s) since the magnetic material to which the current carrying wires are affixed can give rise to an inductive effect which changes during magnetization. This method is also very sensitive, being capable of measuring strains up to  $10^{-8}$ . The minimum dimensions of strain gauges are approximately 2mm. Additional errors that can occur in this measurements is magnetoresistance of the wire. At room temperature this is not greater than  $10^{-7}$ .

When more than one strain gauge (active and dummy) is used in a Wheatstone bridge circuit, this effect is approximately eliminated if care is taken to ensure that all the strain gauges are in the same magnetic field.

### 5.3 Gauge Factor

It is observed experimentally that the resistance of a thin wire varies proportionately to the strain to which it is subjected, provided the temperature is constant and the applied strain is small. This factor of the wire as the fractional change in resistance per unit strain

$$\text{i.e. } G = \left( \frac{\Delta R}{R} \right) / \left( \frac{\Delta L}{L} \right) \quad 5.3$$

### 5.4 Experimental Set up for Measurements of Magnetostriction

The experimental set up consists of a strain sensing device, i.e. strain gauges, D.C. bridge for strain measurements, D.C. amplifier, electromagnet to produce the magnetic field, A specimen holder with an arrangement for rotating the specimen in the magnetic field by definite angles.

### 5.4.1 The D.C. Bridge

A D.C. Wheatstone bridge is slightly out of balance condition measured the fractional change in resistance in the active gauge. The components of the bridge are shown in figure 5.1. When the resistance of the active gauge was changed from  $R$  to  $R + \Delta R$ , a corresponding out of balance voltage developed across the input of the D.C. amplifier. The out put of the amplifier is recorded.

### 5.4.2 The D.C. Amplifier

To measure the small out of balance D.C. voltage, the Model 140 nanovoltmeter was used, which acted as a potentiometric amplifier and had a sensitivity of 0.1 micro-volt for full-scale deflection in the highest sensitivity range. A panel switch selector permitted the meter sensitivity to be altered. Any A.C signal super imposed on the D.C. voltage to be measured was almost entirely attenuated, the filtering factor being inversely proportional to the frequency. The zero drift was less than  $0.1 \mu\text{V}/\text{hour}$  when all sources of thermo E.M.F were reduced by using low thermal solders and protecting the metallic junctions from thermal fluctuations.

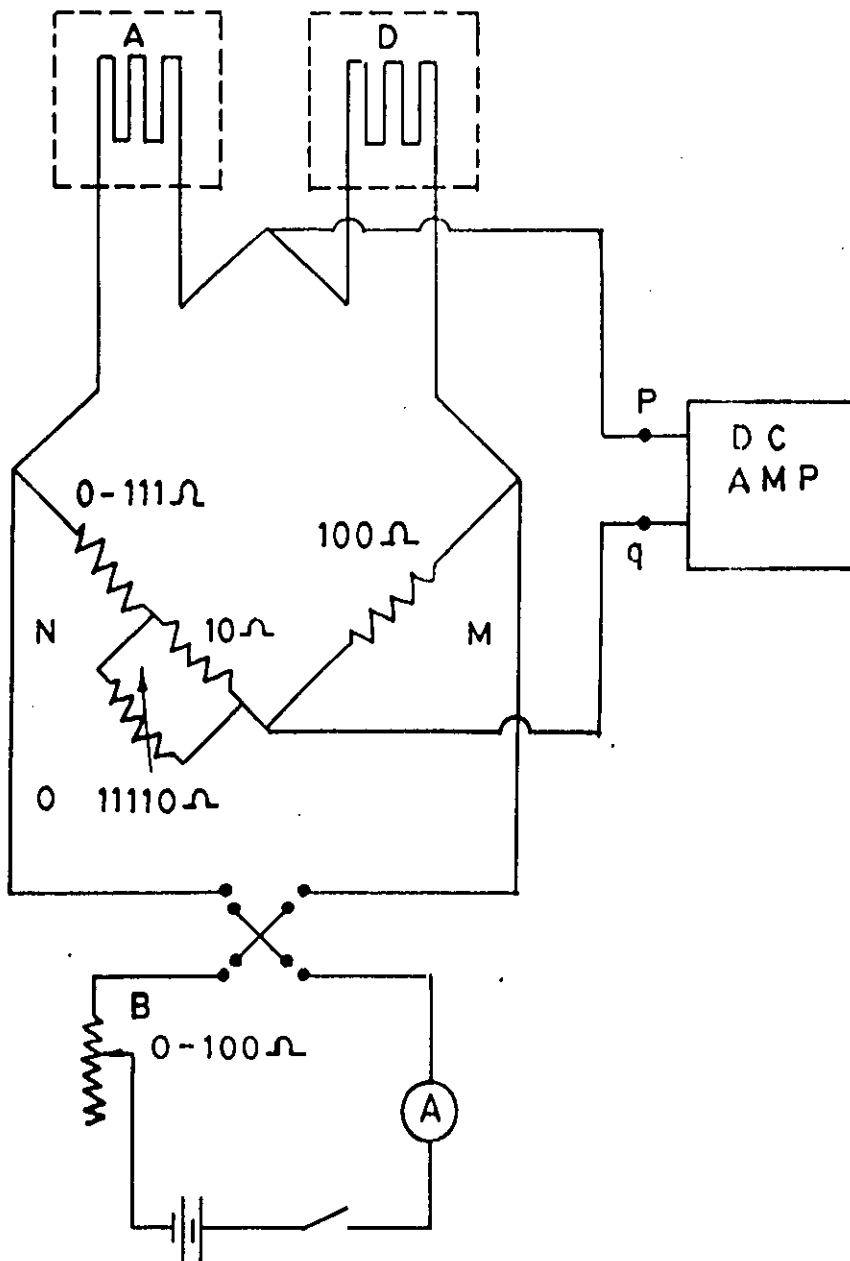


Fig 5.1: D.C. Bridge

### 5.4.3 Low temperature measurement technique

By the same way for measuring magnetostriction at room temperature with the strain gauge technique method and with the Wheatstone Bridge we measured the magnetostriction at liquid nitrogen temperature. We also measured the thermal expansion by equation

$$\alpha = \frac{\frac{\Delta l}{l}}{\Delta T} \quad 5.4$$

where  $\frac{\Delta l}{l}$  is the thermal strain and  $\Delta T$  is the temperature difference.

### 5.5 Bridge current sensitivity and calibration of the D.C. Bridge

The current in the D.C. Bridge circuit, in terms of the parameters of the bridge shown in figure (5.1) is

$$I_g = \frac{E}{\left(B + D + A + \frac{BD}{M}\right)\left(Z + N + A + \frac{ZN}{M}\right)} \times \left(\frac{\Delta A}{1 + K\Delta A}\right) \quad 5.4.1$$

where

$$K = \frac{M(D + Z) + (B + N)(B + D + Z)}{M\left(B + D + A + \frac{BD}{M}\right)\left(Z + N + A + \frac{ZN}{M}\right)}$$

Equation (5.4.1) is an exact algebraic solution for  $I_g$  where the circuit on the right hand side of points PQ has been treated as a current measuring device of input resistance  $Z$ . Since the bridge is only slightly unbalanced  $K\Delta A \ll 1$  and the factor  $(1 + K\Delta A)$  can be replaced by unity. Also, since the input resistance of the measuring unit is of the order of one mega-ohm, we can put  $Z \rightarrow \alpha$  in equation

(5.4) and obtain the expression for the maximum voltage sensitivity corresponding to  $B = 0$  close to the balance condition of the bridge as

$$x = \left( \frac{\Delta I_g}{\Delta A} \right)_o \approx \frac{ED}{(D + A)^2} \quad 5.5$$

In our bridge  $D$  represents the resistance of the dummy gauge and  $A$  that of the active gauge. Both have the same value of 350 ohm in the unstrained condition. Thus the fractional change in resistance can be written as

$$\frac{\Delta A}{A} = \frac{\Delta Z \Delta I_g}{E} \quad 5.6$$

Thus the out of balance voltage  $Z\Delta I_g$  measured by the recorder maintains a linear relationship with  $\frac{\Delta A}{A}$  giving a constant sensitivity. The deviation from linear relationship will only occur if the condition  $1 + K\Delta A = 1$  does not hold. It can be shown that the fractional error 0.01%. The bridge was calibrated by changing the resistance parallel to the 10 ohms resistor in the arm N of the bridge. The minimum voltage that could be measured without noise and drift was of the order of  $10^{-6}$ . The gauge factor of the strain gauge we used was ( $\approx$ ) 2.02 as supplied by the manufacturer and the voltage supplied to the bridge was two volts. Thus maximum strain sensitivity was the order of  $10^{-6}$  from equation (5.6). the sensitivity of the bridge could be increased further either by increasing the current in the circuit or by using higher gain in the amplifier. The upper usable unit was determined by the maximum allowable joule heating in the gauges and the signal-to-noise ratio.

For minimizing the noise, all the connections were made with co-axial cables, so that all parts were screened.



## **5.6 The Choice of Dummy Material**

The identical behavior of the active and dummy gauges is the basic necessity for justifying the use of a compensating gauge for all strain measurements. The nearest approach to this condition can be made by subjecting the two gauges to identical strain and thermal conditions used fused silica, glass as dummy material for its negligible thermal expansion coefficient.

## **5.7 The Specimen Holder**

It is very important to keep the temperature of the specimen and the dummy identical for accurate measurements. Any difference in the thermal environment of the active and dummy gauges affects the result drastically.

To keep the gauges in the same thermal environment a cylindrical shaped specimen holder was made as shown in figure 5.2. It was made from a copper rod of 16 mm diameter. Two identical grooves of approximate thickness 7 mm and width 10 mm were cut separated by a thin section of width 2mm. This arrangement made it assemble to keep the active and dummy specimens as close as possible.

The specimen and the dummy were fixed on the opposite faces of the thin section. Two identical strain gauges one on the face of the active specimen and the other on the dummy specimen were glued. Electrical connections from the gauges were taken out through the hole of 2 mm diameter made in the centre

specimen holder. The thinner section of the specimen holder of diameter 8 mm and length was attached to a copper hollow cylindrical rod of internal bore of 8mm in diameter. This copper hollow rod is then hung from the rotator. A copper hollow tube of 16 mm internal diameter was used as a jacket to keep the active and the dummy at same temperature and to isolate them from thermal fluctuations. The arrangement was found to be quite satisfactory.

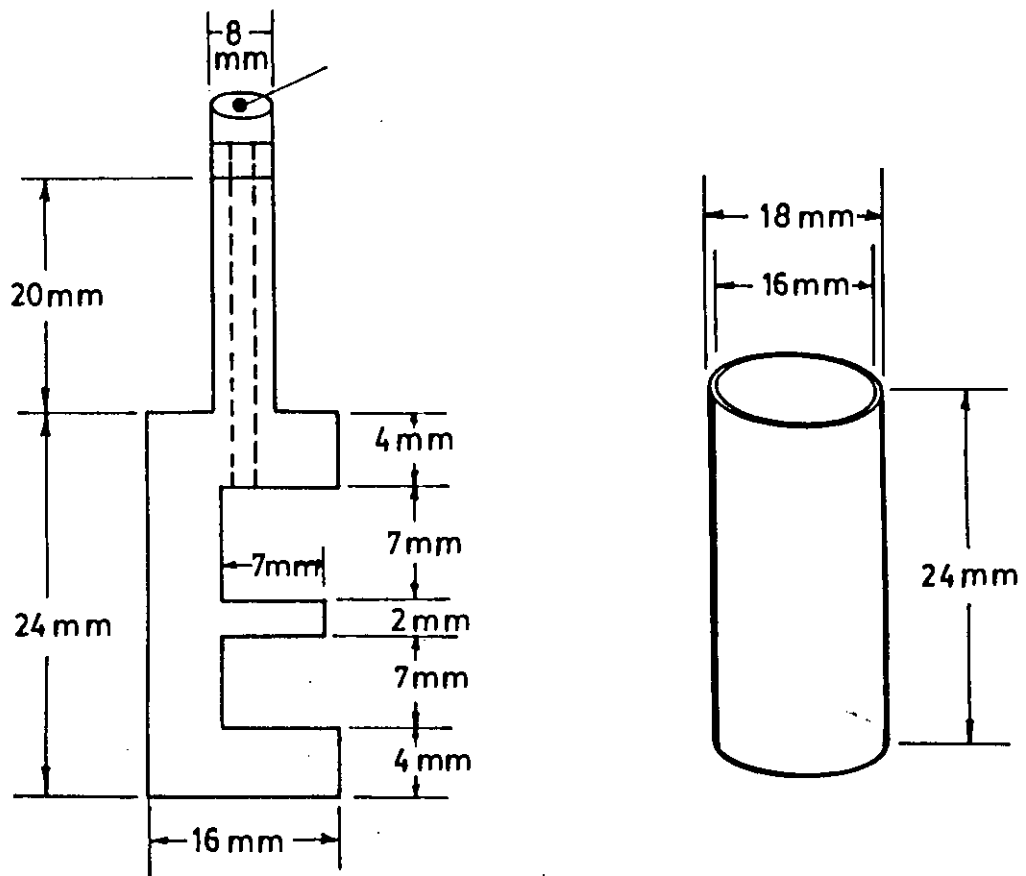


Fig. 5.2: Specimen holder

### **5.9 Specimen mounting**

The mounting of the specimen in the specimen holder has to be flexible in order that the specimen can freely change in dimension. At the same time to avoid any rotation of the specimen due to torque produced by the magnetic field, the specimen must be held sufficiently rigid. The best compromise is made by using a thin cork spacer between the specimen and the base of the specimen holder. The specimen is glued to the cork by Durofix and the cork in turn to the specimen holder. The mosaic pattern of the cork spacer allows the specimen to expand or contract quite freely but constrains it from rotation due to body forces. Comparison of thermal expansion of a brass specimen when fixed to a cork spacer and when free showed that the constraint due to the above mentioned arrangement does not effect the result.

### **5.9 The Gauge Cementing**

For perfect gauge bondage between the gauge and the surface of the specimen it is necessary to have very fine scratches on the gauges and specimen surfaces. The specimen surface is naturally left with fine irregularities of six micron order. The gauge is enclosed in a paper jacket which provides both insulation and protection. The paper base also provides good bonding surface for the gauge on to the specimen.

A thin coat of Durofix was applied to the gauge surface and the gauge area of the specimens. Then the gauge was placed on the specimen surface and the small pressure was applied on the gauge. The adhesive was cured for 24 hours at room temperature.

### 5.10 Calibration curves for magnet

The electromagnet that used for the measurement of magnetostriction calibrated with electronic fluxmeter to an accuracy of about  $\pm 1\%$ . A conventional calibration of current, I vs field strength, H is shown in fig-5.3

### 5.11 Bridge current sensitivity and calibration

The current used for measurement of the resistance changes in the gauges was a D.C Wheatstone Bridge figure 5.1. It was included a reversing switch(s) to ascertain to what extent thermal E.M.F's into the circuit were effecting the nano-voltmeter used was a Model 140 of high sensitivity and a period of 2.5 seconds. This low periodic time of the instrument enabled quick recording of out-of-balance deflections thus minimizing errors due to drift and fluctuations from thermal E.M.F's in the circuit. The bridge sensitivity changes linearly with bridge current Fig.5.4 and Fig 5.5. Bridge current was restricted to a maximum of 25 mA to prevent overheating in the gauge elements.

The components of the bridge are shown in figure 5.1 where A represents the active strain gauge in contact with the specimen and D represents the dummy gauge in the same environment as the active gauge. Any thermal fluctuations which occurred in gauge A also accurate in gauge D and since these are in opposing arms of the bridge, the net effect of the fluctuations should be zero. Work on the bridge arrangement is to continue and it is hoped to amplify small D.C out put voltages from the bridge when measuring very small strains to record the nanovoltmeter scale deflection. Also slow steady thermal drifts would be recorded and allowance made for these in the calculation of results.

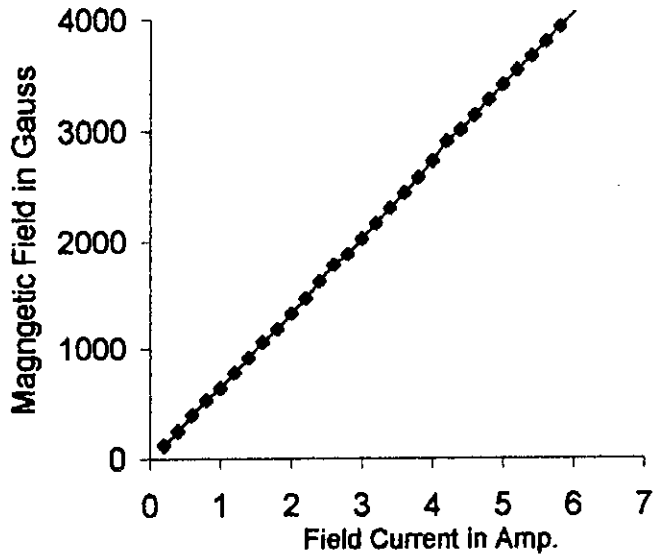


Fig. 5.3: Current vs Magnetic Field

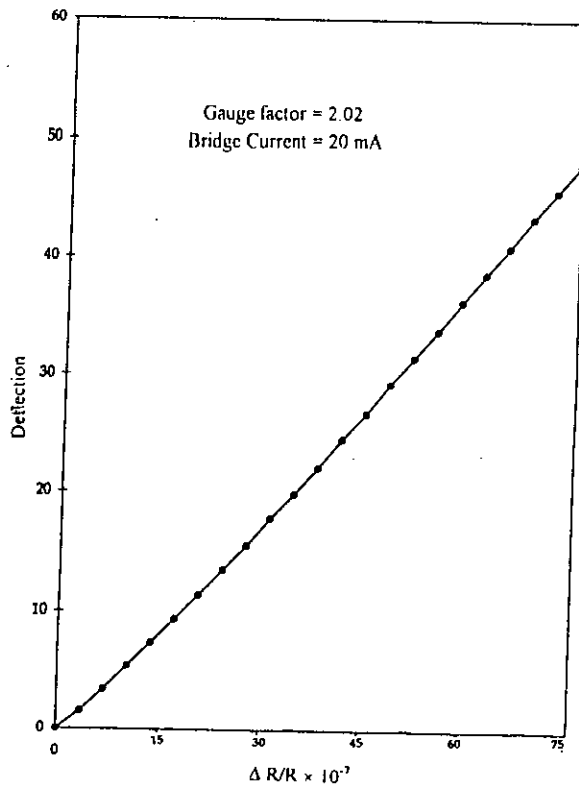


Fig. 5.4: Bridge Sensitivity

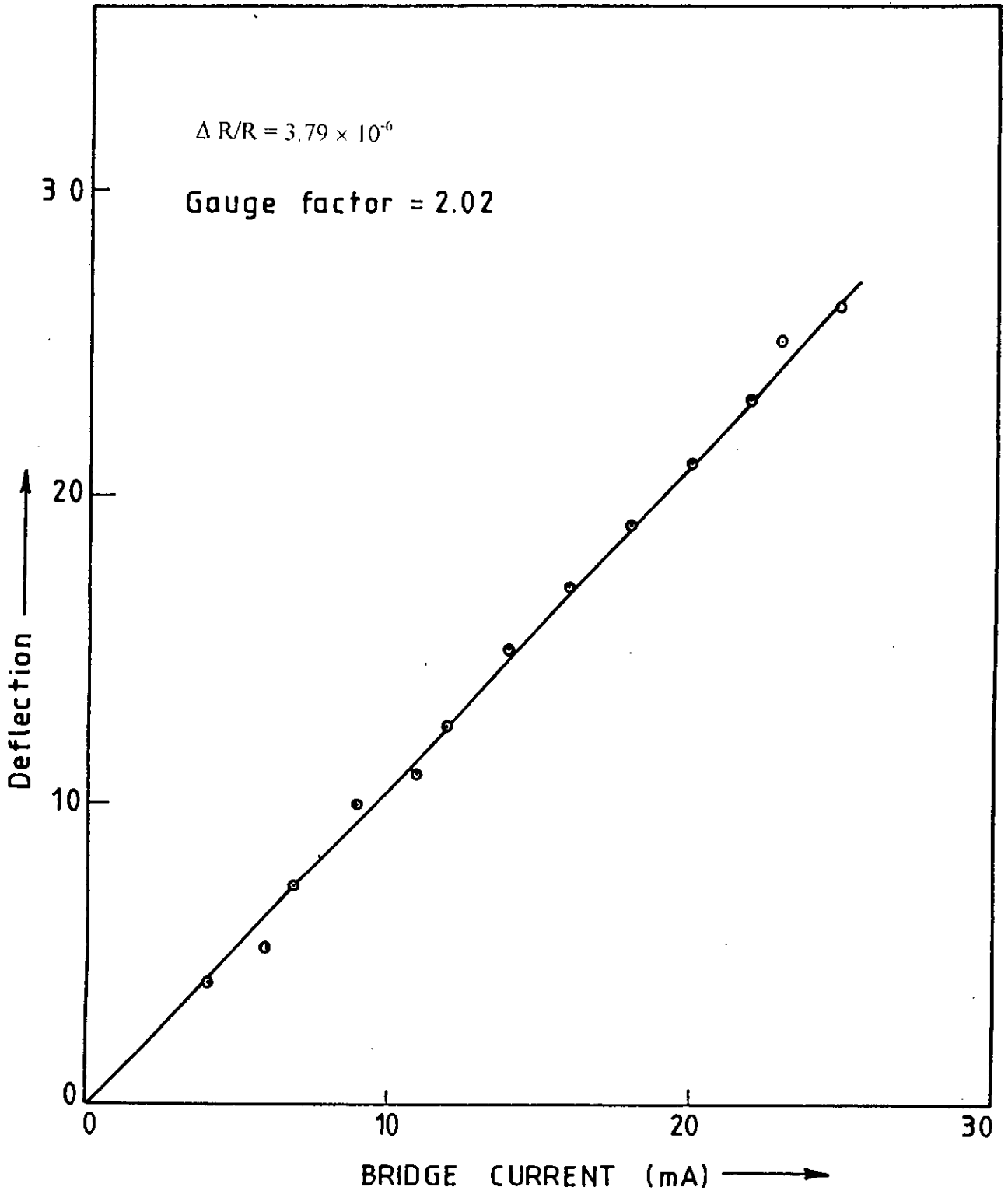
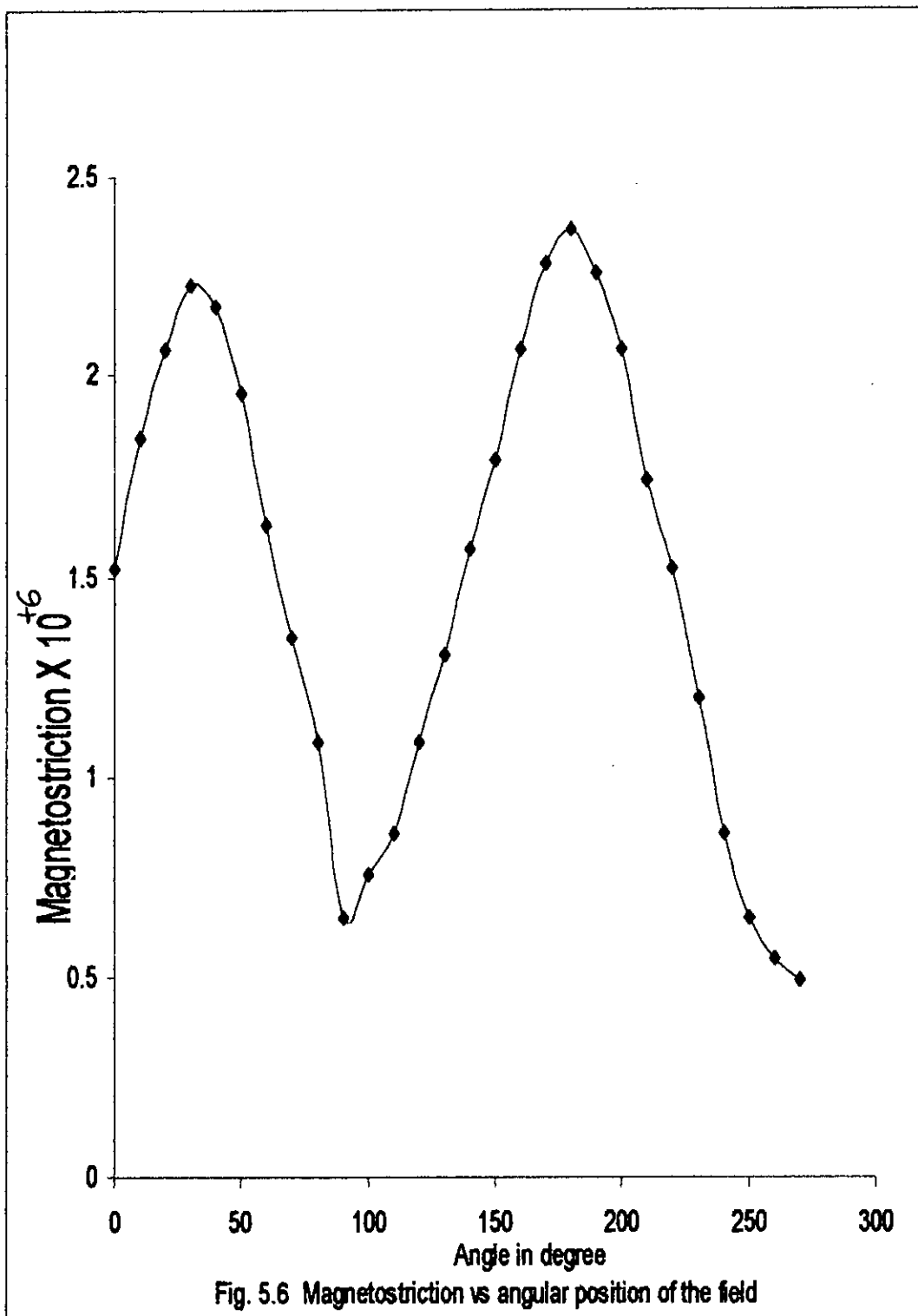


Fig. 5.5: Variation of bridge sensitivity with bridge current

### 5.12 Calibration curve for angle correction

In an amorphous ribbon the magnetic domains of the different micro-crystallites having random orientation make different angles with each other in the demagnetized state. When the magnetic field is applied the magnetic domain wall movement starts. In the initial state due to  $180^\circ$  domain wall movement no contribution is there to the net strain of the amorphous ribbon specimen, because the reversal of the direction of magnetization has no effect on the elongation of the domain. In the second state with increased magnetic field the  $90^\circ$  domain wall movement begins. This gives rise to magnetostriction i.e. changing lattice dimension which in our case is positive. This magnetostriction effect can be looked at as due to predominance of the strain axes in the direction of the measurements. The angle vs magnetostriction curve is shown in figure 5.6. The angle vs magnetostriction curve showed a minimum at  $90^\circ$  and a maximum at  $180^\circ$ . The minimum at  $90^\circ$  is identified as the O-position of magnetic field with respect to the gauge direction and the maximum at  $180^\circ$  is identified as the  $90^\circ$  position of the field with respect to the gauge direction.







**CHAPTER - 6**

## **Results and Discussions on Co-based Amorphous Ribbon**

### **6.1 Field Dependence Magnetostriction of Co-based Amorphous Ribbon**

Magnetostriction of the Co-Fe-B-Si system of composition  $Co_{80-x}Fe_xB_{10}Si_{10}$  [ $x = 2, 4$  and  $6$ ] have been measured using strain gauge technique. Each specimen was subjected to increasing applied field and the differential magnetostriction was measured due to rotation of the magnetic field from parallel to the perpendicular position of the field with respect to the direction for the strain gauge. There is a minimum field needed for saturation magnetostriction for each specimen. The macroscopic magnetostriction representing the fractional change in length of a specimen is related to the macroscopic magnetoelastic constant which is considered as an average over the local elastic contribution. Magnetostriction is measured using the relation

$$\frac{\Delta R}{R} = G \frac{\Delta l}{l} \quad 6.1$$

where  $\frac{\Delta R}{R}$  is the fractional change in resistance,  $G$  is the gauge factor and  $\frac{\Delta l}{l}$  is the strain along the gauge direction. This technique is developed by Goldmann<sup>(6.1)</sup> Lee and Asgar<sup>(6.2)</sup> and others.

Assuming that the amorphous materials can be treated in the same way as polycrystals in respect of the distribution of the strain axes, the linear magnetostrictive strain can be written as

$$\lambda = \frac{3}{2} \lambda_s \left( \cos^2 \theta - \frac{1}{3} \right) \quad 6.2$$

where  $\theta$  is the angle between the direction of the applied field and hence magnetization, and  $\lambda_s$  represents the saturation magnetostriction constant. By

rotating the magnet from perpendicular to the parallel position with respect to the strain measuring direction, we find

$$\lambda_s = \frac{2}{3}(\lambda_{\parallel} - \lambda_{\perp}) \quad 6.3$$

In order to find the exact direction of the strain-measuring gauges, which was carefully bonded on the specimen along the length of the preparation of the specimen, with respect to the direction of magnetization, magnetostriction as a function of position of the field was measured. The direction of the field was initially obtained arbitrarily with respect to the circular scale at the base of the rotating magnet. From the graph of strains Vs field direction is obtained as shown in figure 6.3.

The exact direction of the gauge related to the field was determined. This was done by using the principle mentioned on reference 6.3, where we find that the maximum differential change in strain occurs when the magnetization vector is rotated by  $90^{\circ}$  from the position which is parallel to the gauge direction to the direction which is perpendicular to it.

It is assumed that for sufficiently high field the direction of the field also corresponds to the direction of the saturation magnetization. The magnetostriction of these Co-Fe-B-Si ribbons with composition  $Co_{80-x}Fe_xB_{10}Si_{10}$  [ $x = 2, 4$  and  $6$ ] in as quenched condition is measured, using a strain gauge technique. The magnetostriction of the Co-based amorphous ribbons with different fields are shown in figure 6.1. This field appears to be large enough for the soft amorphous magnetic Co-Fe-B-Si system. This applied field is also much larger than the effective internal field due to the demagnetizing effect, which is

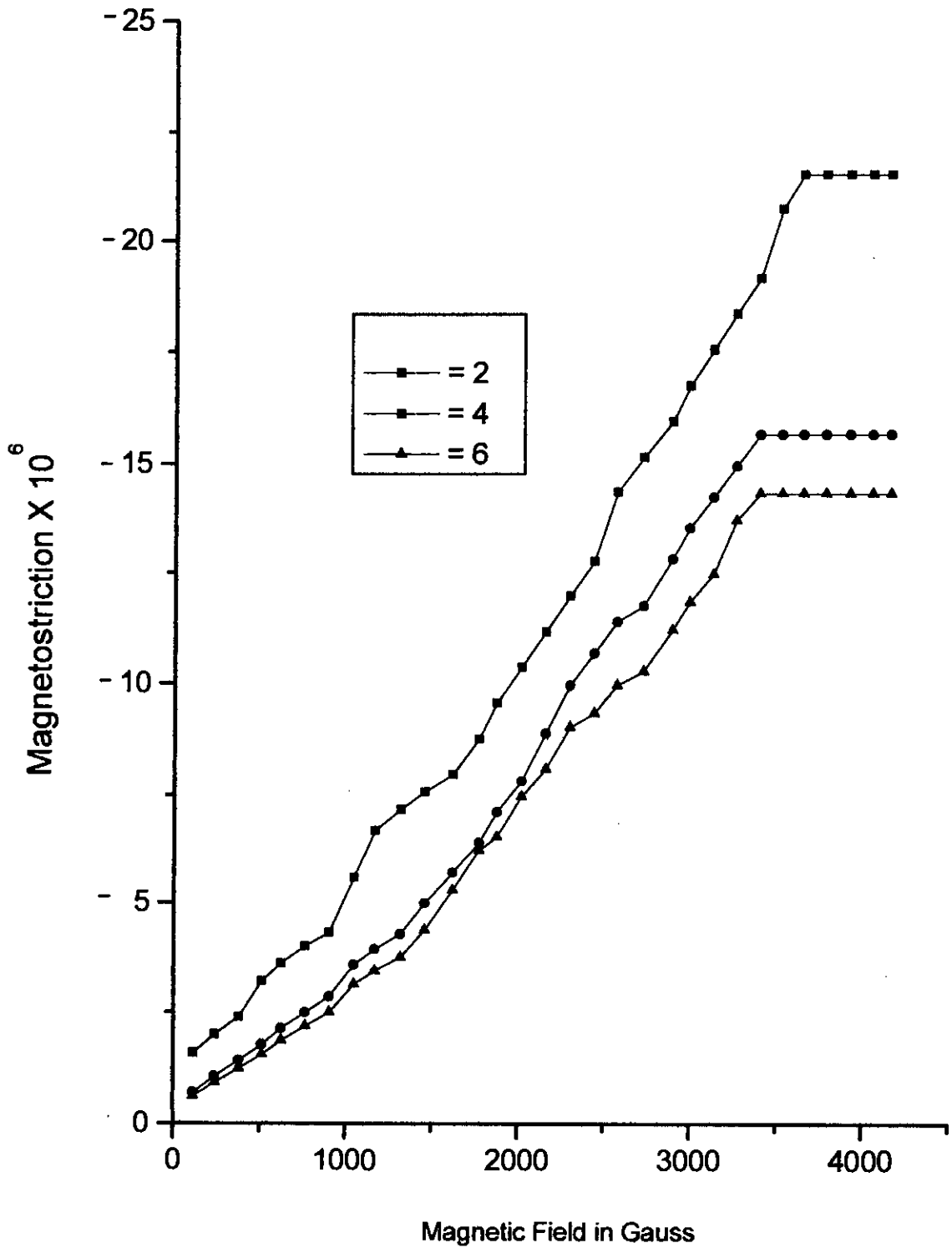


Fig. 6.1: Magnetic field vs magnetostriction of amorphous ribbon with compositions  $\text{Co}_{80-x}\text{Fe}_x\text{B}_{10}\text{Si}_{10}$  at room temperature

## Results and Discussions

necessary condition for saturation magnetization. In order to find the saturation magnetization we only need to measure the strain due to saturation magnetization along the length of the gauge by magnetizing the specimen to saturation value of 3.4 to 3.6 kilogauss. In the direction perpendicular to the gauge and then in the direction parallel to the gauge. By subtracting of the former from the later we obtain the saturation magnetostriction constant using the equation (6.3). Each measurement was taken three times with practically no deviations. After saturation was reached at 3.4 to 3.6 kilogauss, the field was increased in steps up to 4.16 kilogauss. No change in magnetostriction value was observed with increasing field.

The saturation magnetostriction ( $\lambda_s$ ) and saturation field ( $H_s$ ) for different samples as calculated are shown in Table 1.

**Table – 1**

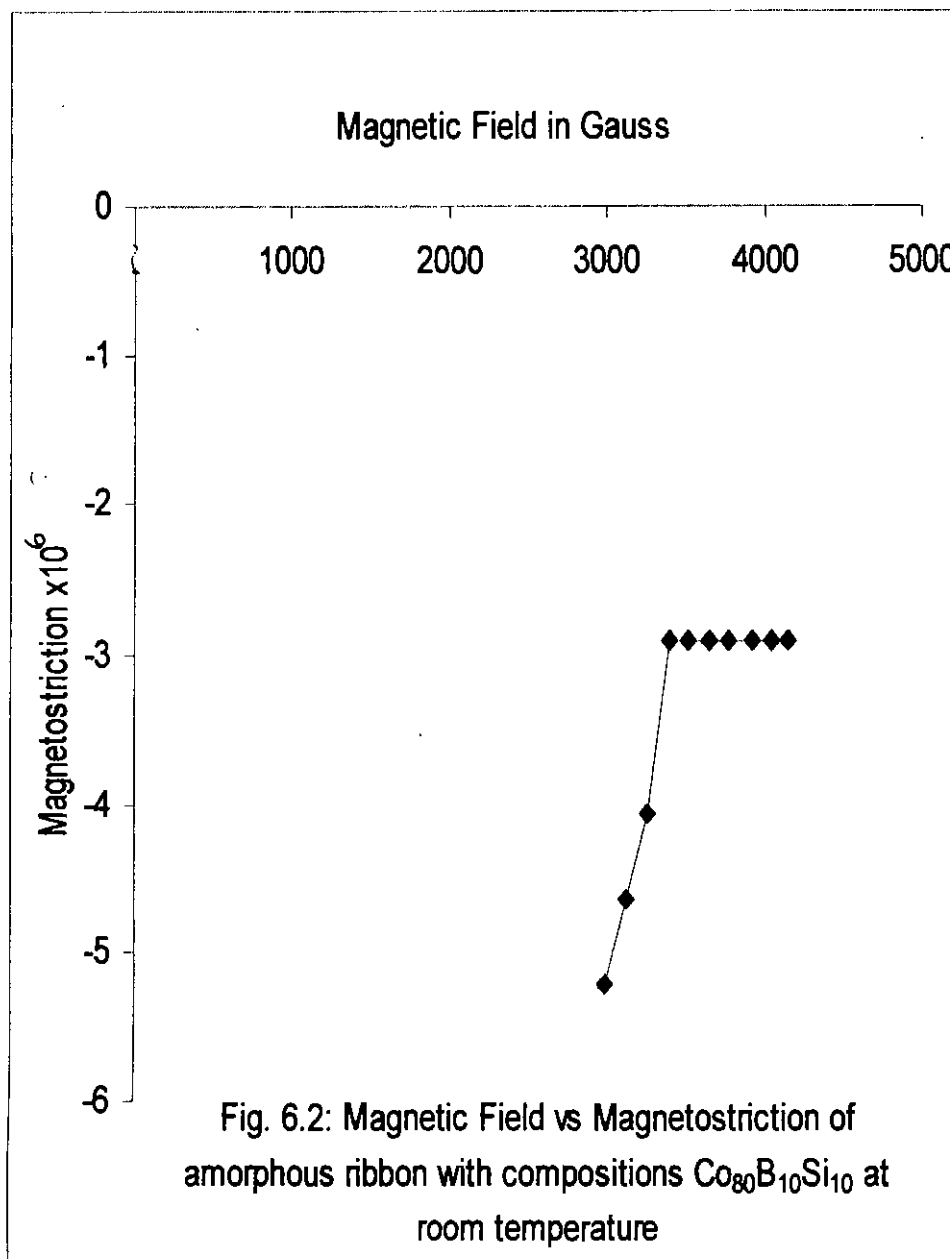
| $Co_{80-x}Fe_xB_{10}Si_{10}$                      | $x = 0$                 | $x = 2$                  | $x = 4$                  | $x = 6$                  |
|---|-------------------------|--------------------------|--------------------------|--------------------------|
| $\lambda_s$ at room temperature                   | $-2.904 \times 10^{-6}$ | $-21.519 \times 10^{-6}$ | $-15.646 \times 10^{-6}$ | $-14.308 \times 10^{-6}$ |
| $H_s$ in kilogauss at room temperature            | 3.4                     | 3.65                     | 3.4                      | 3.4                      |
| $\lambda_s$ at liquid nitrogen temperature        | $-4.356 \times 10^{-6}$ | $-26.301 \times 10^{-6}$ | $-21.336 \times 10^{-6}$ | $-16.174 \times 10^{-6}$ |
| $H_s$ in kilogauss at liquid nitrogen temperature | 2.58                    | 3.92                     | 3.78                     | 3.4                      |

Magnetostriction versus applied fields for positive magnetostriction alloy are displayed in figure 6.1. The minimum value of the saturation magnetostriction measured for the sample of composition  $Co_{76}Fe_6B_{10}Si_{10}$  is  $-14.308 \times 10^{-6}$  and the maximum  $-21.519 \times 10^{-6}$  for 2% Fe. There is evidence of a decrease in magnetostriction of the samples as it passes through the zero magnetostriction composition. The saturation magnetostriction is a material parameter, whereas

## *Results and Discussions*

the longitudinal magnetostriction is essentially a convolution of the saturation magnetostriction and the initial domain orientation of the sample. A connection could be made between the two quantities if the initial domain orientation of the sample were known. Specifically, if the initial domain distribution were random, then the two quantities would be equal and the two sets of data could be compared directly. The behavior of the magnetostriction versus composition curves for the  $Co_{80-x}Fe_xB_{10}Si_{10}$  metallic ribbons is shown in figure 6.1. The rate of decrease of magnetostriction with Fe content and apparent decrease in slope near the zero-magnetostriction composition is shifted to a slightly higher Fe content at 6% Fe. Thus the interpretation of the graph indicating magnetostriction as a function of field is only qualitative except at the saturation magnetostriction, observed value of shown in table-1. Figure 6.2 shows the magnetostriction of  $Co_{80}B_{10}Si_{10}$  as a function field. The saturation field is found to be 3.4 kilogauss. This field appears to be large enough for the amorphous magnetic Co-B-Si system magnetostriction versus field curves are shows negative magnetostriction alloy are displayed in figure 6.2. The measurement at room temperature of the composition  $Co_{80}B_{10}Si_{10}$  and have obtained the following value  $\lambda_s = -2.904 \times 10^{-6}$  for the as-cast sample. The increase of  $\lambda_s$  with magnetic field is associated with negative for Co-rich alloys. The magnetostrictive effects originate from the local strains which correlate  $\lambda_s$  and  $\omega_s$  to the local atomic arrangement. This leads to a strong negative interaction of these properties on the melt-spun technique parameters for Co-based amorphous ribbon.

Co-Fe-B-Si amorphous ribbons are of special interest because these magnetic system, with a high percentage of Co having negative magnetostriction and with small amounts of Fe having positive magnetostriction, are expected to behave as

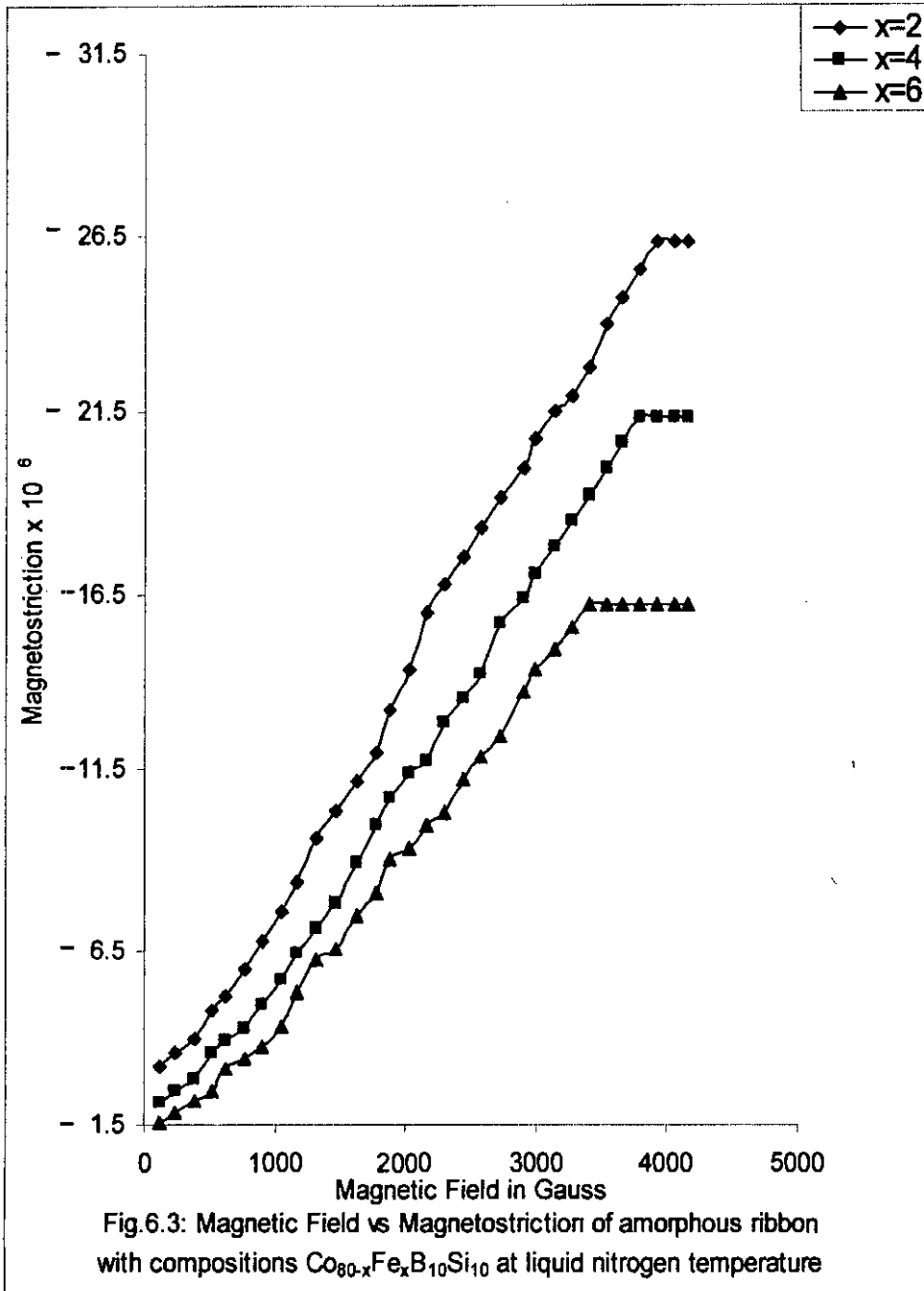


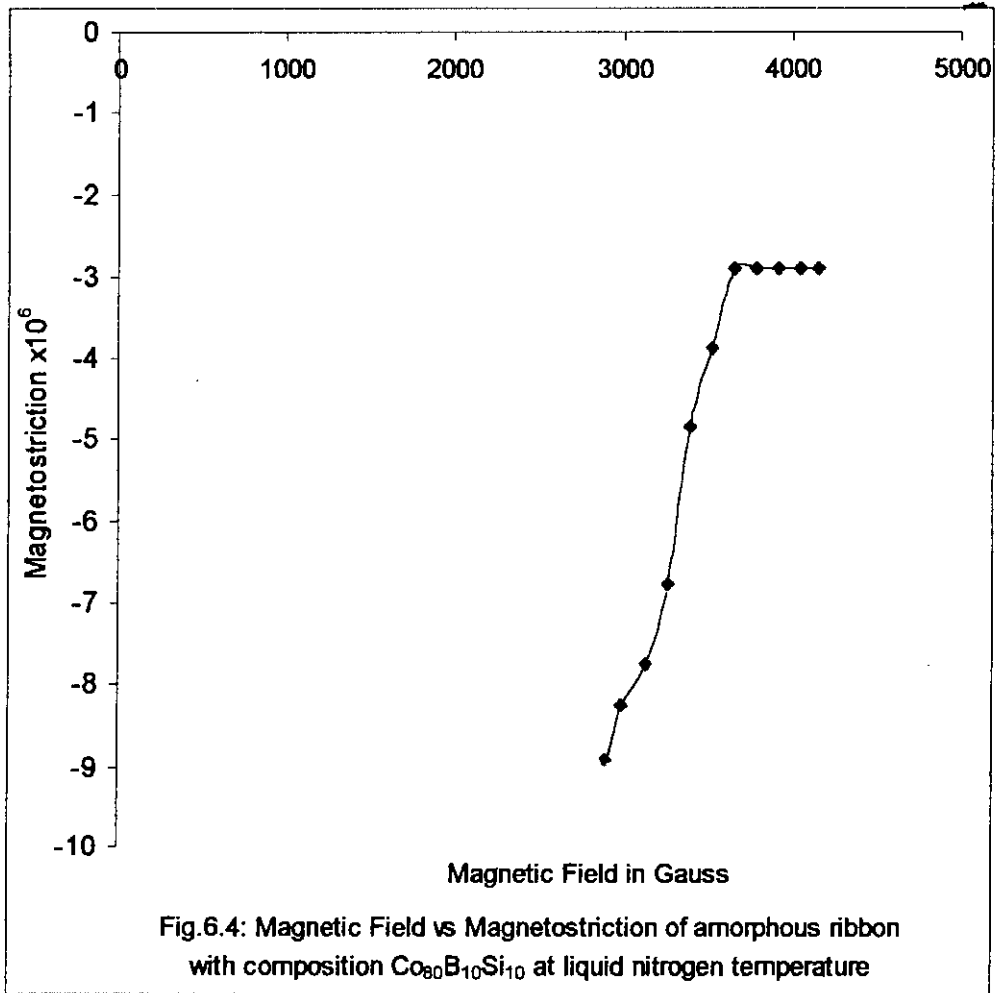
low magnetostrictive materials with high permeability. This expectation is based on the corresponding behavior of crystalline Fe-Co alloys with strong correlation between positive and negative magnetostriction of iron and cobalt giving rise to soft magnetic material. The results are explained as due to minimum magnetostriction of the alloy of composition  $Co_{74}Fe_6B_{10}Si_{10}$  where the positive contribution to magnetostriction due to Fe atoms components the negative magnetostriction of the Co atoms most effectively. Our experimental results show the iron free sample of the composition  $Co_{80}B_{10}Si_{10}$  is negative magnetostrictive. This is explained as due to minimum magnetostriction that results at this composition.

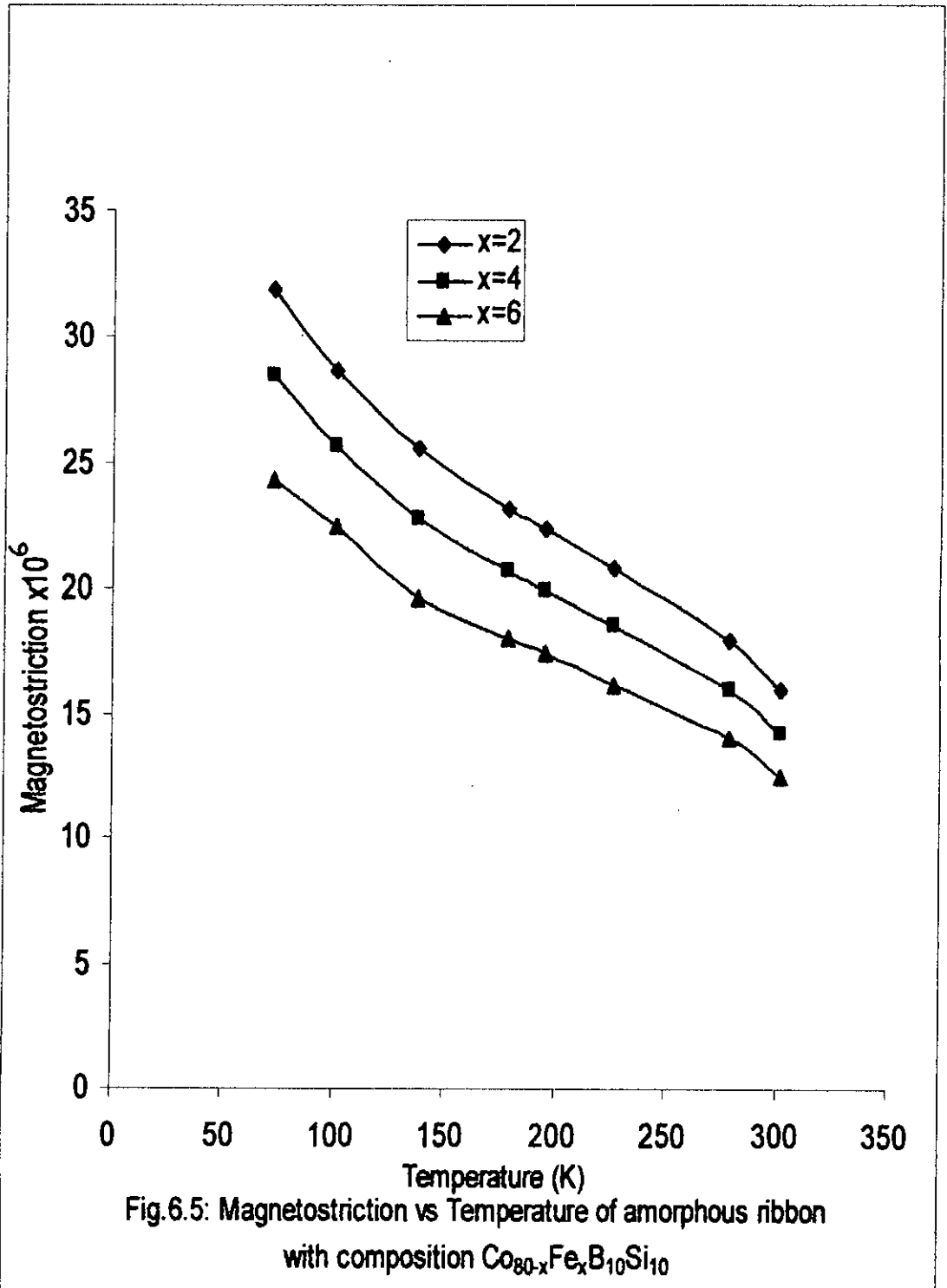
### **6.2 Low Temperature Dependence Magnetostriction of Co-based Amorphous Ribbons.**

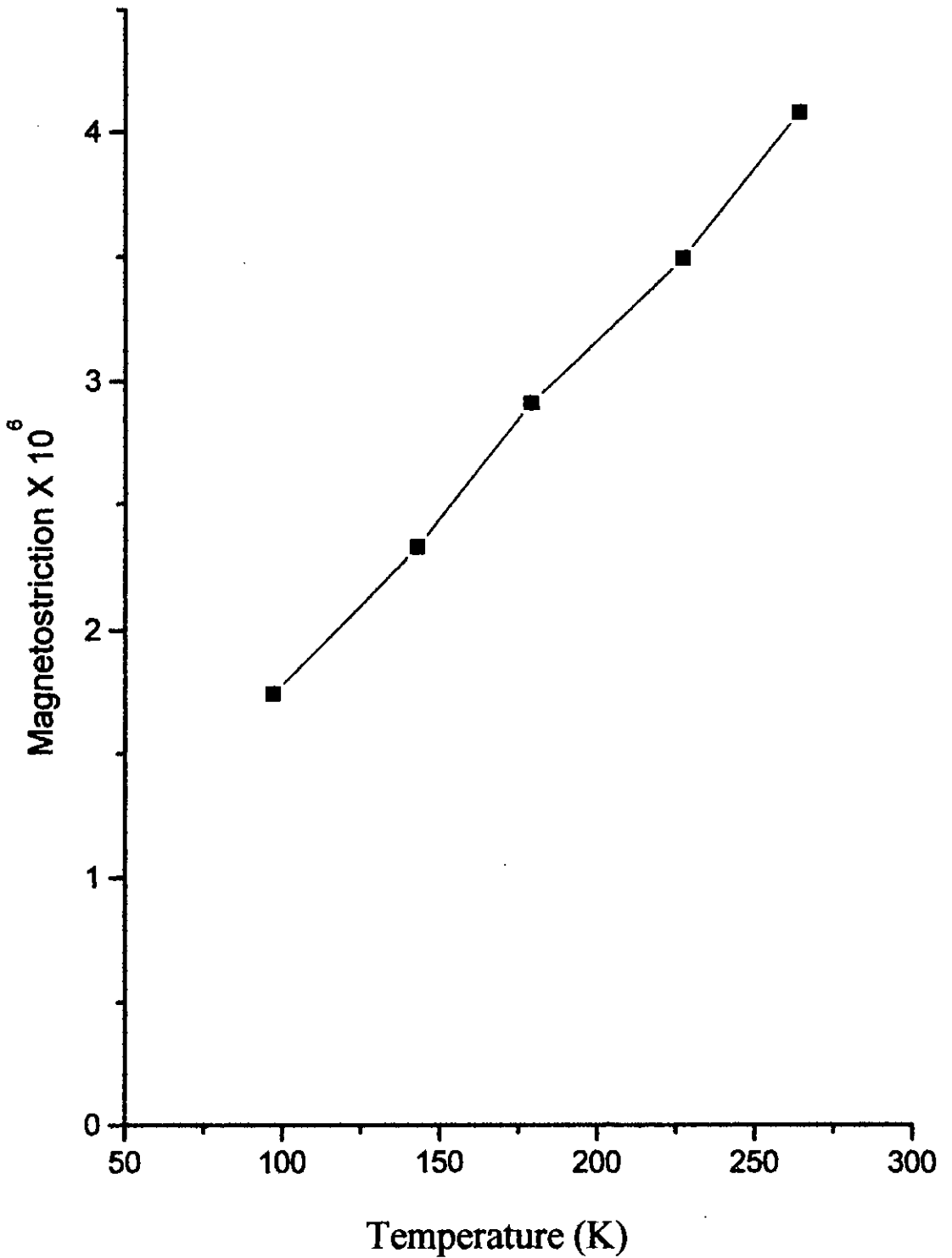
We have performed an extensive and thorough study of the low temperature dependence of the parallel and perpendicular magnetostrictions in the present series of compositions  $Co_{80-x}Fe_xB_{10}Si_{10}$  [ $x = 0, 2, 4$  and  $6$ ], from around 73k up to room temperature and upto maximum applied magnetic field 4.16 kilo gauss. The effect of variation of low temperature on magnetostriction for amorphous ribbons with composition  $Co_{80-x}Fe_xB_{10}Si_{10}$  [ $x = 0, 2, 4$  and  $6$ ] are shown in figure 6.3 and 6.5. Figure 6.4 and 6.6 shows the saturation magnetostriction of  $Co_{80}B_{10}Si_{10}$  as a low temperature dependence at applied magnetic field 4.16 kilo gauss. The low temperature variation of the magnetostriction is increased at maximum applied field for different amorphous ribbon of Co-Fe-B-Si system. Confirming the dominance of single-ion contributions in these alloys, Co and











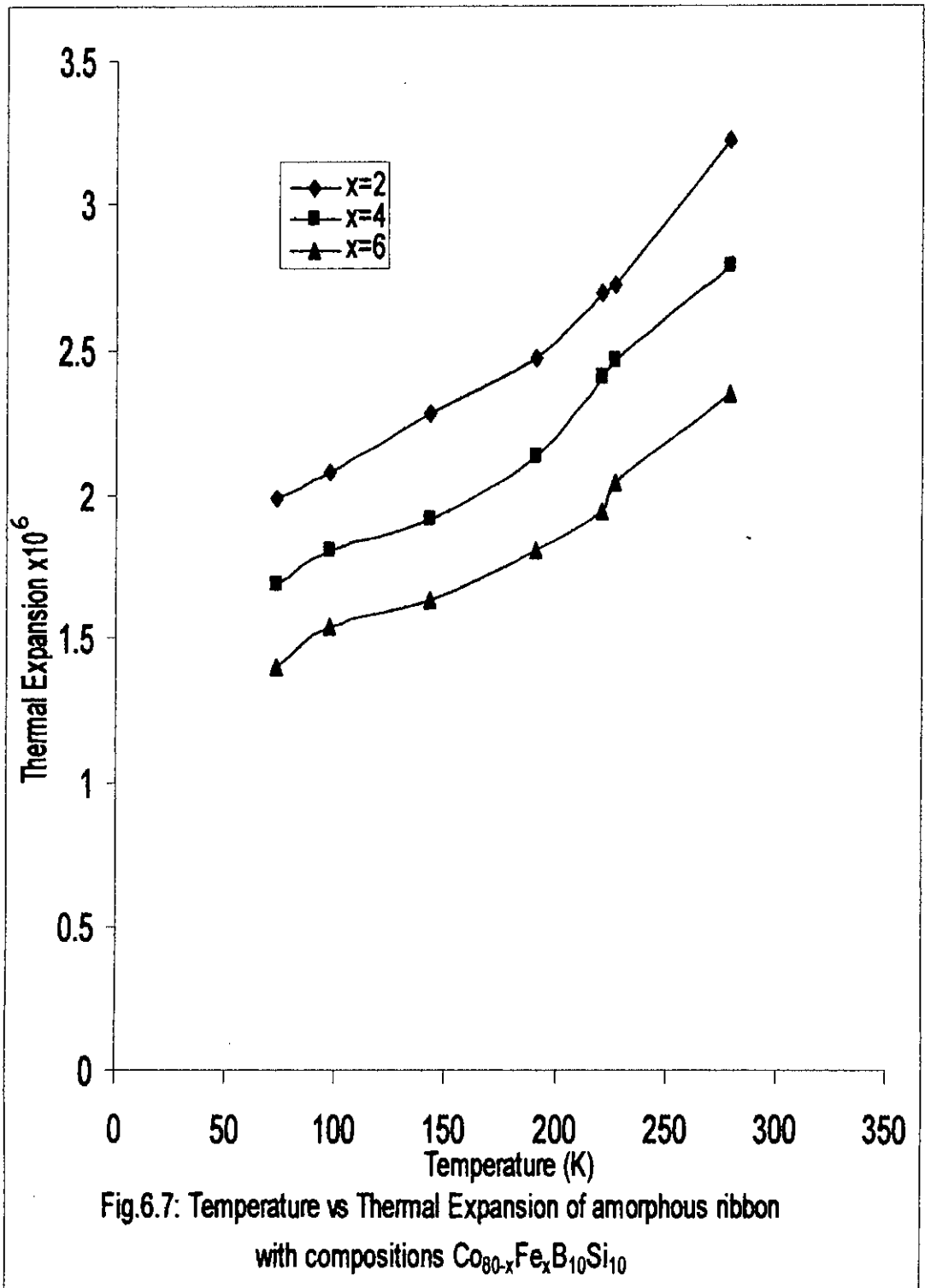
**Fig. 6.6: Magnetostriction vs temperature of amorphous ribbon with composition Co<sub>80</sub>B<sub>10</sub>Si<sub>10</sub>**

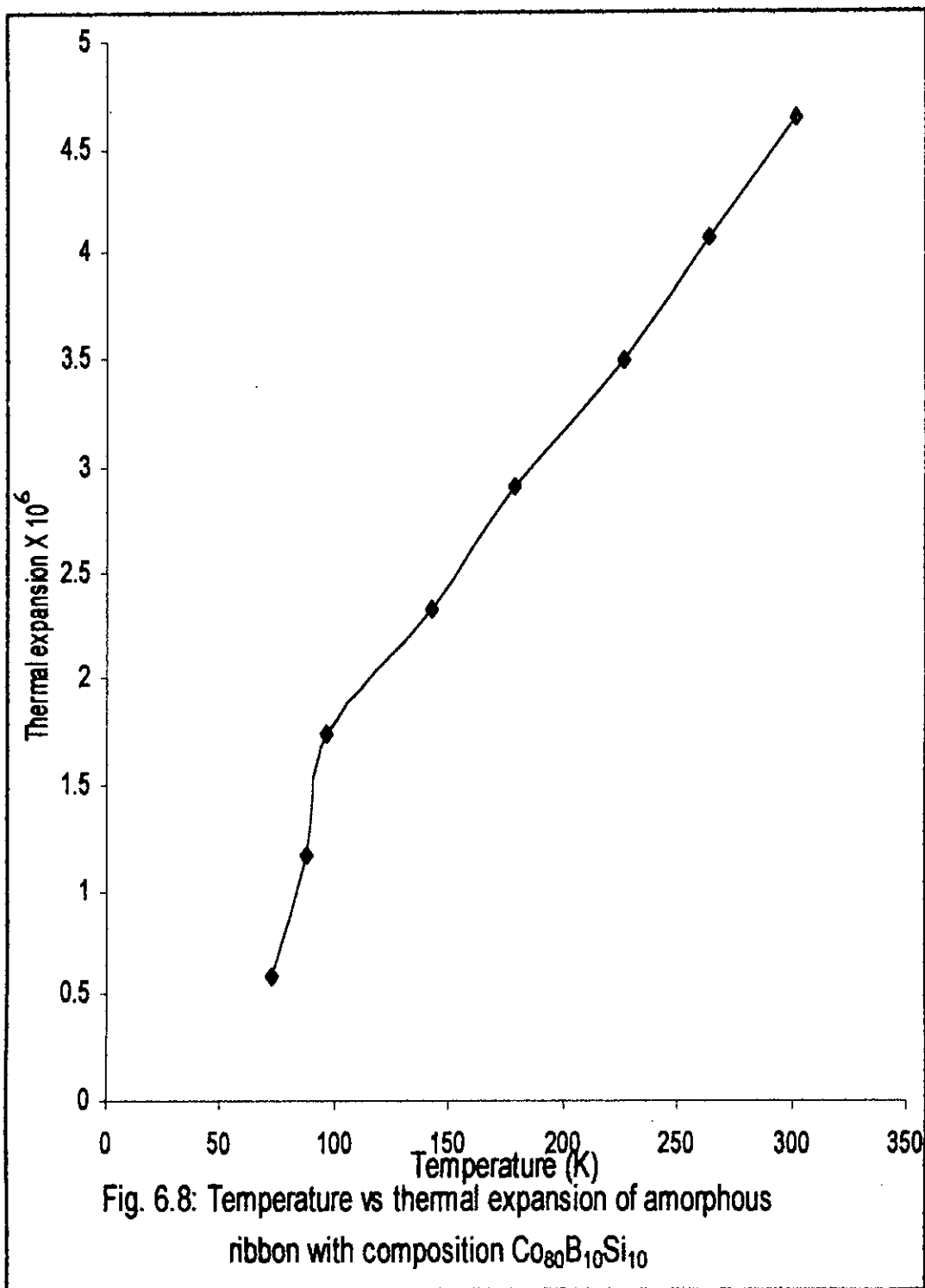
Co-Fe-based alloys again deviate from the pure single-ion behavior and their low temperature dependence suggests the presence of two-ion contributions. The occurrence of a compositional and low temperature compensation of  $\lambda_s$  in Co-Fe-B-Si alloys confirms the presence of the two mechanisms contributing to  $\lambda_s$ .

Experimentally observed modifications of the magnetostriction constant of near-zero magnetostrictive Co-Fe based ribbon with variation of low temperature may be explained by a redistribution of the local easy axis directions while keeping the electronic structure parameters unchanged at constant field. The experiments may be interpreted by assuming that the local magnetostriction value are very small and the low temperature changes upto room temperature increases of the local magnetostriction tensor by amounts which are comparable to the original value.

### **6.3 Low Temperature Dependence Thermal Expansion of Co-based Amorphous Ribbons.**

Thermal expansion measurements were performed between 73 K to 300 K using a strain gauge technique. A sensitive electronic circuit detects the variation in the output of the transformer, the sensitivity being estimated as  $\pm 3.5 \times 10^{-6}$  equivalent strain. The low temperature measurements using liquid nitrogen. The measured temperature accuracy was better than  $\pm 2$ k.





## *Results and Discussions*

The effect of variation of low temperature on thermal expansion for amorphous ribbons with composition  $Co_{80-x}Fe_xB_{10}Si_{10}$  [ $x = 2, 4$  and  $8$ ] are shown in figure 6.7. The low temperature dependence of thermal expansion of amorphous ribbon with composition  $Co_{80}B_{10}Si_{10}$  is shown in figure 6.8. The thermal expansion slightly depends on composition. There is almost monotonous increase of thermal expansion with the increase of temperature for all the samples the fall being sharper. Although these results are of interest from a practical view point they are difficult to interpret quantitatively in terms of directional order theory because of the uncertainty as to the low temperature dependence of thermal expansion and the uncertainty as to whether equilibrium was achieved at any temperature. There is a marked anisotropy on the thermal expansion of these Co-Fe-B-Si and Co-Fe-B ribbons at low temperature Co-Fe-based and Co-based ribbons shows a positive thermal expansion perpendicular to the unique axis even at room temperature. The thermal expansion measurements made continuously and precisely in a temperature range can not only reveal the nature of phase change in amorphous ribbon in that range of temperature but also predict the direction of maximum dielectric anomaly in a amorphous ribbon. The thermal expansion as a function of temperature was positive at all temperature and increased in magnitude as the temperature was increased. The free energy can thus be evaluated as a function of the lattice parameter and temperature. By minimizing the free energy with respect to the lattice parameters, one obtains the lattice constants as a function of temperature. The values obtained are not too different, indicating a similar strain dependence for the Co-Fe exchange or Co-Co exchange interactions along the series are could be anticipated.





**CHAPTER - 7**

## **Results and Discussions on Fe-based Amorphous Ribbon**

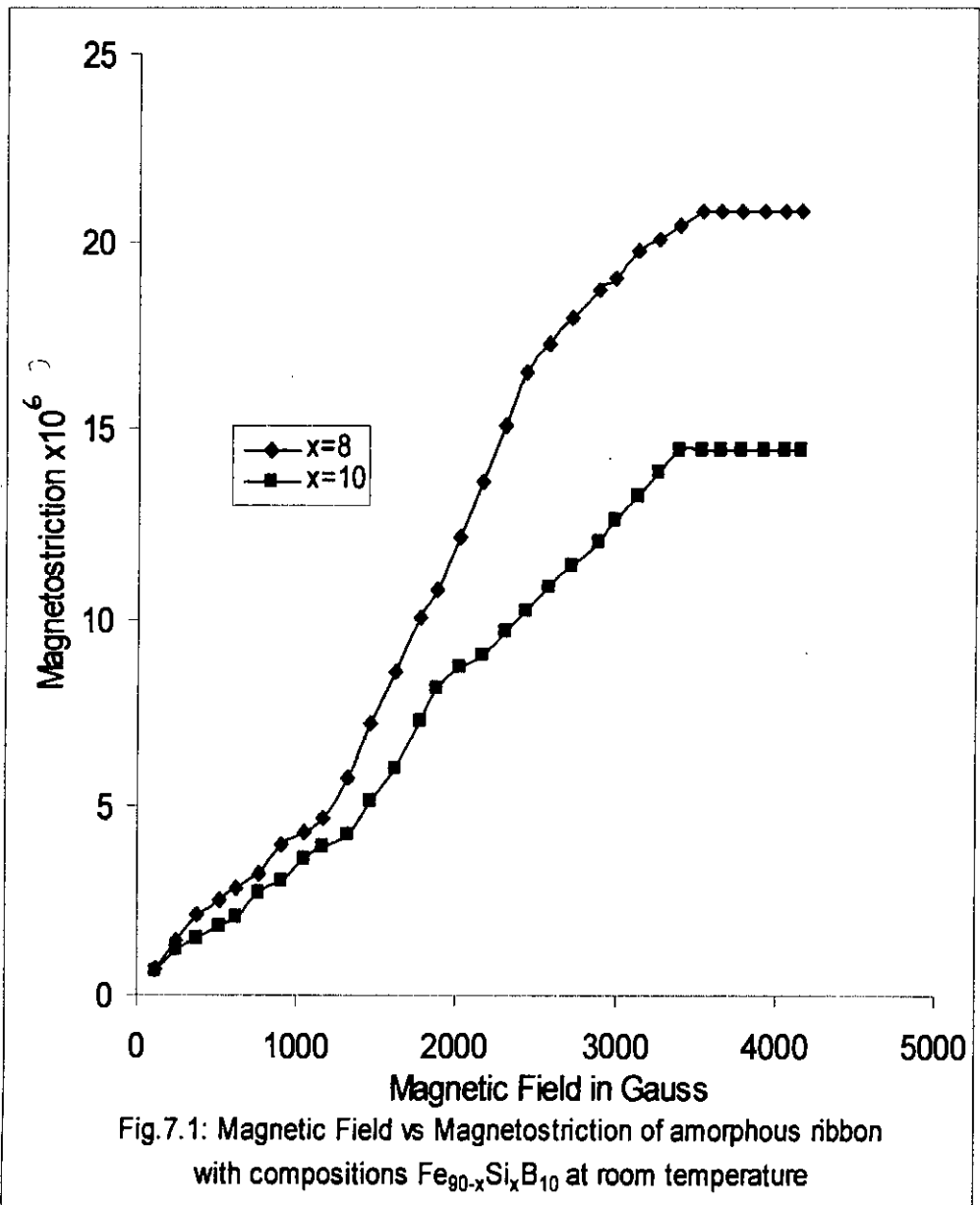
### **7.1 Field Dependence Magnetostriction of Fe-based Amorphous Ribbons.**

The magnetostriction of thin Fe-Si-B ribbons with composition  $Fe_{90-x}Si_xB_{10}$  [ $x = 8$  and  $10$ ] in as quenched condition is measured as a function of magnetic field using a strain gauge technique. The magnetostriction of the amorphous ribbons with different field are shown in figure 7.1. The saturation magnetostriction for these ribbons have higher values for higher percentage of iron. This quite understandable from the consideration of higher contribution of magnetic moments in Fe-rich ribbons.

The saturation magnetostriction ( $\lambda_s$ ) and saturation field ( $H_s$ ) for different sample as calculated are shown in Table-2.

| $Fe_{90-x}Si_xB_{10}$                             | $x = 8$                 | $x = 10$                |
|---|-------------------------|-------------------------|
| $\lambda_s$ at room temperature                   | $20.810 \times 10^{-6}$ | $14.466 \times 10^{-6}$ |
| $H_s$ in kilogauss at room temperature            | 3.53                    | 3.4                     |
| $\lambda_s$ at liquid nitrogen temperature        | $32.291 \times 10^{-6}$ | $24.11 \times 10^{-6}$  |
| $H_s$ in kilogauss at liquid nitrogen temperature | 3.78                    | 3.65                    |

The reason for the variation of magnetostriction with change of composition is assumed to be the varying contribution to positive magnetostriction from Fe in their crystalline forms. The actual understanding of this compositional dependence of magnetostriction requires a complete quantum mechanical calculation of band structures of these amorphous systems. The value of the



## *Results and Discussions*

magnetostriction depends on the electron concentration such that magnetostriction tends to be zero as the Fermi level goes to the degeneracy. Although this theory is of some qualitatively usefulness in understanding our experimental results of magnetostriction in amorphous ribbons it cannot be strictly applied in quantitative terms.

These results are shown in figure 7.1 and studied the magnetostriction of  $Fe_{80}Si_{10}B_{10}$  and  $Fe_{82}Si_8B_{10}$  at room temperature. The perhaps surprising result found was that the material did not appear to be isotropic; value so  $\lambda_s$  varied from  $14.466 \times 10^{-6}$  to  $20.810 \times 10^{-6}$  depending on the direction of field and measurement. O. Handley<sup>[7.1]</sup> has discussed the possible origin of magnetostriction in amorphous alloy. Band models which adequately describes the magnetostriction of crystalline Fe-Ni alloys do not appear to apply to these Fe-Ni and Fe-Co amorphous alloys. A localized spin model, which sums the strain derivative of Pseudo dipolar interaction energies over nearest neighbors adequately describes the magnetostrictions of crystalline Fe and Co. When generalized to consider the amorphous alloys the model suggests that the short range order of Fe-rich amorphous alloys resembles that of their crystalline counterparts. Interpretation of the results in terms of a quantum statistical mechanics theory suggests that one anisotropic mechanism for positive magnetostriction dominates in the Fe-based amorphous ribbons.

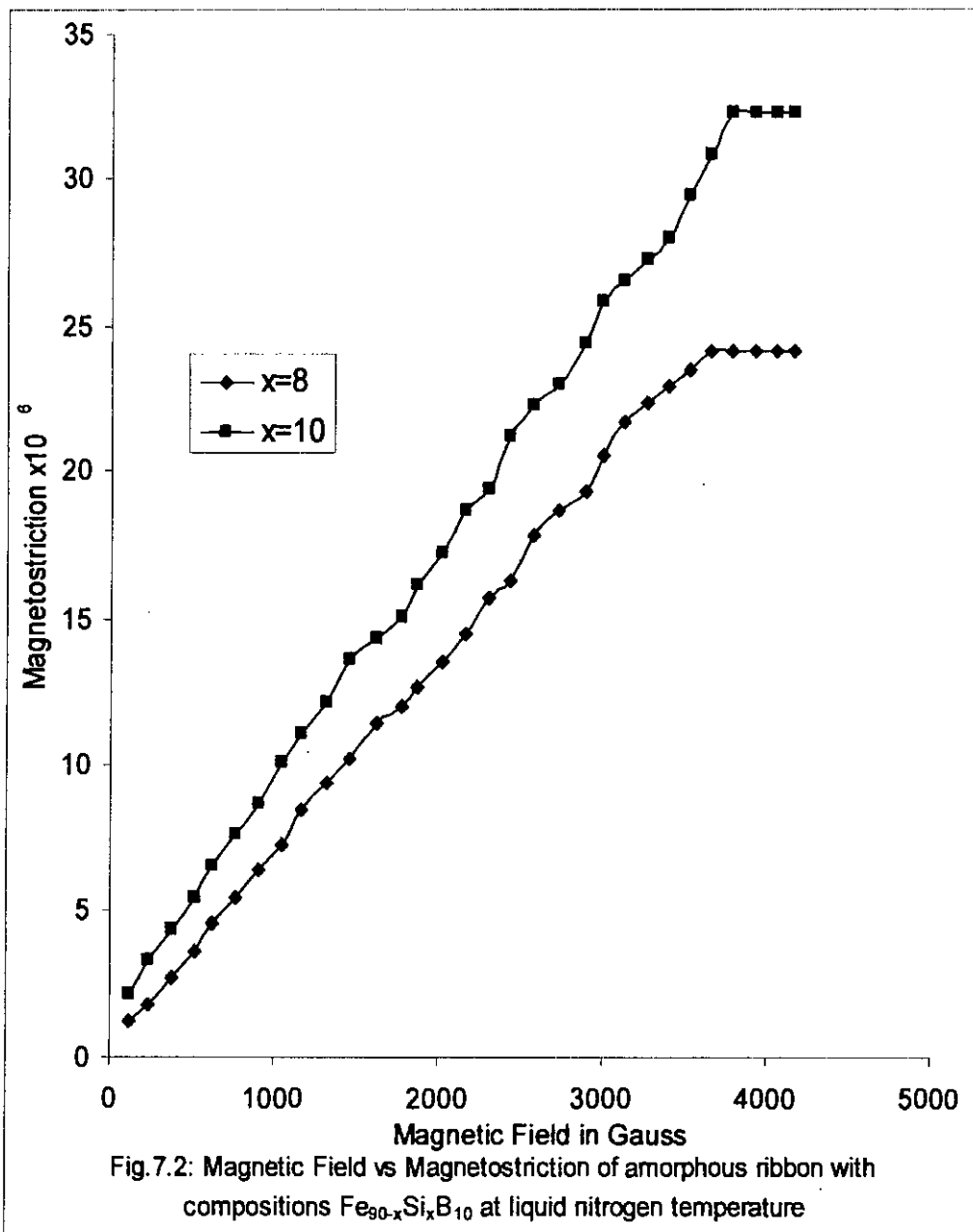
## **7.2 Low Temperature Dependence Magnetostriction of Fe-based Amorphous Ribbons.**

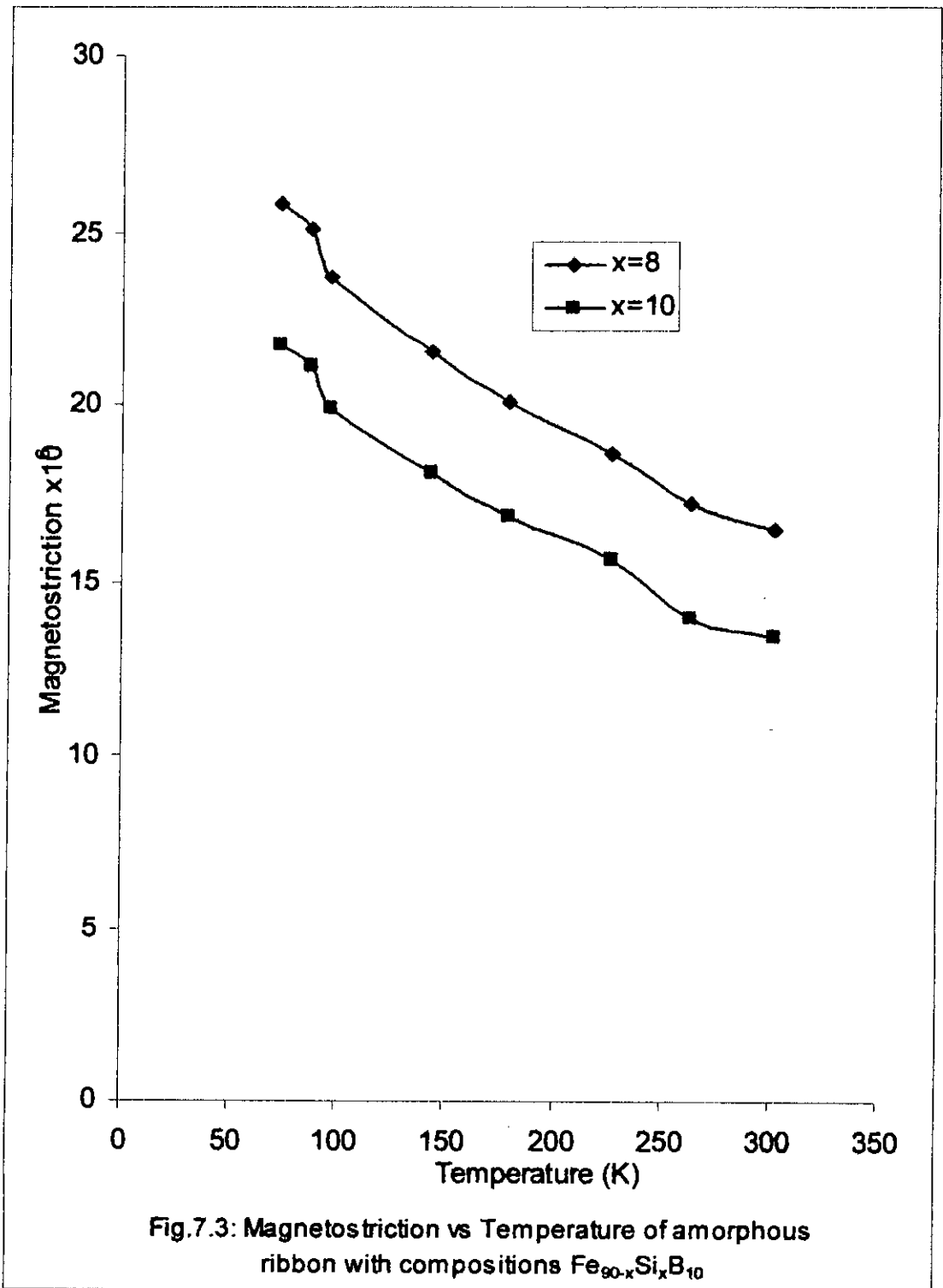
Study of low temperature dependence of the parallel and perpendicular magnetostriction in the present composition  $Fe_{80}Si_{10}B_{10}$  and  $Fe_{82}Si_8B_{10}$  from around 73K upto room temperature and constant applied magnetic field 4.16 kilo gauss, the low temperature dependence of magnetostriction of amorphous ribbon with composition  $Fe_{90-x}Si_xB_{10}$  [ $x=8$  and  $10$ ] are shown in figure 7.2 and 7.3. The origin of magnetostriction, in this case is most likely the internal stress. In this case, it should be possible to substantially reduce magnetostriction by the stress relieving due to the increase of temperature. This evolution can be associated with a relaxation process, since relaxation produces an increase of the magnetostriction in Fe-based amorphous ribbons. After the maximum magnetostriction decreases with increasing temperature. This evolution of the effective magnetostriction with low temperature dependence can be understood from the two phase nature of the crystallized material. As already indicated the value of the effective magnetostriction of the samples results from the balance between the magnetostriction of the  $\alpha$ FeSi crystallites and that of the amorphous phase matrix according to

$$\lambda_x = V_{Fe-Si} \lambda_s^{Fe-Si} + (1 - V_{Fe-Si}) \lambda_s^{amor}$$

where  $v_{Fe-Si}$  denotes the volume percentage of crystallized material.

The value measured in the fully relaxed amorphous  $\lambda_s = 20.8101 \times 10^{-6}$ , which can be considered as good estimation of the magnetostriction of the remaining amorphous matrix. In particular, in this system near low magnetostriction





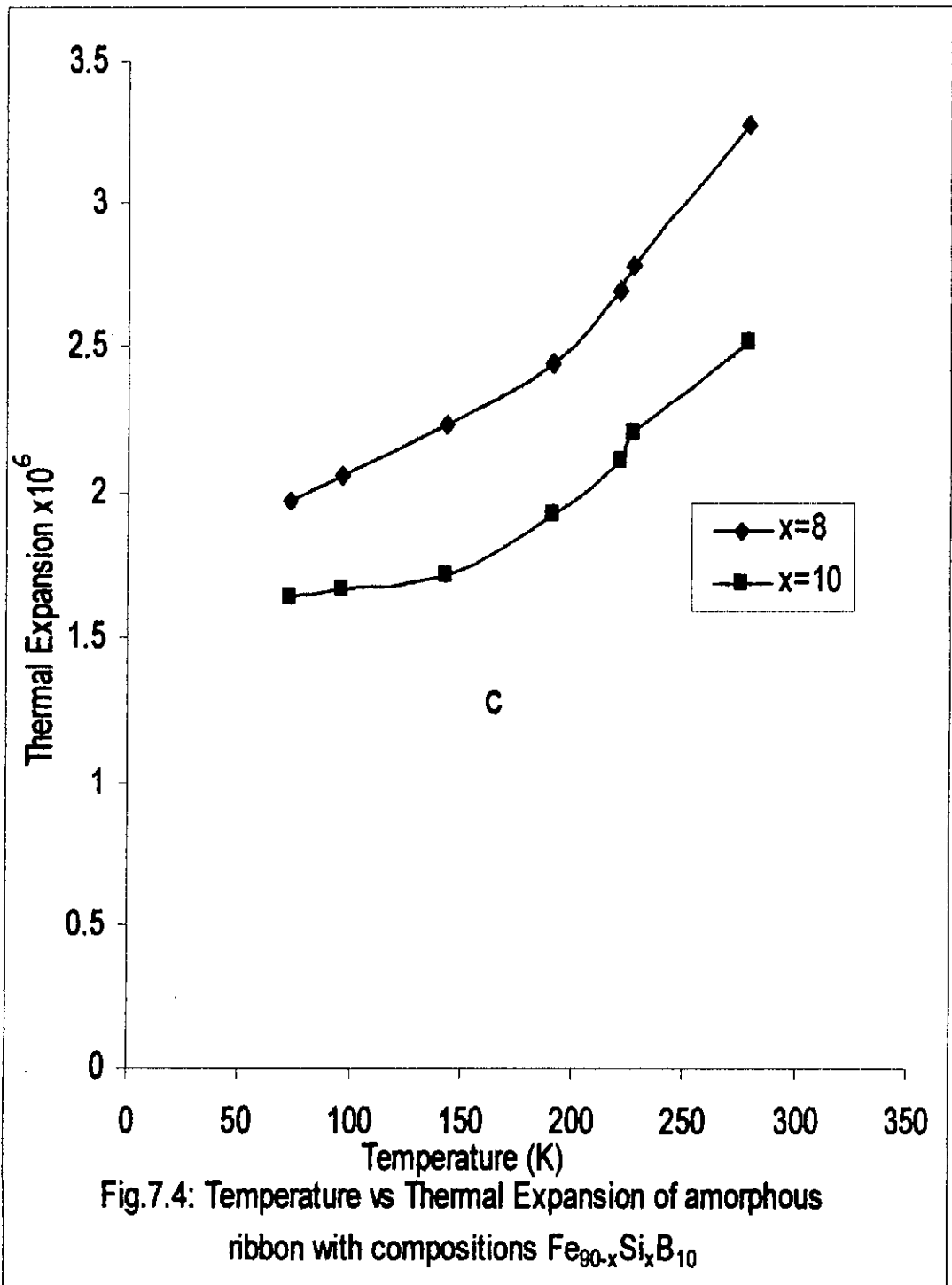
samples can be achieved by controlled crystallization leading to a compensation of the contribution of the negative magnetostriction  $\alpha$ FeSi crystallites with that of the positive magnetostriction amorphous matrix.

### **7.3 Low Temperature Dependence Thermal Expansion of Fe-based Amorphous Ribbons.**

Low temperature dependence of thermal expansion of as quenched Fe-Si-B system with composition  $Fe_{90-x}Si_xB_{10}$  [ $x = 8$  and  $10$ ] have been measured by strain gauge technique. A sensitive electronic circuit detects the variation in the output of the transformer, the sensitivity being estimated as  $\pm 3.5 \times 10^{-6}$  equivalent strain. The measured temperature accuracy better than  $\pm 2$  K. Temperature dependence of thermal expansion of the samples measured by using a strain gauge technique from 73 K to room temperature are shown in figure 7.4. With increasing temperature thermal expansion monotonously increases for all the samples, the fall on an average sharper. The thermal expansion of Fe-Si-B amorphous alloy slightly depends on composition. These values obtained are not too different, indicating a similar strain dependence for the Fe-Fe exchange interaction along the series.

Anisotropic amorphous ribbon like Fe-based exhibit positive value of thermal expansion at low temperature along one of the two principal directions. The thermal expansion arise from the contributions from the acoustic and optic modes such that optic mode are more effective in the c-direction whereas the acoustic modes are highly predominant along directions normal to the c-axis





## *Results and Discussions*

positive values of thermal expansion found in Fe-Si-B amorphous alloys arise from magnetic interaction or the 3d electron. Instability of normal modes of vibration may arise from positive thermal expansion in amorphous ribbons. The sign of the thermal expansion coefficient is governed by the sign of the volume magnetostriction.



**CONCLUSIONS**

### **Conclusions**

Amorphous ribbons as a potential new medium for understanding secondary magnetic effects by parameters like magnetostriction and thermal expansion has been studied. Two sets of amorphous alloys were chosen with composition  $Fe_{90-x}Si_xB_{10}$  [ $x = 8$  and  $10$ ] and  $Co_{80-x}Fe_xB_{10}Si_{10}$  [ $x = 0, 2, 4$  and  $6$ ] the melt spinning technique has been confirmed as a very useful method of preparing amorphous ribbons.

Amorphous Fe-B-Si and Co-Fe-B-Si ribbons are metastable form of alloy, which has a great potential as a soft magnetic material. This material is magnetically soft and is not likely to have magnetocrystalline anisotropy due to the absence of crystalline structure. However, due to the preparation technique some induced anisotropy is created in the samples because the ribbons are subjected to a tension along the length during the preparation. Since this material is obtained in the form of thin ribbons; it needs no further processing for the reduction of thickness, as in the case of silicon iron transformer core material, for high frequency uses. However, since Co-Fe-Si-B, Co-Si-B and Fe-Si-B are metastable materials, their stabilities are affected by thermal and other agencies. This is very important factor to be considered for technological uses.

## Conclusions

Although the magnetic characteristics of amorphous materials are discussed in general, on the assumption that the amorphous state of magnetic alloy of a given composition is independent of the technique used in preparing the specimen, in reality the secondary effects like domain orientation and strain induced magnetostriction of amorphous ribbons depend very much on the preparation process. We have shown that non-local corrections play only a minor role for the case of strongly magnetostrictive amorphous ferromagnets with  $\lambda_s^{eff}$  around as in  $-14.466 \times 10^{-6}$  to  $-20.810 \times 10^{-6}$  for instance, Fe-Si-B alloys. Magnetostriction is very important for technological uses. The magnetostriction of Co-based alloys is around  $-2.904 \times 10^{-6}$  and for Co-Fe-based alloy is around  $-14.308 \times 10^{-6}$  to  $-21.519 \times 10^{-6}$ . Fe-Si-B and Co-Fe-Si-B system is very important to study the effect of these elements on magnetostriction. Since Fe has positive magnetostriction while Co has negative magnetostriction, it is possible to reduce the value of magnetostriction by changing the relative amount of the two elements.

The effect of low temperature dependence on magnetostriction has also been measured using strain gauge and a systematic increase of saturation magnetostriction is observed with lowering of Fe materials.

Thermal expansion coefficient has been estimated by strain gauge technique and it is observed that the value of the expansion coefficient as well as its change with temperature is low compared to crystalline material which is an advantage for the application of amorphous materials when temperature change is involved.

## ***Conclusions***

Since there was no temperature control system available, the temperature measurement could not be made exactly in the low temperature region.



**REFERENCES**

## References

### Chapter - 1.

- 1.1 W. Klement , Jr., R. H. Willens and P. Dewez, *Nature* , 187(1960) 869.
- 1.2 Gubanov, A.I. 1960, *FIZ*, Tver ,Tel .2,502.
- 1.3 Brenner , A. D. E. Couch and E. K. Williams, 1950, *J Res, Nat., Bureau Standards* 44, 109.
- 1.4 Dewez, P. R. H. Willens and W. Klement, Jr., 1960, *J. Appl. Phys.* 31, 1136.
- 1.5 Miroshnickenko, L. S. and I. V. Salli., 1959, *Ind. Lab.* 25, 1463 (in english) *Fran Zavatskaya Lab*, 25, 1394 (1959).
- 1.6 Mader, S. and A. S. Nowick, 1965, *Appl. Phys, Lett.* 7, 57
- 1.7 B. T. Cong, *J. Magn. Magn. Mater* 117 (1992) 126.
- 1.8 T. Miyaki, K. Yamanchi, S. Arakawa, Y. Yoshizawa and S. Nakajima, *Bulletin Japan, Inst. Metals.* 26 (1987), 299.
- 1.9 O. Komoto, H. Hujishima, S. Sumiya, H. Itomasa and T. Ojima, *Bulletin Japan Inst, Metals.* 27 (1988), 293.
- 1.10 H. Fujimori, M. Kikuchi Y. obi and T. Masumoto, *Sci. Rep. RITO*, A- 26 (1976), 36.
- 1.11 H. Warliment and R. Bolli, *J, Magn. Magn. Mat.* 26 (1982), 97.
- 1.12 S. S. Sikder, M. A. Asgar, M. A. Hakim and M. A. Mazid "The effect annealing on the magnetization Process of Iron- Boron ribbon", *Journal of Bangladesh Academy of Science*, Vol. 20, N.2, 237-245 ( 1996).
- 1.13 Simpson, A. W. and D. R. Brambley, 1971, *Phys. Stat. Sol. (b)* 43, 291.
- 1.14 Sherwood, R.C., E. M. Gyorgy, H. S. Chen, S. D. Ferris, G. Norman and H .J. Leamy 1975, *AIP Conf. Proc.* 24, 745.
- 1.15 Arai, K., N. Tsuya, M. Yamada H. Shirae, H. Fujimori, H. Saito and T. Masumoto, 1976, in *Rapidly quenched metals, Section 1* (eds. N. J. Grand and B. C. Giessen ) ( M.I. T. Press, Cambridge, Mass.) P. 489.
- 1.16 O, Hadley, R. C.1977, in *Amorphous magnetism* (eds.R. A. Levy and R, Hasegawa ) ( Plenum Press. New Youk ) p-379.
- 1.17 M. A. Asgar and S. S. Sikder, *Indian J. Phys .* 71A (6), 689-696 (1999).
- 1.18 A. Hernando, M. Vazuez and J. M. Barandiaran, *J. Phys.* E21 (1988) 1129.
- 1.19 H. K. Lachowicz, in: *Amorphous Metats*, eds, H. Matyja and P. G. Zielinski (World Scientific, Singapor, (1986) P 313.
- 1.20 S. Chikazumi, *Physics of Magetism* (Krienger, Florida ,1964) P.431.
- 1.21 P. Predeeki, A. Mullendoro and N, Grant *Trans, Metall. Soc. AIME* 223, 1581(1965).
- 1.22 M. S. Cohen, *J. Appl. Phys.* 32, 87s (1961).
- 1.23 K. Hara, *J. Sci. Hiroschima Univ. Ser. II* 34, 139 (1970).
- 1.24 F. E. Luborsky, J. J. Becker and R.O. McCary *IEEE Trans, Magnetics* MAG - 11,1644 ( 1975).
- 1.25 T. Egami, P. J. Flanders and C. D. Grahm ( Jr) *AIP Conf. Proc.* 24, 697 (1975).
- 1.26 P. A. Algarabel, M. R. Ibarra, C. Marquina and A.del Moral. *J. Magn. Magn. Mater.* 84 (1990)109.



## References

- 1.27 M. R. Ibarra, P. A. Agarabel, A. del Alberdi, J. Bartolone and A. Moral, J. M. Fernandez, M. R. Ibarra, C. Marquina, R. Navarro and C. Rillo, *ibid.* ref. (2).
- 1.28 K. H. J. Buschow and R. Grossinger, *J. Less -Common Met.* 135 (1987) 39.
- 1.29 D. Givord, H. S. Li, J. M. Moreau, R. Perrier de la Bathie and E. du Tremolet de Lacheisserie, *Physica B.* 130 (1985) 323.
- 1.30 Sikder, S. S. Ph.D. Thesis (1999), Physics Department, BUET.

## Chapter - 2.

- 2.1. Brenner, A., D. E. Couch and E.K. Williams 1950, *J. Res. Nat. Bureau standards* 44, 109.
- 2.2. W. Klement Jr., R. H. Williens and P. Duwez, *Nature* (1960), 187, 809.
- 2.3. Gubanov, A. L. 1960, *FIZ Tver. Tel.* 2, 502.
- 2.4. Pond, R. Jr. and R. Maddin, 1969, *Trans. Met. SOC. AIME* 245, 2475.
- 2.5. Mader, S. and A. S. Nowick, 1965, *Appl. Phys. Lett.* 7, 57.
- 2.6. Tsuei, C. C. and P. Duwez, 1966, *J. Appl. Phys.* 37, 435.
- 2.7. T. Mizoguchi, IBM Research Report RC 6054, 1976.
- 2.8. R. Alben, J.I. Budnick, G.S. Cargill, III, *Metallic Glasses* ( American SOC. for Metals.1978) P-304.
- 2.9. E. M. Gyorgy, *ibid* P- 275.
- 2.10. G.S. Cargill III, *Solid State Physics*, Vol-30 Ed. Ehrenreich et. al., Academic Press, New York ( 1975) P-257.
- 2.11. T. Masumoto, S. Ohnuma K. Shirakawa, M. Nose and K. Kobayshi, *Int. Conf. on Liquiid and Amorphous Metals*, Grenoble France, 1980.
- 2.12. Cargill III, G.S., 1975 a, *Solid State Physics* 30, 227.
- 2.13. M.A. Asgar, (1984) *Mechanical Engineering Research Bulletin* (BUET) P.I.
- 2.14. S. S. Sikder, Ph.D Thesis (BUET) , July, 1999.
- 2.15. Alben R., J.I. Budnick and G. S. Cargill III, 1977in *Metallic glasses* (eds . H. S. Leamy and J. J. Gilman) ( American Society for Metals, Metals Park, Ohio) ch. 12.
- 2.16. Cargill III, G.S. , 1975 b, *Solid State Phys.* Vol. 30, eds H. Ehrenreich, F. Seitz and D. Turnbull ( Academic Press, New york) P. 227.
- 2.17. Turnbull, D. 1969, *Contenys. Phys.* 10,473.
- 2.18. Duwez, P., R.H. willens and W. Klement, Jr., *J. Appl. Phys.* 31,1136, 1960.
- 2.19. H.S. Chen, *Rep. Prog. Phys.* 43,23 (1980)

## References

### Chapter - 3.

- 3.1. M.A. Asgar, Proceeding of the International Conference on Physics and energy for development, Dhaka, 26-19 Jan. 1985. 153P.
- 3.2. J. H. Van Vleck Phys Rev.52,1178 (1938).
- 3.3. E.R. Callen and H.B. Callen, Phys. Rev. 129,578 (1963).
- 3.4. L. Berger, Phys. Rev. 138A, 1083(1965).
- 3.5. I. A. Campbell. Sol., St. Comm., 10,953 (1972)
- 3.6. A. Hernando, M. Vazquez and J.M.Barandiaran, J, Phys. E 21 (1988) 1129.
- 3.7. H. K. Lachowicz, in: Amorphous Metals , eds. H. Matyja and P. G. Zielinski (World Scientific, Singapore, 1986) P. 313.
- 3.8. S. Chikazumi, Physics of Magnetism ( Krieger, Florida, 1964) P.431.
- 3.9. M. L. Spano, K. B. Hathaway and H. T. Savage, J. Appl. Phys. 53 (1982).
- 3.10. J. D. Livingston, Harris and M. Plischke, 1974, J. Mon-Cryst. Solids 15, 239.
- 3.11. Cochrane, R.W., R. Harris and M. Plischke, 1974, J. Non- Crys. Solids 15, 239.
- 3.12. Fahnel, M., and T. Egami, 1982, J. Appl. Phys, 53,2319.
- 3.13. Suzuki, Y., and T. Egami, 1983, J. Magn. & Magn. Mater. 31-34, 1459.
- 3.14. Lachowicz, H. K., and H. Szymczak., 1984, J. Magn. & Magn. Mater. 41, 327.
- 3.15. O' Handley, R. C., and N. J. Grant, 1985, Proceedings on Rapidly Quenched Metals, eds S. Steed and H. warlimont ( North- Holland, Amsterdam) P. 1125.
- 3.16. Furthmüller, J., M. Fahnel and G. Herzer, 1986, J. Phys. F 16, L 255.
- 3.17. Furthmüller,J., M. Fahnel and G. Herzer, 1987, J. Magn. & Magn. Mater, 69, 79.
- 3.18. Furthmüller,J., M.Fahnel and G. Herzer 1987b, J. Magn. & Magn. Mater. 69, 89.
- 3.19. Szymczak, H., 1987, J. Magn. & Magn. Mater. 67, 227.
- 3.20. Fahnel, M., and J. Farthmüller, 1988, J. Magn. & Magn. Mater. 72, 6.
- 3.21. Fahnel, M., and J. Furthmüller, 1989, Phys, Status Solidi A 116, 819.
- 3.22. Pawellek, R., J. Furthmüller and M. Fahnel, 1988, J. Magn & Magn. Mater, 75, 225.
- 3.23. Suzuki, Y., and N. Ohta, 1988, J. Appl. Phys. 63, 3633.
- 3.24. Boll, R. H. R. Hilzingen and H. Warlimont, 1983, in : Metallic Glasses, Chemical and structural Properties, ed. R. Hasegawa ( CRC Press, Boca Raton ) P. 183.
- 3.25. Tago, A. C. Nishimura and K. Yanagisawa, 1985, IEEE Trans. Magn. MAG-21, 2032.
- 3.26. Sherwood, R. C., E. M. Gyorgy, H.S. Chen, S.D. Ferris, G. Norman and H.J. Leamy, 1975, AIP Conf, Proc. 24, 745.
- 3.27. O' Handley, R. C., L. I. Mendelsohn and E. A. Nesbitt, 1976, IEEE Trans. Magn. MAG-12, 942.
- 3.28. Gyorgy, E. M., 1978, in Metallic Glasses, eds J. J. Gilman and H. J. Leamy (American Society for Metals, Metals Park, OH) P.275.

## References

- 3.29. O' Handley, R. C. 1978, Phys. Rev. B 18, 930.
- 3.30. O' Handley, R. C., and M.O. Sullivan, 1981, J. Appl. Phys. 52, 1841.
- 3.31. Fujimori, H., N.S. Kazama, K. Hirose, J. Zhang, H. Moita, I. Sato and H. Sagawara, 1984, J. Appl. Phys. 55, 1769.
- 3.32. Chen, D. X., and K. V. Rao, 1986 IEEE Trans, Magn. MAG-22, 451.
- 3.33. Shiba, K. F. S. Tsurnashima, S. Uchiyama and S. Yoshino, 1986 IEEE Trans. Magn. MAG-22, 1104.
- 3.34. Jergel, M., G. Vlasa'k and P. Duhaj, 1989, Phys. Status solidi A 111, 597.
- 3.35. Callen, E. R., and H. B. Callen, 1965, Phys. Rev. A 139, 45.
- 3.36. du Tremolet de Lachessrie, E., 1982, J. Magn. & Magn. Mater. 25, 251.
- 3.37. Hernando, A., V. Madurga, C. Nunez de Villavicencio and M. Vasquez, 1984, Appl. Phys. Lett. 45, 802.
- 3.38. Chen, D. X., and K. V. Rao, 1986, IEEE Trans. Magn. MAG-22, 451.
- 3.39. du Tremolet de Lachessrie, E., and R. Yavari, 1988, J. de Phys. (France) 12, Suppl. C8-1327.
- 3.40. Cullen, J, and A. del Moral, 1990, J. Magn. & Magn. Mater. 83, 157.
- 3.41. Clark, A. E., 1980, in Handbook on Ferromagnetic Materials , Vol. 1, ed. E. P. Wohlfarth ( North Holland, Amsterdam) P.531.
- 3.42. Hubbard, J. 1979a, Phys. Rev. B 19, 2626.
- 3.43. Hubbard, J. 1979a, Phys. Rev. B 20, 4584.
- 3.44. Hubbard, J. 1981a, Phys, Rev. B 23, 5974.
- 3.45. Hubbard, J. 1981b, in: Electron Correlation and Magnetism in Narrow- Band System, ed. T. Moriya ( Springer, Berlin) p. 29.
- 3.46. Hasegawa, H., 1979, J. Phys. Soc, Jpn. 46, 1504.
- 3.47. Hasegawa, H., 1980a, J. Phys. Soc. Jpn 49, 178.
- 3.48. Hasegawa, H., 1980b, J. Phys. Soc. Jpn. 49, 963.
- 3.49. Hasegawa. H., 1983, J. Phys. F13, 2655.
- 3.50. Hasegawa, H., 1984, J. Phys. F14, 1235.
- 3.51. Oguchi, T., K. Terakura and N. Hamada, 1983, J, Phys. F13, 145.
- 3.52. Moruzzi, V. L., and P.M. Marcus, K. Schwarz and P. Mohn, 1986, Phys. Rev. B 34, 1784.
- 3.53. Motuzzi, V. L., and P. M. Marcus, 1988, Phys. Rev. B 38, 1613.
- 3.54. Capellmann, H., 1979, J. Phys. (1966) F4.
- 3.55. Prange, R. E. and V. Korenman, 1975, AIP Conf. Proc. 325.
- 3.56. Prange, R. E., and V. Korenman, 1976 AIP Conf. Proc. 29, 321.
- 3.57. Prange, R. E. and V. Korenman, 1979a, Phys, Rev. B, 19, 4691.
- 3.58. Prange, R. E. and V. Korenman, 1979b, Phy. Rev. B 19, 4698.
- 3.59. Korenman, V. J. L. Murray and R. E. Prange, 1977a, Phys. Rev. B 16, 4032.
- 3.60. Korenman, V., J. L. Murray and R. E. Prange, 1977b, Phys. Rev. B16, 4048.
- 3.61. Korenman, V. J. L. Murray and R. E. Prange, 1977c. Phys. Rev. B16, 4058.
- 3.62. Korenman, V., 1985 J. Appl. Phys. 57, 3000.
- 3.63. Terakura, K., and J. Kanamori, 1971, Proc. Theor. Phys. 46. 1007.
- 3.64. Terakura, K., 1976, J. Phys. F6, 1385.

## References

- 3.65. K. Malozamoff, A. P.; A. R. Williams, K. Terakura, and V.L. Moruzzi , 1983, *J. Magn. & Magn. Mater.* 35, 192.
- 3.66. Malozamoff, A. P. , A. R. Williams, V. L. Moruzzi, 1984, *Phys. Rev. B* 29 1620.
- 3.67. Willams, A. R., V. L. Moruzzi, C. D. Gelatt Jr. and J. Kubler, 1983, *J. Mang. & Magn Mater*, 31-34, 88.
- 3.68. Williams, A. R., V. L. Moruzzi, A. P. Malozemoff and K. Terakura, 1983b, *IEEE Trans. Magn. MAG-19*, 1983.
- 3.69. Friedel ., 1958, *Nuovo Cimmento*, Suppl. 7 ( 2) 287.
- 3.70. Beebey, J. L. 1964, *Phys. Rev. A.* 135, 130.
- 3.71. Velicky, B., S. Kirkpatrick and H. Ehrenreich ,1968, *Phys. Rev.* 175, 747.
- 3.72. Oelhafen, P., E. Hanser, H. J. Güntherodt and K. Bennemann, 1979, *Phys. Rev. Lett.* 49, 1134.
- 3.73. O. Handley , R. C., 1978a , *Phys. Rev. B*18, 930.
- 3.74. O. Handley , R.C., And L. Berger 1978, in : *Physics of Transition Metals* ,eds M. J. G. Lee, J. M. Perz and E. Fawcett (Institute of Physics, Bristol ) P. 477.
- 3.75. Corb, B. W., R. C. O. Handley and N. J. Grant .1982, *J. Appl. Phys.* 53, 7728.
- 3.76. Corb ,B.W., 1985 ,*Phys. Rev. B* 31, 2521.
- 3.77. Corb, B. W., R. C. O. Handley and N. S. Grant,1983, *Phys. Rev. B* 27, 636.
- 3.78. O. Handley, R. C., 1987a, *J. Appl. Phys.* 62, R15.
- 3.79. Stein, F., and G. Dietz, 1989, *J. Magn. & Magn. Mater.* 81, 294.
- 3.80. Jaccarino, V., and L. R. Walker, 1965, *Phys. Rev. Lett.* 15, 259.
- 3.81. Keffer, F., 1966, in : *Ferromagnetism*, ed. H. P. J. Wijn (Springer, Berlin) Vol. XVII, 2, P.1.
- 3.82. Dyson, J. F., 1956, *Phys. Rev.* 102, 1217,1230.
- 3.83. Mathon, J., and E. P. Wohlfarth, 1968, *Proc. R. Soc.* A302, 409.
- 3.84. Suran, G., J. S. Sztern, J. A. Aboaf and T. R. McGuire, 1981 *IEEE Trans. Magn. MAG-17*, 3065.
- 3.85. Hüller, K., 1986, *J. Magn. & Magn. Mater.* 61, 347.
- 3.86. Rhyne, J. J., G. E. Fise and J. W. Lynn, 1982, *J. Appl. Phys.* 53, 2316.
- 3.87. Maczymbowicz, L. J., D. Dendorek , and R. Zuberek, 1985, *Thin Solid Films*, 125, 269.
- 3.88. Yu. S. C., J. W. Lynn, J. S. Rhyne and G. E. Fish, 1988, *J. Appl. Phys.* 63, 4083.
- 3.89. Gangulee, A., and R. J. Kobliska 1978b, *J. Appl. Phys.* 49, 4896.
- 3.90. Vittoria, C., P. Lubitz and V. Ritz, 1978, *J. Appl. Phys.* 49, 4908.
- 3.91. Lubitz, P., J. H. Schelleng and C. Vittoria,1976, *AIP Conf. Proc.* 29, 178.
- 3.92. Frenandez -Baca, J. A., J. W. Lynn, J. J. Rhyne and G. E. Fish, 1987, *Phys. Rev. B*, 36, 8497.
- 3.93. L. Neel *Anr., de Physique*, 3, 137 (1948).
- 3.94. W. P. Mason and J. A. Lewis, *Phys. Rev.* 94, 1439 (1954).
- 3.95. E. R. Callen and H. B.Callen, *Phys. Rev.* 129 (1963) 578; *ibid*, *Phys. Rev. A* 139 (1965) 455.
- 3.96. A. E. Clark ,B. F. De Savage and R. Bozorth, *Phys. Rev. A*138 (1965) 216

## References

### Chapter - 4.

- 4.1 O. G. Peterson, D. N. Batchelde, and R.O. Simmons, Phys. Rev. 150, 703 (1966).
- 4.2 M. R. Ibarra, P. A. Algarabel, A. Alberdi, J. Bartolome and A. del Moral, J. Appl. Phys. 61 (1987) 3451.
- 4.3 M. Shiga, J. Phys. Soc. Jpn. 59 (1981) 2573.
- 4.4 J. P. Gavigan, D. Givord, H. S. Li and J. Voiron, Physica B 149 (1988) 345.
- 4.5 J. F. Janak and A. R. Williams, Phys. Rev. B 14 (1976) 4199.

### Chapter -5.

- 5.1 H. P. Rooksby and B. T. M. Willis, Nature, 172, 1054 ( 1953).
- 5.2 L. Kraus and J. Schneider, Phys. Stat .Sol. (a) 39, K 161 (1977).
- 5.3 H. Nogaoka, Phil. Mag. 37, 131 (1844).
- 5.4 J. E. Goldman, Phys. Rev. 72, 529 (1947).
- 5.5 Y. Shirakawa and I . Oguma, Sci. Rep. Inot. Tohoku university, A 188, 532 (1966).
- 5.6 M. A. Michell, A. E. Clark, H. T. Savage and R. J. Abbund, IEEE Magn, 14, 1169 (1978).
- 5.7 J. E. Goldman, Phys. Rev. 72, 529 (1947).
- 5.8 M. A. Asgar, Ph.D. Thesis, University of Southampton (1970).
- 5.9 H. P. Rooksby as B. T. M .Willis, Nature, 172, 1054 (1953).

### Charpter – 6

- 6.1 J. E. goldman Phys. Rev. 72, 529 (1947).
- 6.2 E. W. Lee and M. A. Asgar, Phys. Rev. Lett. 22, 1436 (1969).
- 6.3 Berger, A., Physics Rev. (1965), 138A, 1083.

### Chapter – 7

- 7.1 O. Handley, R. C. 1977, in Amorphous magnetism II (eds. R. A. Levy and R. Hasegawa) (Plenum Press, New York) P 379.



**APPENDIX**

**Table 1: Data for Magnetic Field Strength**

| <b>Field Current<br/>(Amp)</b> | <b>Flux meter<br/>Reading (+)</b> | <b>Flux meter<br/>Reading (-)</b> | <b>Average<br/>Deflection</b> | <b>Magnetic Field<br/>(Gauss)</b> |
|--------------------------------|-----------------------------------|-----------------------------------|-------------------------------|-----------------------------------|
| 0.2                            | 10                                | 13                                | 11.5                          | 115                               |
| 0.4                            | 22                                | 26                                | 24.0                          | 240                               |
| 0.6                            | 35                                | 41                                | 38.0                          | 380                               |
| 0.8                            | 48                                | 54                                | 51.0                          | 514                               |
| 1.0                            | 60                                | 65                                | 62.5                          | 625                               |
| 1.2                            | 73                                | 80                                | 76.5                          | 765                               |
| 1.4                            | 86                                | 95                                | 90.5                          | 905                               |
| 1.6                            | 100                               | 110                               | 105.0                         | 1050                              |
| 1.8                            | 113                               | 121                               | 117.0                         | 1170                              |
| 2.0                            | 127                               | 137                               | 132.0                         | 1320                              |
| 2.2                            | 142                               | 150                               | 146.0                         | 1460                              |
| 2.4                            | 155                               | 169                               | 162.0                         | 1620                              |
| 2.6                            | 169                               | 186                               | 177.5                         | 1775                              |
| 2.8                            | 183                               | 192                               | 187.5                         | 1875                              |
| 3.0                            | 197                               | 207                               | 202.0                         | 2020                              |
| 3.2                            | 211                               | 221                               | 216.0                         | 2160                              |
| 3.4                            | 224                               | 236                               | 230.0                         | 2300                              |
| 3.6                            | 239                               | 249                               | 244.0                         | 2440                              |
| 3.8                            | 252                               | 263                               | 257.5                         | 2575                              |
| 4.0                            | 268                               | 277                               | 272.5                         | 2725                              |
| 4.2                            | 281                               | 298                               | 289.5                         | 2895                              |
| 4.4                            | 295                               | 304                               | 299.5                         | 2995                              |
| 4.6                            | 308                               | 318                               | 313.0                         | 3130                              |
| 4.8                            | 322                               | 331                               | 326.5                         | 3265                              |
| 5.0                            | 335                               | 345                               | 340.0                         | 3400                              |
| 5.2                            | 350                               | 356                               | 353.0                         | 3530                              |
| 5.4                            | 362                               | 369                               | 365.5                         | 3655                              |
| 5.6                            | 376                               | 381                               | 378.5                         | 3785                              |
| 5.8                            | 391                               | 394                               | 392.5                         | 3925                              |
| 6.0                            | 405                               | 406                               | 405.5                         | 4055                              |
| 6.2                            | 416                               | 416                               | 416.0                         | 4160                              |

**Table 2: Data for Calibration of the D.C. Bridge**  
 Gauge Factor: 2.02  
 Bridge Current: 20 mA

| <b>Deflection in Nanovoltmeter</b> | <b><math>\Delta R/R \times 10^{-6}</math></b> |
|------------------------------------|---|
| 0                                  | 0   |
| 4                                  | 1.6   |
| 7                                  | 3.5   |
| 8                                  | 5.5   |
| 9                                  | 7.4   |
| 10                                 | 9.4   |
| 11                                 | 11.4  |
| 13                                 | 13.5  |
| 15                                 | 15.5  |
| 20                                 | 17.8  |
| 29                                 | 19.8  |
| 33                                 | 22.0  |
| 38                                 | 24.4  |
| 43                                 | 26.6  |
| 51                                 | 29.2  |
| 70                                 | 31.5  |
| 71                                 | 33.8  |
| 72                                 | 36.3  |
| 73                                 | 38.6  |
| 74                                 | 40.9  |
| 75                                 | 43.4  |
| 76                                 | 45.7  |
| 76                                 | 48.0  |



**Table 3: Variation of Bridge Sensitivity with Bridge Current**

Gauge Factor: 2.02

Sensitivity per deflection  $\Delta R/R=3.79 \times 10^{-6}$

| Bridge Current (Amp) | Nano voltmeter Reading |
|----------------------|------------------------|
| 4                    | 4                      |
| 6                    | 5.8                    |
| 9                    | 8                      |
| 11                   | 10.4                   |
| 12                   | 12.5                   |
| 14                   | 15                     |
| 16                   | 17                     |
| 18                   | 19                     |
| 20                   | 21                     |
| 22                   | 22.5                   |
| 23                   | 25                     |
| 25                   | 26.6                   |

**Table 4: Variation of Magnetostriction with the Angle of Field**  
 Bridge Current: 20mA,  
 Gauge Factor: 2.02,  
 Sensitivity per deflection  $\Delta R/R = 4.39 \times 10^{-6}$

| Magnet Position(Degree) | Nanovoltmeter Reading | Magnetostriction $\times 10^{-6}$ |
|-------------------------|-----------------------|-----------------------------------|
| 0                       | 7.0                   | 1.5213                            |
| 10                      | 8.0                   | 1.8472                            |
| 20                      | 9.0                   | 2.0646                            |
| 30                      | 10.25                 | 2.2276                            |
| 40                      | 10.0                  | 2.1733                            |
| 50                      | 9.0                   | 1.9559                            |
| 60                      | 7.5                   | 1.6299                            |
| 70                      | 6.25                  | 1.3582                            |
| 80                      | 5.0                   | 1.0866                            |
| 90                      | 3.0                   | 0.6520                            |
| 100                     | 3.5                   | 0.7606                            |
| 110                     | 5.0                   | 0.8631                            |
| 120                     | 6.0                   | 1.3039                            |
| 130                     | 7.0                   | 1.5213                            |
| 140                     | 7.25                  | 1.5756                            |
| 150                     | 8.25                  | 1.7929                            |
| 160                     | 9.5                   | 2.0646                            |
| 170                     | 10.5                  | 2.2819                            |
| 180                     | 10.9                  | 2.3688                            |
| 190                     | 10.4                  | 2.2602                            |
| 200                     | 9.5                   | 2.0646                            |
| 210                     | 8.0                   | 1.7386                            |
| 220                     | 7.0                   | 1.5213                            |
| 230                     | 5.5                   | 1.1953                            |
| 240                     | 4.0                   | 0.8631                            |
| 250                     | 3.0                   | 0.6519                            |
| 260                     | 2.5                   | 0.5433                            |
| 270                     | 2.25                  | 0.4889                            |

**Table 5: Table for Magnetostriction Measurement at Room Temperature**Sample:  $\text{Co}_{78}\text{Fe}_2\text{B}_{10}\text{Si}_{10}$ 

Gauge Factor: 2.02

Sensitivity per deflection  $\Delta R/R=4.83 \times 10^{-6}$ 

| Field Current (Amp) | Magnetic Field Strength (Gauss) | Nano voltmeter Reading | Magnetostriction $\times 10^{-6}$ |
|---------------------|---------------------------------|------------------------|-----------------------------------|
| 0.2                 | 115                             | -1.0                   | -1.5941                           |
| 0.4                 | 240                             | -1.25                  | -1.9925                           |
| 0.6                 | 380                             | -1.5                   | -2.3911                           |
| 0.8                 | 514                             | -2.0                   | -3.1881                           |
| 1.0                 | 625                             | -2.25                  | -3.5866                           |
| 1.2                 | 765                             | -2.5                   | -3.9851                           |
| 1.4                 | 905                             | -2.7                   | -4.3039                           |
| 1.6                 | 1050                            | -3.5                   | -5.5792                           |
| 1.8                 | 1170                            | -4.0                   | -6.3762                           |
| 2.0                 | 1320                            | -4.5                   | -7.1733                           |
| 2.2                 | 1460                            | -4.75                  | -7.5717                           |
| 2.4                 | 1620                            | -5.0                   | -7.9703                           |
| 2.6                 | 1775                            | -5.5                   | -8.7673                           |
| 2.8                 | 1875                            | -6.0                   | -9.5643                           |
| 3.0                 | 2020                            | -6.5                   | -10.3614                          |
| 3.2                 | 2160                            | -7.0                   | -11.1584                          |
| 3.4                 | 2300                            | -7.5                   | -11.9554                          |
| 3.6                 | 2440                            | -8.0                   | -12.7525                          |
| 3.8                 | 2575                            | -9.0                   | -14.3465                          |
| 4.0                 | 2725                            | -9.5                   | -15.1435                          |
| 4.2                 | 2895                            | -10.0                  | -15.9405                          |
| 4.4                 | 2995                            | -10.5                  | -16.7376                          |
| 4.6                 | 3130                            | -11.0                  | -17.5346                          |
| 4.8                 | 3265                            | -11.5                  | -18.3316                          |
| 5.0                 | 3400                            | -12.0                  | -19.1287                          |
| 5.2                 | 3530                            | -13.0                  | -20.7227                          |
| 5.4                 | 3655                            | -13.5                  | -21.5198                          |
| 5.6                 | 3785                            | -13.5                  | -21.5198                          |
| 5.8                 | 3925                            | -13.5                  | -21.5198                          |
| 6.0                 | 4055                            | -13.5                  | -21.5198                          |
| 6.2                 | 4160                            | -13.5                  | -21.5198                          |

**Table 6: Table for Magnetostriction Measurement at Room Temperature**Sample :  $\text{Co}_{76}\text{Fe}_4\text{B}_{10}\text{Si}_{10}$ 

Gauge Factor : 2.02

Sensitivity per deflection  $\Delta R/R = 4.31 \times 10^{-6}$ 

| Field Current<br>(Amp) | Magnetic Field<br>Strength(Gauss) | Nano voltmeter<br>Reading | Magnetostriction<br>$\times 10^{-6}$ |
|------------------------|-----------------------------------|---------------------------|--------------------------------------|
| 0.2                    | 115                               | -0.5                      | -0.7112                              |
| 0.4                    | 240                               | -0.75                     | -1.0668                              |
| 0.6                    | 380                               | -1.0                      | -1.4224                              |
| 0.8                    | 514                               | -1.25                     | -1.7781                              |
| 1.0                    | 625                               | -1.5                      | -2.1337                              |
| 1.2                    | 765                               | -1.75                     | -2.4893                              |
| 1.4                    | 905                               | -2.0                      | -2.8448                              |
| 1.6                    | 1050                              | -2.5                      | -3.5561                              |
| 1.8                    | 1170                              | -2.75                     | -3.9117                              |
| 2.0                    | 1320                              | -3.0                      | -4.2633                              |
| 2.2                    | 1460                              | -3.5                      | -4.9785                              |
| 2.4                    | 1620                              | -4.0                      | -5.6897                              |
| 2.6                    | 1775                              | -4.5                      | -6.4010                              |
| 2.8                    | 1875                              | -5.0                      | -7.1122                              |
| 3.0                    | 2020                              | -5.5                      | -7.8234                              |
| 3.2                    | 2160                              | -6.25                     | -8.8903                              |
| 3.4                    | 2300                              | -7.0                      | -9.9571                              |
| 3.6                    | 2440                              | -7.5                      | -10.6683                             |
| 3.8                    | 2575                              | -8.0                      | -11.3795                             |
| 4.0                    | 2725                              | -8.25                     | -11.7351                             |
| 4.2                    | 2895                              | -9.0                      | -12.8019                             |
| 4.4                    | 2995                              | -9.5                      | -13.5132                             |
| 4.6                    | 3130                              | -10.0                     | -14.2244                             |
| 4.8                    | 3265                              | -11.0                     | -14.9356                             |
| 5.0                    | 3400                              | -11.0                     | -15.6469                             |
| 5.2                    | 3530                              | -11.0                     | -15.6469                             |
| 5.4                    | 3655                              | -11.0                     | -15.6469                             |
| 5.6                    | 3785                              | -11.0                     | -15.6469                             |
| 5.8                    | 3925                              | -11.0                     | -15.6469                             |
| 6.0                    | 4055                              | -11.0                     | -15.6469                             |
| 6.2                    | 4160                              | -11.0                     | -15.6469                             |

**Table 7: Table for Magnetostriction Measurement at Room Temperature**Sample:  $\text{Co}_{74}\text{Fe}_6\text{B}_{10}\text{Si}_{10}$ 

Gauge Factor: 2.02

Sensitivity per deflection  $\Delta R/R=3.77 \times 10^{-6}$ 

| Field Current (Amp) | Magnetic Field Strength (Gauss) | Nano voltmeter Reading | Magnetostriction $\times 10^{-6}$ |
|---------------------|---------------------------------|------------------------|-----------------------------------|
| 0.2                 | 115                             | -0.5                   | -0.6221                           |
| 0.4                 | 240                             | -0.75                  | -0.93317                          |
| 0.6                 | 380                             | -1.0                   | -1.2442                           |
| 0.8                 | 514                             | -1.25                  | -1.5553                           |
| 1.0                 | 625                             | -1.5                   | -1.8663                           |
| 1.2                 | 765                             | -1.75                  | -2.1774                           |
| 1.4                 | 905                             | -2.0                   | -2.4884                           |
| 1.6                 | 1050                            | -2.5                   | -3.1106                           |
| 1.8                 | 1170                            | -2.75                  | -3.4216                           |
| 2.0                 | 1320                            | -3.0                   | -3.7327                           |
| 2.2                 | 1460                            | -3.5                   | -4.3548                           |
| 2.4                 | 1620                            | -4.25                  | -5.2880                           |
| 2.6                 | 1775                            | -5.0                   | -6.2211                           |
| 2.8                 | 1875                            | -5.25                  | -6.5322                           |
| 3.0                 | 2020                            | -6.0                   | -7.4653                           |
| 3.2                 | 2160                            | -6.5                   | -8.0875                           |
| 3.4                 | 2300                            | -7.25                  | -9.0206                           |
| 3.6                 | 2440                            | -7.5                   | -9.3317                           |
| 3.8                 | 2575                            | -8.0                   | -9.9538                           |
| 4.0                 | 2725                            | -8.25                  | -10.2649                          |
| 4.2                 | 2895                            | -9.0                   | -11.1980                          |
| 4.4                 | 2995                            | -9.5                   | -11.8201                          |
| 4.6                 | 3130                            | -10.0                  | -12.4422                          |
| 4.8                 | 3265                            | -11.0                  | -13.6865                          |
| 5.0                 | 3400                            | -11.5                  | -14.3086                          |
| 5.2                 | 3530                            | -11.5                  | -14.3086                          |
| 5.4                 | 3655                            | -11.5                  | -14.3086                          |
| 5.6                 | 3785                            | -11.5                  | -14.3086                          |
| 5.8                 | 3925                            | -11.5                  | -14.3086                          |
| 6.0                 | 4055                            | -11.5                  | -14.3086                          |
| 6.2                 | 4160                            | -11.5                  | -14.3086                          |

**Table 8: Table for Magnetostriction Measurement at Liquid Nitrogen Temperature**Sample:  $\text{Co}_{78}\text{Fe}_2\text{B}_{10}\text{Si}_{10}$ 

Gauge Factor: 2.02

Sensitivity per deflection  $\Delta R/R=4.83 \times 10^{-6}$ 

| Field Current (Amp) | Magnetic Field Strength (Gauss) | Nano voltmeter Reading | Magnetostriction $\times 10^{-6}$ |
|---------------------|---------------------------------|------------------------|-----------------------------------|
| 0.2                 | 115                             | -2.0                   | -3.1881                           |
| 0.4                 | 240                             | -2.25                  | -3.5866                           |
| 0.6                 | 380                             | -2.5                   | -3.9851                           |
| 0.8                 | 514                             | -3.0                   | -4.7822                           |
| 1.0                 | 625                             | -3.25                  | -5.1807                           |
| 1.2                 | 765                             | -3.75                  | -5.9778                           |
| 1.4                 | 905                             | -4.25                  | -6.7747                           |
| 1.6                 | 1050                            | -4.75                  | -7.5717                           |
| 1.8                 | 1170                            | -5.25                  | -8.3688                           |
| 2.0                 | 1320                            | -6.0                   | -9.5644                           |
| 2.2                 | 1460                            | -6.5                   | -10.3614                          |
| 2.4                 | 1620                            | -7.0                   | -11.1584                          |
| 2.6                 | 1775                            | -7.5                   | -11.9554                          |
| 2.8                 | 1875                            | -8.25                  | -13.1509                          |
| 3.0                 | 2020                            | -9.0                   | -14.3465                          |
| 3.2                 | 2160                            | -10.0                  | -15.9405                          |
| 3.4                 | 2300                            | -10.5                  | -16.7376                          |
| 3.6                 | 2440                            | -11.0                  | -17.5347                          |
| 3.8                 | 2575                            | -11.5                  | -18.3317                          |
| 4.0                 | 2725                            | -12.0                  | -19.1287                          |
| 4.2                 | 2895                            | -12.5                  | -19.9257                          |
| 4.4                 | 2995                            | -13.0                  | -20.7227                          |
| 4.6                 | 3130                            | -13.5                  | -21.5198                          |
| 4.8                 | 3265                            | -13.75                 | -21.9183                          |
| 5.0                 | 3400                            | -14.25                 | -22.7153                          |
| 5.2                 | 3530                            | -15.0                  | -23.9108                          |
| 5.4                 | 3655                            | -15.5                  | -24.7079                          |
| 5.6                 | 3785                            | -16.0                  | -25.5049                          |
| 5.8                 | 3925                            | -16.5                  | -26.3019                          |
| 6.0                 | 4055                            | -16.5                  | -26.3019                          |
| 6.2                 | 4160                            | -16.5                  | -26.3019                          |

**Table 9: Table for Magnetostriction Measurement at Liquid Nitrogen Temperature**Sample:  $\text{Co}_{76}\text{Fe}_4\text{B}_{10}\text{Si}_{10}$ 

Gauge Factor: 2.02

Sensitivity per deflection  $\Delta R/R=4.31 \times 10^{-6}$ 

| Field Current (Amp) | Magnetic Field Strength (Gauss) | Nano voltmeter Reading | Magnetostriction $\times 10^{-6}$ |
|---------------------|---------------------------------|------------------------|-----------------------------------|
| 0.2                 | 115                             | -1.5                   | -2.1337                           |
| 0.4                 | 240                             | -1.75                  | -2.4893                           |
| 0.6                 | 380                             | -2.0                   | -2.8448                           |
| 0.8                 | 514                             | -2.5                   | -3.5561                           |
| 1.0                 | 625                             | -2.75                  | -3.9117                           |
| 1.2                 | 765                             | -3.0                   | -4.2633                           |
| 1.4                 | 905                             | -3.5                   | -4.9785                           |
| 1.6                 | 1050                            | -4.0                   | -5.6897                           |
| 1.8                 | 1170                            | -4.5                   | -6.4010                           |
| 2.0                 | 1320                            | -5.0                   | -7.1122                           |
| 2.2                 | 1460                            | -5.0                   | -7.8234                           |
| 2.4                 | 1620                            | -6.25                  | -8.8903                           |
| 2.6                 | 1775                            | -7.0                   | -9.9571                           |
| 2.8                 | 1875                            | -7.5                   | -10.6683                          |
| 3.0                 | 2020                            | -8.0                   | -11.3795                          |
| 3.2                 | 2160                            | -8.25                  | -11.7351                          |
| 3.4                 | 2300                            | -9.0                   | -12.8019                          |
| 3.6                 | 2440                            | -9.5                   | -13.5132                          |
| 3.8                 | 2575                            | -10.0                  | -14.2244                          |
| 4.0                 | 2725                            | -11.0                  | -15.6469                          |
| 4.2                 | 2895                            | -11.5                  | -16.3581                          |
| 4.4                 | 2995                            | -12.0                  | -17.0693                          |
| 4.6                 | 3130                            | -12.5                  | -17.7805                          |
| 4.8                 | 3265                            | -13.0                  | -18.4917                          |
| 5.0                 | 3400                            | -13.5                  | -19.2029                          |
| 5.2                 | 3530                            | -14.0                  | -19.9142                          |
| 5.4                 | 3655                            | -14.5                  | -20.6254                          |
| 5.6                 | 3785                            | -15.0                  | -21.3366                          |
| 5.8                 | 3925                            | -15.0                  | -21.3366                          |
| 6.0                 | 4055                            | -15.0                  | -21.3366                          |
| 6.2                 | 4160                            | -15.0                  | -21.3366                          |

**Table 10: Table for Magnetostriction Measurement at Liquid Nitrogen Temperature**Sample:  $\text{Co}_{74}\text{Fe}_6\text{B}_{10}\text{Si}_{10}$ 

Gauge Factor: 2.02

Sensitivity per deflection  $\Delta R/R=3.77 \times 10^{-6}$ 

| Field Current (Amp) | Magnetic Field Strength (Gauss) | Nano voltmeter Reading | Magnetostriction $\times 10^{-6}$ |
|---------------------|---------------------------------|------------------------|-----------------------------------|
| 0.2                 | 115                             | -1.25                  | -1.5553                           |
| 0.4                 | 240                             | -1.5                   | -1.8663                           |
| 0.6                 | 380                             | -1.75                  | -2.1774                           |
| 0.8                 | 514                             | -2.0                   | -2.4884                           |
| 1.0                 | 625                             | -2.5                   | -3.1106                           |
| 1.2                 | 765                             | -2.75                  | -3.4216                           |
| 1.4                 | 905                             | -3.0                   | -3.7327                           |
| 1.6                 | 1050                            | -3.5                   | -4.3547                           |
| 1.8                 | 1170                            | -4.25                  | -5.2879                           |
| 2.0                 | 1320                            | -5.0                   | -6.2211                           |
| 2.2                 | 1460                            | -5.25                  | -6.5322                           |
| 2.4                 | 1620                            | -6.0                   | -7.4653                           |
| 2.6                 | 1775                            | -6.5                   | -8.0874                           |
| 2.8                 | 1875                            | -7.25                  | -9.0206                           |
| 3.0                 | 2020                            | -7.5                   | -9.3317                           |
| 3.2                 | 2160                            | -8.0                   | -9.9538                           |
| 3.4                 | 2300                            | -8.25                  | -10.2648                          |
| 3.6                 | 2440                            | -9.0                   | -11.1980                          |
| 3.8                 | 2575                            | -9.5                   | -11.8201                          |
| 4.0                 | 2725                            | -10.0                  | -12.4422                          |
| 4.2                 | 2895                            | -11.0                  | -13.6865                          |
| 4.4                 | 2995                            | -11.5                  | -14.3085                          |
| 4.6                 | 3130                            | -12.0                  | -14.9306                          |
| 4.8                 | 3265                            | -12.5                  | -15.5528                          |
| 5.0                 | 3400                            | -13.0                  | -16.1749                          |
| 5.2                 | 3530                            | -13.0                  | -16.1749                          |
| 5.4                 | 3655                            | -13.0                  | -16.1749                          |
| 5.6                 | 3785                            | -13.0                  | -16.1749                          |
| 5.8                 | 3925                            | -13.0                  | -16.1749                          |
| 6.0                 | 4055                            | -13.0                  | -16.1749                          |
| 6.2                 | 4160                            | -13.0                  | -16.1749                          |



**Table 11: Table for Temperature Dependence**

Sample:  $\text{Co}_{78}\text{Fe}_2\text{B}_{10}\text{Si}_{10}$

Gauge Factor: 2.02.

Sensitivity per deflection  $\Delta R/R=4.83 \times 10^{-6}$

| <b>E.M.F (mV)</b> | <b>Temperature (°K)</b> | <b>Nano-voltmeter reading</b> | <b>Magnetostriction <math>\times 10^{-6}</math></b> |
|-------------------|-------------------------|-------------------------------|---|
| -5.543            | 77                      | 20                            | 31.8812   |
| -4.920            | 101                     | 18                            | 28.6931   |
| -4.123            | 138                     | 16                            | 25.5049   |
| -3.214            | 179                     | 15                            | 23.9108   |
| -2.845            | 196                     | 14.5                          | 22.3168   |
| -2.168            | 227                     | 13                            | 20.7228   |
| -1.013            | 279                     | 11.25                         | 17.9332   |
| -0.514            | 302                     | 10                            | 15.9406   |

**Table 12: Table for Temperature Dependence**Sample:  $\text{Co}_{76}\text{Fe}_4\text{B}_{10}\text{Si}_{10}$ 

Gauge Factor: 2.02.

Sensitivity per deflection  $\Delta R/R=4.31 \times 10^{-6}$ 

| E.M.F (mV) | Temperature (°K) | Nano-voltmeter reading | Magnetostriction $\times 10^{-6}$ |
|------------|------------------|------------------------|-----------------------------------|
| -5.543     | 73               | 20                     | 28.4488                           |
| -4.920     | 101              | 18                     | 25.6039                           |
| -4.123     | 138              | 16                     | 22.7591                           |
| -3.214     | 179              | 14.5                   | 20.6254                           |
| -2.845     | 196              | 14.0                   | 19.9142                           |
| -2.168     | 227              | 13                     | 18.4917                           |
| -1.013     | 279              | 11.25                  | 16.0024                           |
| -0.514     | 302              | 10                     | 14.2244                           |

**Table 13: Table for Temperature Dependence**Sample:  $\text{Co}_{74}\text{Fe}_6\text{B}_{10}\text{Si}_{10}$ 

Gauge Factor: 2.02

Sensitivity per deflection  $\Delta R/R=3.77 \times 10^{-6}$ 

| E.M.F (mV) | Temperature (°K) | Nano-voltmeter deflection | Magnetostriction $\times 10^{-6}$ |
|------------|------------------|---------------------------|-----------------------------------|
| -5.543     | 77               | 19.5                      | 24.2624                           |
| -4.920     | 101              | 18                        | 22.3960                           |
| -4.123     | 138              | 15.75                     | 19.5965                           |
| -3.214     | 179              | 14.5                      | 18.0413                           |
| -2.845     | 196              | 14.0                      | 17.4191                           |
| -2.168     | 227              | 13                        | 16.1749                           |
| -1.013     | 279              | 11.25                     | 13.9975                           |
| -0.514     | 302              | 10                        | 12.4422                           |

**Table 14: Table for Thermal Expansion Measurement**

Sample:  $\text{Co}_{78}\text{Fe}_2\text{B}_{10}\text{Si}_{10}$

Gauge Factor: 2.02.

Sensitivity per deflection  $\Delta R/R=4.83 \times 10^{-6}$

| E.M.F (mV) | Temperature (K) | Nano voltmeter Reading | Mean Temperature (K) | Thermal Expansion $\alpha=(\Delta l/l)/\Delta T \times 10^{-6}$ |
|------------|-----------------|------------------------|----------------------|---|
| -5.543     | 77              | 20                     | 85                   | 1.9926  |
| -5.012     | 97              | 40                     | 120                  | 2.0792  |
| -4.019     | 143             | 44                     | 167                  | 2.2871  |
| -2.970     | 191             | 31                     | 206                  | 2.4708  |
| -2.313     | 221             | 76.75                  | 224                  | 2.6899  |
| -2.168     | 227             | 59                     | 253                  | 2.7129  |
| -1.021     | 279             | 31                     | 290.5                | 3.2228  |
| -0.532     | 302             |                        |                      |   |

**Table 15: Table for Thermal Expansion Measurement**Sample:  $\text{Co}_{76}\text{Fe}_4\text{B}_{10}\text{Si}_{10}$ 

Gauge Factor: 2.02.

Sensitivity per deflection  $\Delta R/R=4.31 \times 10^{-6}$ 

| E.M.F (mV) | Temperature (K) | Nano voltmeter Reading | Mean Temperature (K) | Thermal Expansion $\alpha=(\Delta l/l)/\Delta T \times 10^{-6}$ |
|------------|-----------------|------------------------|----------------------|---|
| -5.543     | 77              | 19                     | 85                   | 1.6892  |
| -5.012     | 97              | 39                     | 120                  | 1.8089  |
| -4.019     | 143             | 43                     | 167                  | 1.9114  |
| -2.970     | 191             | 30                     | 206                  | 2.1337  |
| -2.313     | 221             | 6.75                   | 224                  | 2.4004  |
| -2.168     | 227             | 60                     | 253                  | 2.4619  |
| -1.021     | 279             | 30                     | 290.5                | 2.7830  |
| -0.532     | 302             |                        |                      |   |

**Table 16: Table for Thermal Expansion Measurement**Sample:  $\text{Co}_{74}\text{Fe}_6\text{B}_{10}\text{Si}_{10}$ 

Gauge Factor: 2.02.

Sensitivity per deflection  $\Delta R/R=3.77 \times 10^{-6}$ 

| E.M.F (mV) | Temperature (K) | Nano voltmeter Reading | Mean Temperature (K) | Thermal Expansion $\alpha=(\Delta l/l)/\Delta T \times 10^{-6}$ |
|------------|-----------------|------------------------|----------------------|---|
| -5.543     | 77              | 18                     | 85                   | 1.3997  |
| -5.012     | 97              | 38                     | 120                  | 1.5418  |
| -4.019     | 143             | 42                     | 167                  | 1.6330  |
| -2.970     | 191             | 29                     | 206                  | 1.8041  |
| -2.313     | 221             | 6.25                   | 224                  | 1.9441  |
| -2.168     | 227             | 57                     | 253                  | 2.0458  |
| -1.021     | 279             | 29                     | 290.5                | 2.3532  |
| -0.532     | 302             |                        |                      |   |

**Table 17: Table for Magnetostriction Measurement at Room Temperature**Sample:  $\text{Co}_{80}\text{B}_{10}\text{Si}_{10}$ 

Gauge Factor: 2.02

Sensitivity per deflection  $\Delta R/R=3.52 \times 10^{-6}$ 

| Field Current (Amp) | Magnetic Field Strength (Gauss) | Nano voltmeter Reading | Magnetostriction $\times 10^{-6}$ |
|---------------------|---------------------------------|------------------------|-----------------------------------|
| 0.2                 | 115                             | -0.5                   | -0.5809                           |
| 0.4                 | 240                             | -0.55                  | -0.6389                           |
| 0.6                 | 380                             | -0.75                  | -0.8713                           |
| 0.8                 | 514                             | -1.0                   | -1.1617                           |
| 1.0                 | 625                             | -1.25                  | -1.4521                           |
| 1.2                 | 765                             | -1.5                   | -1.7426                           |
| 1.4                 | 905                             | -1.5                   | -1.7426                           |
| 1.6                 | 1050                            | -1.75                  | -2.0330                           |
| 1.8                 | 1170                            | -2.0                   | -2.3234                           |
| 2.0                 | 1320                            | -2.25                  | -2.6139                           |
| 2.2                 | 1460                            | -2.5                   | -2.9043                           |
| 2.4                 | 1620                            | -2.75                  | -3.1947                           |
| 2.6                 | 1775                            | -2.75                  | -3.1947                           |
| 2.8                 | 1875                            | -3.0                   | -3.4851                           |
| 3.0                 | 2020                            | -3.0                   | -3.4851                           |
| 3.2                 | 2160                            | -3.5                   | -4.0660                           |
| 3.4                 | 2300                            | -3.5                   | -4.0660                           |
| 3.6                 | 2440                            | -3.75                  | -4.3564                           |
| 3.8                 | 2575                            | -3.75                  | -4.3564                           |
| 4.0                 | 2725                            | -4.0                   | -4.6469                           |
| 4.2                 | 2895                            | -4.25                  | -4.9373                           |
| 4.4                 | 2995                            | -4.5                   | -5.2277                           |
| 4.6                 | 3130                            | -4.0                   | -4.6469                           |
| 4.8                 | 3265                            | -3.5                   | -4.0660                           |
| 5.0                 | 3400                            | -2.5                   | -2.9043                           |
| 5.2                 | 3530                            | -2.5                   | -2.9043                           |
| 5.4                 | 3655                            | -2.5                   | -2.9043                           |
| 5.6                 | 3785                            | -2.5                   | -2.9043                           |
| 5.8                 | 3925                            | -2.5                   | -2.9043                           |
| 6.0                 | 4055                            | -2.5                   | -2.9043                           |
| 6.2                 | 4160                            | -2.5                   | -2.9043                           |

**Table 18 : Table for Magnetostriction at Liquid Nitrogen Temperature**Sample:  $\text{Co}_{80}\text{B}_{10}\text{Si}_{10}$ 

Gauge Factor: 2.02

Sensitivity per deflection  $\Delta R/R=3.52 \times 10^{-6}$ 

| Field Current (Amp) | Magnetic Field Strength (Gauss) | Nano voltmeter Reading | Magnetostriction $\times 10^{-6}$ |
|---------------------|---------------------------------|------------------------|-----------------------------------|
| 0.2                 | 115                             | -0.75                  | -0.8713                           |
| 0.4                 | 240                             | -1.0                   | -1.9362                           |
| 0.6                 | 380                             | -1.25                  | -2.4202                           |
| 0.8                 | 514                             | -1.5                   | -2.9043                           |
| 1.0                 | 625                             | -1.5                   | -2.9043                           |
| 1.2                 | 765                             | -1.75                  | -3.3883                           |
| 1.4                 | 905                             | -2.0                   | -3.8724                           |
| 1.6                 | 1050                            | -2.25                  | -4.3564                           |
| 1.8                 | 1170                            | -2.5                   | -4.8404                           |
| 2.0                 | 1320                            | -2.75                  | -5.3245                           |
| 2.2                 | 1460                            | -2.75                  | -5.3245                           |
| 2.4                 | 1620                            | -3.0                   | -5.8085                           |
| 2.6                 | 1775                            | -3.0                   | -5.8085                           |
| 2.8                 | 1875                            | -3.5                   | -6.7767                           |
| 3.0                 | 2020                            | -3.5                   | -6.7767                           |
| 3.2                 | 2160                            | -3.75                  | -7.2607                           |
| 3.4                 | 2300                            | -3.75                  | -7.2607                           |
| 3.6                 | 2440                            | -4.0                   | -7.7447                           |
| 3.8                 | 2575                            | -4.25                  | -8.2288                           |
| 4.0                 | 2725                            | -4.5                   | -8.7129                           |
| 4.2                 | 2895                            | -4.6                   | -8.9064                           |
| 4.4                 | 2995                            | -4.5                   | -8.2288                           |
| 4.6                 | 3130                            | -4.0                   | -7.7447                           |
| 4.8                 | 3265                            | -3.5                   | -6.7767                           |
| 5.0                 | 3400                            | -2.5                   | -4.8404                           |
| 5.2                 | 3530                            | -2.0                   | -3.8724                           |
| 5.4                 | 3655                            | -1.5                   | -2.9043                           |
| 5.6                 | 3785                            | -1.5                   | -2.9043                           |
| 5.8                 | 3925                            | -1.5                   | -2.9043                           |
| 6.0                 | 4055                            | -1.5                   | -2.9043                           |
| 6.2                 | 4160                            | -1.5                   | -2.9043                           |

**Table 19: Table for Temperature Dependence**Sample:  $\text{Co}_{80}\text{B}_{10}\text{Si}_{10}$ 

Gauge Factor: 2.02

Sensitivity per deflection  $\Delta R/R=3.52 \times 10^{-6}$ 

| E.M.F (mV) | Temperature (°K) | Nano-voltmeter deflection | Magnetostriction $\times 10^{-6}$ |
|------------|------------------|---------------------------|-----------------------------------|
| -5.543     | 77               | -05                       | -0.5809                           |
| -5.213     | 88               | -1.0                      | -1.1617                           |
| -5.012     | 97               | -1.5                      | -1.7426                           |
| -4.019     | 143              | -2.0                      | -2.3234                           |
| -3.219     | 179              | -2.5                      | -2.9043                           |
| -2.168     | 227              | -3.0                      | -3.4851                           |
| -1.363     | 264              | -3.5                      | -4.0660                           |
| -0.532     | 302              | -4.0                      | -4.6469                           |

**Table 20: Table for Thermal Expansion Measurement**Sample:  $\text{Co}_{80}\text{B}_{10}\text{Si}_{10}$ 

Gauge Factor: 2.02.

Sensitivity per deflection  $\Delta R/R=3.52 \times 10^{-6}$ 

| E.M.F (mV) | Temperature (K) | Nano voltmeter Reading | Mean Temperature (K) | Thermal Expansion $\alpha=(\Delta l/l)/\Delta T \times 10^{-6}$ |
|------------|-----------------|------------------------|----------------------|---|
| -5.543     | 77              | 18                     | 85                   | 1.3069  |
| -5.012     | 97              | 40                     | 120                  | 1.5153  |
| -4.019     | 143             | 46                     | 167                  | 1.6699  |
| -2.970     | 191             | 32                     | 206                  | 1.8587  |
| -2.313     | 221             | 7                      | 224                  | 2.0330  |
| -2.168     | 227             | 63                     | 253                  | 2.1112  |
| -1.021     | 279             | 30                     | 290.5                | 2.2729  |
| -0.532     | 302             |                        |                      |   |

**Table 21: Table for Magnetostriction Measurement at Room Temperature**Sample: Fe<sub>82</sub>B<sub>8</sub>Si<sub>10</sub>

Gauge Factor: 2.02

Sensitivity per deflection  $\Delta R/R=4.3486 \times 10^{-6}$ 

| Field Current (Amp) | Magnetic Field Strength (Gauss) | Nano voltmeter Reading | Magnetostriction $\times 10^{-6}$ |
|---------------------|---------------------------------|------------------------|-----------------------------------|
| 0.2                 | 115                             | 0.5                    | 0.7176                            |
| 0.4                 | 240                             | 1.0                    | 1.4352                            |
| 0.6                 | 380                             | 1.5                    | 2.1528                            |
| 0.8                 | 514                             | 1.75                   | 2.5116                            |
| 1.0                 | 625                             | 2.0                    | 2.8704                            |
| 1.2                 | 765                             | 2.25                   | 3.2292                            |
| 1.4                 | 905                             | 2.75                   | 3.9467                            |
| 1.6                 | 1050                            | 3.0                    | 4.3055                            |
| 1.8                 | 1170                            | 3.25                   | 4.6643                            |
| 2.0                 | 1320                            | 4.0                    | 5.7407                            |
| 2.2                 | 1460                            | 5.0                    | 7.1759                            |
| 2.4                 | 1620                            | 6.0                    | 8.6111                            |
| 2.6                 | 1775                            | 7.0                    | 10.0463                           |
| 2.8                 | 1875                            | 7.5                    | 10.7639                           |
| 3.0                 | 2020                            | 8.5                    | 12.1990                           |
| 3.2                 | 2160                            | 9.5                    | 13.6342                           |
| 3.4                 | 2300                            | 10.5                   | 15.0694                           |
| 3.6                 | 2440                            | 11.5                   | 16.5046                           |
| 3.8                 | 2575                            | 12.0                   | 17.2222                           |
| 4.0                 | 2725                            | 12.5                   | 17.9398                           |
| 4.2                 | 2895                            | 13.0                   | 18.6574                           |
| 4.4                 | 2995                            | 13.25                  | 19.0162                           |
| 4.6                 | 3130                            | 13.75                  | 19.7337                           |
| 4.8                 | 3265                            | 14.0                   | 20.0925                           |
| 5.0                 | 3400                            | 14.25                  | 20.4513                           |
| 5.2                 | 3530                            | 14.5                   | 20.8101                           |
| 5.4                 | 3655                            | 14.5                   | 20.8101                           |
| 5.6                 | 3785                            | 14.5                   | 20.8101                           |
| 5.8                 | 3925                            | 14.5                   | 20.8101                           |
| 6.0                 | 4055                            | 14.5                   | 20.8101                           |
| 6.2                 | 4160                            | 14.5                   | 20.8101                           |



**Table 22: Table for Magnetostriction at Liquid Nitrogen Temperature**Sample: Fe<sub>82</sub>B<sub>8</sub>Si<sub>10</sub>

Gauge Factor: 2.02

Sensitivity per deflection  $\Delta R/R=4.3486 \times 10^{-6}$ 

| Field Current (Amp) | Magnetic Field Strength (Gauss) | Nano voltmeter Reading | Magnetostriction $\times 10^{-6}$ |
|---------------------|---------------------------------|------------------------|-----------------------------------|
| 0.2                 | 115                             | 1.5                    | 2.1528                            |
| 0.4                 | 240                             | 2.25                   | 3.3292                            |
| 0.6                 | 380                             | 3.0                    | 4.3055                            |
| 0.8                 | 514                             | 3.75                   | 5.3819                            |
| 1.0                 | 625                             | 4.5                    | 6.4583                            |
| 1.2                 | 765                             | 5.25                   | 7.5347                            |
| 1.4                 | 905                             | 6.0                    | 8.6111                            |
| 1.6                 | 1050                            | 7.0                    | 10.0463                           |
| 1.8                 | 1170                            | 7.75                   | 11.1226                           |
| 2.0                 | 1320                            | 8.5                    | 12.1990                           |
| 2.2                 | 1460                            | 9.5                    | 13.6342                           |
| 2.4                 | 1620                            | 10.0                   | 14.3518                           |
| 2.6                 | 1775                            | 10.5                   | 15.0694                           |
| 2.8                 | 1875                            | 11.25                  | 16.1458                           |
| 3.0                 | 2020                            | 12.0                   | 17.2222                           |
| 3.2                 | 2160                            | 13.0                   | 18.6573                           |
| 3.4                 | 2300                            | 13.5                   | 19.3749                           |
| 3.6                 | 2440                            | 14.75                  | 21.1689                           |
| 3.8                 | 2575                            | 15.5                   | 22.2453                           |
| 4.0                 | 2725                            | 16.0                   | 22.9629                           |
| 4.2                 | 2895                            | 17.0                   | 24.3981                           |
| 4.4                 | 2995                            | 18.0                   | 25.8333                           |
| 4.6                 | 3130                            | 18.5                   | 26.5508                           |
| 4.8                 | 3265                            | 19.0                   | 27.2684                           |
| 5.0                 | 3400                            | 19.5                   | 27.9860                           |
| 5.2                 | 3530                            | 20.5                   | 29.4212                           |
| 5.4                 | 3655                            | 21.5                   | 30.8564                           |
| 5.6                 | 3785                            | 22.5                   | 32.2916                           |
| 5.8                 | 3925                            | 22.5                   | 32.2916                           |
| 6.0                 | 4055                            | 22.5                   | 32.2916                           |
| 6.2                 | 4160                            | 22.5                   | 32.2916                           |

**Table 23: Table for Temperature Dependence**Sample: Fe<sub>82</sub>B<sub>10</sub>Si<sub>10</sub>

Gauge Factor: 2.02

Sensitivity per deflection  $\Delta R/R=4.3486 \times 10^{-6}$ 

| E.M.F (mV) | Temperature (°K) | Nano-voltmeter deflection | Magnetostriction $\times 10^{-6}$ |
|------------|------------------|---------------------------|-----------------------------------|
| -5.543     | 73               | 18.0                      | 25.8333                           |
| -5.213     | 88               | 17.5                      | 25.1156                           |
| -5.012     | 97               | 16.5                      | 23.6805                           |
| -4.019     | 143              | 15.0                      | 21.5277                           |
| -3.219     | 179              | 14.0                      | 20.0925                           |
| -2.168     | 227              | 13                        | 18.6574                           |
| -1.363     | 264              | 12.0                      | 17.2222                           |
| -0.532     | 302              | 11.5                      | 16.5045                           |

**Table 24: Table for Thermal Expansion Measurement**Sample: Fe<sub>82</sub>Si<sub>8</sub>B<sub>10</sub>

Gauge Factor: 2.02.

Sensitivity per deflection  $\Delta R/R=4.3486 \times 10^{-6}$ 

| E.M.F (mV) | Temperature (K) | Nano voltmeter Reading | Mean Temperature (K) | Thermal Expansion $\alpha=(\Delta l/l)/\Delta T \times 10^{-6}$ |
|------------|-----------------|------------------------|----------------------|---|
| -5.543     | 77              | 22                     | 85                   | 1.9734  |
| -5.012     | 97              | 44                     | 120                  | 2.0592  |
| -4.019     | 143             | 50                     | 167                  | 2.2425  |
| -2.970     | 191             | 34                     | 206                  | 2.4398  |
| -2.313     | 221             | 7.5                    | 224                  | 2.6909  |
| -2.168     | 227             | 67                     | 253                  | 2.7738  |
| -1.021     | 279             | 15                     | 290.5                | 3.2760  |
| -0.532     | 302             |                        |                      |   |

**Table 25: Table for Magnetostriction Measurement at Room Temperature**Sample: Fe<sub>80</sub>B<sub>10</sub>Si<sub>10</sub>

Gauge Factor: 2.02

Sensitivity per deflection  $\Delta R/R=3.6527 \times 10^{-6}$ 

| Field Current (Amp) | Magnetic Field Strength (Gauss) | Nano voltmeter Reading | Magnetostriction $\times 10^{-6}$ |
|---------------------|---------------------------------|------------------------|-----------------------------------|
| 0.2                 | 115                             | 0.5                    | 0.66028                           |
| 0.4                 | 240                             | 1.0                    | 1.2055                            |
| 0.6                 | 380                             | 1.25                   | 1.5069                            |
| 0.8                 | 514                             | 1.5                    | 1.8083                            |
| 1.0                 | 625                             | 1.75                   | 2.1096                            |
| 1.2                 | 765                             | 2.25                   | 2.7124                            |
| 1.4                 | 905                             | 2.5                    | 3.0138                            |
| 1.6                 | 1050                            | 3.0                    | 3.6165                            |
| 1.8                 | 1170                            | 3.25                   | 3.9179                            |
| 2.0                 | 1320                            | 3.5                    | 4.2193                            |
| 2.2                 | 1460                            | 4.25                   | 5.1234                            |
| 2.4                 | 1620                            | 5.0                    | 6.0276                            |
| 2.6                 | 1775                            | 6.0                    | 7.2331                            |
| 2.8                 | 1875                            | 6.75                   | 8.1372                            |
| 3.0                 | 2020                            | 7.25                   | 8.7399                            |
| 3.2                 | 2160                            | 7.5                    | 9.0413                            |
| 3.4                 | 2300                            | 8.0                    | 9.6441                            |
| 3.6                 | 2440                            | 8.5                    | 10.2468                           |
| 3.8                 | 2575                            | 9.0                    | 10.8496                           |
| 4.0                 | 2725                            | 9.5                    | 11.4524                           |
| 4.2                 | 2895                            | 10.0                   | 12.0551                           |
| 4.4                 | 2995                            | 10.5                   | 12.6578                           |
| 4.6                 | 3130                            | 11.0                   | 13.2606                           |
| 4.8                 | 3265                            | 11.5                   | 13.8634                           |
| 5.0                 | 3400                            | 12.0                   | 14.4661                           |
| 5.2                 | 3530                            | 12.0                   | 14.4661                           |
| 5.4                 | 3655                            | 12.0                   | 14.4661                           |
| 5.6                 | 3785                            | 12.0                   | 14.4661                           |
| 5.8                 | 3925                            | 12.0                   | 14.4661                           |
| 6.0                 | 4055                            | 12.0                   | 14.4661                           |
| 6.2                 | 4160                            | 12.0                   | 14.4661                           |

**Table 26: Table for Magnetostriction at Liquid Nitrogen Temperature**Sample: Fe<sub>80</sub>B<sub>10</sub>Si<sub>10</sub>

Gauge Factor: 2.02

Sensitivity per deflection  $\Delta R/R=3.6527 \times 10^{-6}$ 

| Field Current (Amp) | Magnetic Field Strength (Gauss) | Nano voltmeter Reading | Magnetostriction $\times 10^{-6}$ |
|---------------------|---------------------------------|------------------------|-----------------------------------|
| 0.2                 | 115                             | 1.0                    | 1.2055                            |
| 0.4                 | 240                             | 1.5                    | 1.8083                            |
| 0.6                 | 380                             | 2.25                   | 2.7124                            |
| 0.8                 | 514                             | 3.0                    | 3.6165                            |
| 1.0                 | 625                             | 3.75                   | 4.5207                            |
| 1.2                 | 765                             | 4.5                    | 5.4248                            |
| 1.4                 | 905                             | 5.25                   | 6.3289                            |
| 1.6                 | 1050                            | 6.0                    | 7.2331                            |
| 1.8                 | 1170                            | 7.0                    | 8.4385                            |
| 2.0                 | 1320                            | 7.75                   | 9.3427                            |
| 2.2                 | 1460                            | 8.5                    | 10.2468                           |
| 2.4                 | 1620                            | 9.5                    | 11.4524                           |
| 2.6                 | 1775                            | 10.0                   | 12.0551                           |
| 2.8                 | 1875                            | 10.5                   | 12.6579                           |
| 3.0                 | 2020                            | 11.25                  | 13.5620                           |
| 3.2                 | 2160                            | 12.0                   | 14.4661                           |
| 3.4                 | 2300                            | 13.0                   | 15.6716                           |
| 3.6                 | 2440                            | 13.5                   | 16.2744                           |
| 3.8                 | 2575                            | 14.75                  | 17.7813                           |
| 4.0                 | 2725                            | 15.5                   | 18.6854                           |
| 4.2                 | 2895                            | 16.0                   | 19.2882                           |
| 4.4                 | 2995                            | 17.0                   | 20.4937                           |
| 4.6                 | 3130                            | 18.0                   | 21.6992                           |
| 4.8                 | 3265                            | 18.5                   | 22.3019                           |
| 5.0                 | 3400                            | 19.0                   | 22.9047                           |
| 5.2                 | 3530                            | 19.5                   | 23.5075                           |
| 5.4                 | 3655                            | 20.0                   | 24.1102                           |
| 5.6                 | 3785                            | 20.0                   | 24.1102                           |
| 5.8                 | 3925                            | 20.0                   | 24.1102                           |
| 6.0                 | 4055                            | 20.0                   | 24.1102                           |
| 6.2                 | 4160                            | 20.0                   | 24.1102                           |

**Table 27: Table for Temperature Dependence**Sample: Fe<sub>80</sub>B<sub>10</sub>Si<sub>10</sub>

Gauge Factor: 2.02

Sensitivity per deflection  $\Delta R/R=3.6527 \times 10^{-6}$ 

| E.M.F (mV) | Temperature (°K) | Nano-voltmeter deflection | Magnetostriction $\times 10^{-6}$ |
|------------|------------------|---------------------------|-----------------------------------|
| -5.543     | 77               | 18.0                      | 21.6992                           |
| -5.213     | 88               | 17.5                      | 21.0964                           |
| -5.012     | 97               | 16.5                      | 19.8909                           |
| -4.019     | 143              | 15.0                      | 18.0826                           |
| -3.219     | 179              | 14.0                      | 16.8772                           |
| -2.168     | 227              | 13                        | 15.6716                           |
| -1.363     | 264              | 12.0                      | 13.9839                           |
| -0.532     | 302              | 11.5                      | 13.4012                           |

**Table 28: Table for Thermal Expansion Measurement**Sample: Fe<sub>80</sub>B<sub>10</sub>Si<sub>10</sub>

Gauge Factor: 2.02.

Sensitivity per deflection  $\Delta R/R=3.6527 \times 10^{-6}$ 

| E.M.F (mV) | Temperature (K) | Nano voltmeter Reading | Mean Temperature (K) | Thermal Expansion $\alpha=(\Delta l/l)/\Delta T \times 10^{-6}$ |
|------------|-----------------|------------------------|----------------------|---|
| -5.543     | 77              | 21                     | 85                   | 1.6330  |
| -5.012     | 97              | 41                     | 120                  | 1.6635  |
| -4.019     | 143             | 44                     | 167                  | 1.7108  |
| -2.970     | 191             | 31                     | 206                  | 1.9285  |
| -2.313     | 221             | 7                      | 224                  | 2.1096  |
| -2.168     | 227             | 63.5                   | 253                  | 2.2082  |
| -1.021     | 279             | 31                     | 290.5                | 2.5154  |
| -0.532     | 302             |                        |                      |   |

